Czech University of Life Sciences
Faculty of Environmental Sciences
Department of Water Resources and Environmental Modeling

Czech University of Life Sciences Prague
Faculty of Environmental Sciences

Numerical modelling of freezing soil and snow considering coupled water and heat flow

Dissertation thesis

Ing. Johanna Ruth Blöcher

Ph.D. programme: Environmental Modelling
Branch of study: Landscape Engineering
Supervisor: Doc. Ing. Michal Kuraz, Ph.D.

Prague, February 2022

Thesis Supervisor:
Doc. Ing. Michal Kuraz, Ph.D.
Department of Water Resources and Environmental Modelling
Faculty of Environmental Sciences
Czech University of Life Sciences
Kamycka 129
165 00 Prague 6
Czech Republic

Declaration

I hereby declare I have written this doctoral thesis independently and quoted all the sources of information used in accordance with methodological instructions on ethical principles for writing an academic thesis. Moreover, I state that this thesis has neither been submitted nor accepted for any other degree.

In Prague, February 2022

.....
Ing. Johanna Ruth Blöcher

I dedicate this work

to my furry lockdown heroines Luna, Peaky, Sesame and Sand

Acknowledgements

First, I would like to thank all the people of the Department of Water Resources and Environmental Modeling. In particular I would like to acknowledge my supervisor Michal Kuraz, our head of department Martin Hanel and Yannis Markonis for their mentorship and support. I would also like to acknowledge all members of the IGA project this work is based on. First, Roman Juras for the introduction to the world of snow and for leading the rain-on-snow experiments, and the master students Veronika Cejkova, Ibrahim Bello, Krystof Dytrt and Simon Audes. I would also like to express my gratitude towards Helenka Michalkova for her support and patience with complicated administrative matters. Then, also a special shout-out to my office comrades over the years, especially Tugba Dogan and Eva Melisova. I would also like to acknowledge the people at the department of soil science and soil physics at TU Braunschweig, and would like to especially thank Sascha C. Iden for guidance, mentorship and friendship when times were tough. Finally, I would like to thank my sister for always having an open ear and my husband for all the love, support and patience.

Funding

I acknowledge funding through the internal grant agency of the Faculty of Environmental Sciences, Czech University of Life Sciences Prague, Czech Republic (Grant number `20184236`, Project: *Experimental investigation and mathematical modelling of hydraulic properties of snowpacks*).

Abstract

Frozen soil plays an important role in simulation of land surface processes, hydrology and degrading permafrost. An accurate description of liquid water flow through snowpacks is essential to improve forecasting of disasters such as avalanches and floods, and is important for river and reservoir management. Liquid water flow through snow does not only occur during snow-melt, but also during rain-on-snow events. Freezing and melting tightly couple the water and heat flow, where temperature and temperature gradients influence the water flow and phase changes, and water content and flow influences temperature distribution. In most porous media, the interface between liquid and frozen water is not sharp and a slushy zone is present and unfrozen water can exist at sub-zero temperatures. A mathematical model can be derived using the Clausius-Clapeyron equation, which allows the derivation of a freezing curve relating temperature to pressure head.

Implementing the freezing rate is not straight-forward. Using the Clausius-Clapeyron equation creates a discontinuity at the freezing temperature in the freezing rate term in the water transport equation and latent heat term in the heat transport equation. This model assumes instant equilibrium between the ice phase. This assumption often leads to an overestimation of the ice content that is not reproduced in freezing soil experiments. This suggests that during freezing the ice and liquid water phases may not be in equilibrium. Models governing water flow in snow often neglect capillary action and tend to be derived from bucket models instead of physical laws.

This thesis aims to derive a robust coupled water and heat flow model for freezing soil and snow, and to implement the derived models into the Fortran-based open-source codebase DRUtES. Specifically, this thesis investigated the use of a regularization term to deal with the discontinuity, the use of a non-equilibrium water-ice-phase model (hereafter, ICENE) to reduce overestimation of the ice-content near freezing fronts. The models were first derived for freezing soil and then extended for snow, specifically to be applied to artificial rain-on-snow events. Here, we test the applicability of the Clausius-Clapeyron equation and adapt the non-equilibrium formulation to construct mathematical models governing coupled water and heat flow for snow. To validate the models, previously published freezing soil column experiments were used. For snow, artificial rain-on-snow experiments were conducted as part of this research in Czech mountain regions using a portable rain simulator with a brilliant blue dye tracer methodology.

The results of this thesis showed that the application of regularization of the discontinuous term successfully stabilizes the computation and can remove oscillations. As the degree of regularization is problem dependent, a simple method to determine optimal regularization parameters was presented. Volumetric water content and temperature profiles of previously published soil freezing experiments are reproduced well in the simulations. This approach could be added to other codebases easily, and the method therefore allows for broad applicability. For the ICENE model, the change in ice content was solved in a separate equation and then linked back as a non-linear zero order term. The zero-order term contains a non-equilibrium time constant and we found these time constants can vary dramatically. Overall, the ICENE decreases overestimation reported, but changes how far the freezing front propagates. Therefore, an updated formulation may additionally take into account a dependent equilibrium time constant based

on how fast temperature changes.

Two coupled water and heat flow models were adapted for snow. We show that instantaneous freezing has massive limitations to simulate water flow in snow accurately, and a phase non-equilibrium approach is required. As hydraulic and thermal properties are difficult to measure directly, cryo-transfer functions are needed to estimate them. Cryo-transfer functions based on dry snow density and mean snow grain diameter exist and were used to obtain hydraulic and thermal properties. These result in very steep retention properties. When using one-dimensional simulations for rain-on-snow experiments, moisture distribution and outflow are difficult to recreate. In this thesis, we confirm that snow often results in complicated flow patterns, showing fingering flow and horizontal flow structures. No major melt crusts or ice layers were present to explain horizontal flow structures. Horizontal flow structures can also be attributed to capillary barriers. With the cryo-transfer functions, these capillary barriers can only be recreated in simulations with significant differences in grain size and snow density between the layers. The horizontal flow structures observed after the rain-on-snow experiments, however, were more frequent than capillary barriers predicted with cryo-transfer functions. An additional mechanism would need to be taken into account to understand how horizontal flow patterns are created. We suggest that a formulation for anisotropy of the permeability may be key. Further, this work confirms that that the heterogeneity in snow structure and in flow patterns makes it difficult to take representative point measurements of moisture and temperature that can be used for comparison. Image processing could help to obtain a general overview of flow paths and may provide a useful tool to indicate regions with moisture content.

List of Tables

List of Figures

Contents

Chapter 1

Preface

All models are wrong, but some are useful (attributed to George Box).

1.1 Foreword

I believe that we were all born with a deep curiosity to want to understand how the world works. What better way to do that than with mathematical models? For me my curiosity always brought me back to soil. The phrase *"All models are wrong, but some are useful"* was chosen by Prof. Durner when he first introduced me to the Richards equation in my 3rd semester of my Bachelor's study at TU Braunschweig, and it stuck with me. The Richards equation is at the center of this thesis. It describes water flow in unsaturated soil - well to some extent it does. Representing our world in models can give us useful tools to perform experiments on what happens if we change that system. So, why did I choose this quote? Although mathematical models may seem objective, they really are quite subjective and I believe that we as *modellers* have to find better ways to communicate the assumptions we are making. Box was a statistician and probably had statistical uncertainty in mind, but I mean assumptions in the very physics we are trying to describe, and how we think processes should be described, so in this work the equilibrium assumption of freezing is put under the microscope. We have our beautiful equations and now we want to use them for our world. When we apply the models we create, it is really not only about physical laws, but also suddenly becomes about mathematics. There are very few instances where analytical solutions can be derived in a usable manner. So we go to numerical modeling. This means that we need to find ways to approximate our equations in a reasonable manner. This can be difficult for a number of reasons.

For freezing porous media, for instance freezing soil and snow, we solve coupled water and heat flow. Here, small changes in the solution can rapidly change constitutive function values. With one model assumption, we also deal with a discontinuity in the constitutive function. In one of the models derived here, we solve a set of two equations, and in the other a set of three equations. We solve systems where the physical properties result in very different ranges causing the linearized system to include entries of massively different magnitude. Some of these issues remain open research questions, for others simple solutions are presented.

1.2 Motivation

Under the threat of climate change, cold regions are changing and the need to accurately model these changes is becoming increasingly important. Many aspects of cold region hydrology and associated change were included in community paper of Blöschl et al. (2019). Aspects touched in this work include assumptions associated with hydrological laws that govern water flow in freezing soil and snow. The main motivation lies in the disentangling of when model assumptions apply, and if these models and assumptions for the porous medium of freezing soil can be extrapolated to the porous medium snow. This doctoral study began with the ambitious aim to develop a model for snow that can be used to simulate rain-on-snow experiments based on the Richards equation, fairly naively not realizing what a difficult task this might be. For snow, it is only recently that more complicated physical approaches such as the Richards equation are used, leaving a lot of scope for model improvements. As a first step, a model governing coupled water and heat flow for freezing soil should be constructed, which in some respects is an easier version of snow. When I was going through prior studies, many reported numerical issues and oscillations that went unexplored. Further, most studies reported that the common approach used tends to overestimate freezing under certain conditions, with few studies offering approaches to counteract these effects. The recent development of the use of the Richards equation for snow created a hype, which now leaves scope to see how well a model would simulate rain-on-snow experiments of natural snow.

1.3 Thesis structure

This thesis begins with an introductory section on theory and background of coupled water and heat flow in freezing soil and snow, which is followed by three research chapters, chapters 4, 5 and 6. The first research chapter deals with the implementation of a coupled water and heat model flow for freezing

soil based on the Clausius-Clapeyron equations. A system of equations is derived and a discontinuity in the constitutive function identified, which is treated with a regularization approach. The second research chapter deals with the assumption that freezing does not occur instantaneously and should be described by a non-equilibrium ice-phase approach. The third research chapter adapts these two models to allow simulating water and heat flow in snow. In the third research chapter the models are used to simulate rain-on-snow experiments conducted as part of this thesis work.

Chapter 2

Targets of dissertation

The aim of this thesis is to derive and implement models of coupled water and heat flow in freezing soil with two different assumptions on freezing and to adapt these models for water and heat flow in snow. Specifically, the thesis addresses: 1) the applicability of regularization in managing oscillations on a coupled water and heat flow model assuming instantaneous freezing based on the Clausius-Clapeyron equation; 2) the effect on freezing and redistribution of water in freezing soil when the ice and water phase are not in equilibrium and freezing is not instantaneous; 3) the applicability of these models and their assumptions for snow and in particular for rain-on-snow events using experiments which were conducted as part of this thesis.

Chapter 3

Theory and background

3.1 Introduction

This thesis focuses on the numerical modelling of freezing soil and snow. Both are natural porous media that undergo phase changes and transport of water is tightly coupled to heat transport. In some respects freezing soil and snow are quite similar and coupled water and heat transport can be described using similar approaches. Although numerical simulations of both porous media are important and bring plenty of challenges in their own right, here we see soil freezing as less complex snow and build a numerical model for snow based on assumptions for freezing soil.

Freezing and thawing in soil occur in high altitude regions and in boreal regions with seasonally frozen soil as well as regions with permafrost and therefore affects a large region. Permafrost thawing in particular can release carbon and methane and could act as a positive feedback mechanism to climate change (Kurylyk and Watanabe 2013). An accurate model of freezing and thawing in soil is required for many applications including simulation of land surface processes, hydrology and degrading permafrost (Frampton et al. 2013; Dall'Amico et al. 2011; Painter et al. 2013).

Precipitation patterns are changing (Markonis et al. 2019) which may affect the occurance of rain-on-snow events (Juras et al. 2021). The presence of snow cover can impact the hydrological cycle strongly, because it can delay the routing from precipitation to streamflow (Juras et al. 2021). Snow does not only provide the material for many winter sports, but also has an important insulation function protecting plants and animals from harsh winter winds, which have been shown to be detrimental to many plant and animal species. Snow is also important for the cooling of our planet (Sturm et al. 2017). Furthermore, snowmelt is recharging groundwater tables and is important to assure drinking water supply (Knowles

et al. 2006; Niu and Yang 2006; Godsey et al. 2014). The value of snow in monetary terms is difficult to measure. With its important role in water management, Sturm et al. (2017) estimated snow to have a trillion dollar value. The discharge behavior of snow can become very complicated during so-called Rain-on-snow (ROS) events. The discharge behavior is highly dependent on precedent conditions of the snow. Due to its complexity, physical-based models are required to model the many processes occurring during and as a result of ROS events. Water flow in snow occurs during ROS, and ROS events are expected to become more frequent.

In the sections below, background to the theory governing coupled water and heat flow in freezing soil and snow is given. Use of mathematical equations is avoided and placed with the model derivations in the following research chapters, instead conceptual equations are used.

3.2 Coupled water and heat flow theory for freezing soil

Water flow in frozen soil and thawing ground is important for a range of fields such as infiltration capacity during snowmelt (Zhao and Gray 1999), mechanical stability (Hansson et al. 2004), redistribution of solutes and increasingly for investigation of permafrost under climate change (Watanabe and Flury 2008). Dall'Amico et al. (2011) divides freezing soil models into three categories, namely (1) empirical and semiempirical, (2) analytical and (3) numerical-physically-based. The first group is based on experimentally established coefficients. The second group includes specific solutions to heat conduction problems under certain assumptions, e.g. Stefan's formulation, which simulates freezing/thawing fronts using accumulated ground surface degree-days. The last group solve the complete energy equation often coupled with transient water flow in the soil, which is assumed to give the best accuracy (Zhang et al. 2008), but is also most difficult to implement. Phase changes can cause discontinuities, which can create numerical oscillations (Hansson et al. 2004). The focus of this section is on the theory behind the numerical-physically-based approaches.

Water transport in unsaturated soil is governed by the Richards equation. The Richards equation assumes that water flows due to gravity (convection) and capillary forces (diffusion). The Richards equation in its original form is iso-thermal and does not take into account phase change. Freezing tightly couples water and heat flow, where temperature and temperature gradients influence the water flow through the soret effect (Tan et al. 2011), while phase change, water content and flow influence the temperature distribution. Therefore, a mathematical model of freezing soil requires an extension of the Richards equation, which includes these missing processes, which can conceptually be expressed as:

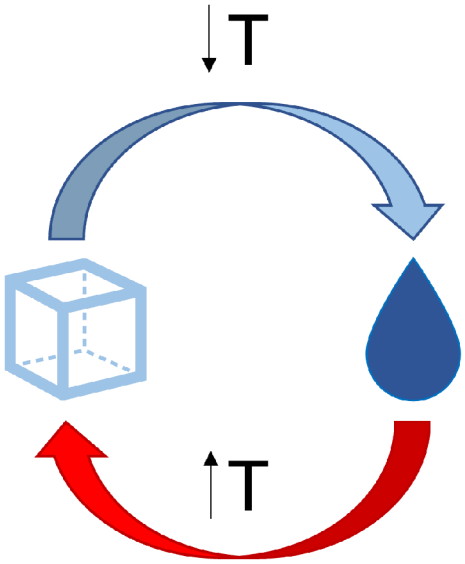

Figure 3.1: Schematic of how latent heat releases heat during freezing and consumes heat during melting.

$$\boxed{\text{Retention}} + \boxed{\text{Phase Change}} = \boxed{\text{Diffusion}} + \boxed{\text{Convection}} + \boxed{\text{Diffusion}}, \tag{3.1}$$

where the processes that are coupled to the heat equation are marked in red. As freezing is a non-isothermal process, a heat equation is also required. In many regards, this equation is quite similar to the Richards equation, containing a capacity term, which is similar to retention, a diffusive flux, a convective flux due to the movement of water, and a latent heat term due to phase change:

$$\boxed{\text{Capacity}} + \boxed{\text{Latent Heat}} = \boxed{\text{Diffusion}} + \boxed{\text{Convection}}. \tag{3.2}$$

The latent heat is known to cause numerical issues, which are discussed in the first research chapter 4. When water freezes, heat is released, and when water melts, heat is consumed.

Latent heat of fusion is causing an interesting effect, called a zero-curtain effect observed in alpine and arctic permafrost (Dall'Amico et al. 2011). While water in the soil is freezing, the temperature at that point in the soil remains 0 °C due to the the release of energy during phase change. Similar effects can be observed during melting.

The major assumption for freezing soil is that the process of freezing is analogous to that of drying, and conversely melting to that of wetting. This means that mathematical models of freezing were developed where a decrease in temperature decreases the pressure head in the soil, similar to that of drying soil. This

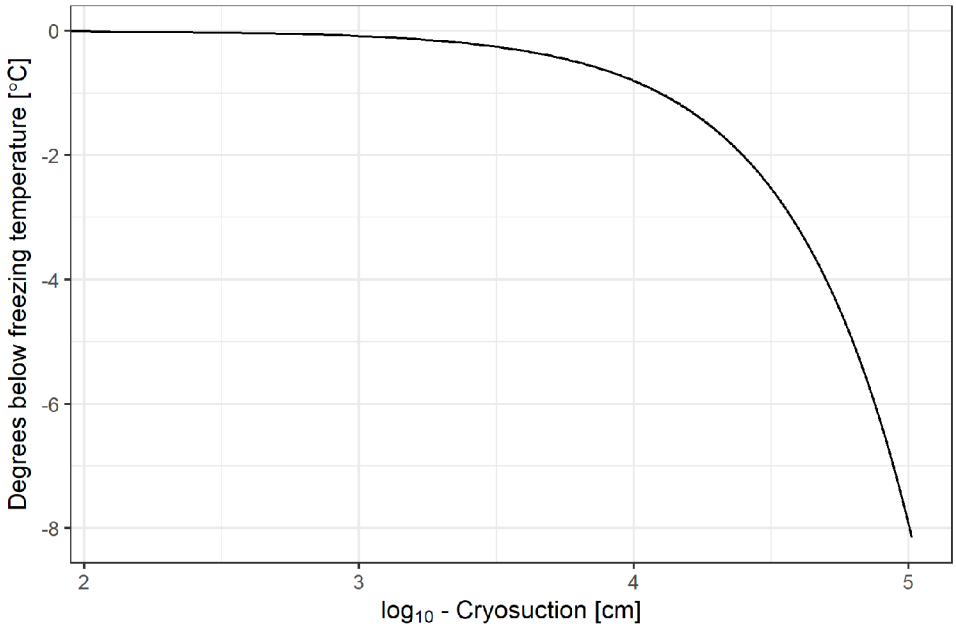

Figure 3.2: Temperature induced cryo-suction.

effect is also often referred to as "Cryo-suction". The actual amount of liquid water is then dependent on the soils retention curve, which is the equilibrium curve between water content and the pressure head. This assumption can also cause changes to the zero-curtain effect. The change in temperature is still mediated by latent heat of fusion, but not necessarily at 0 °C, but rather dependent on the pressure head in the soil.

This relation can be derived using the Clausius-Clapeyron equation, where the change in pressure can be related to the change in temperature, or in more general terms, it explains the existence of a pressure-temperature relationship. This equation is not only used for freezing soil, but widely used in physics. For instance it also explains the expansion of water due to temperature increase.

The model derived from this assumes instantaneous freezing. Some researchers Peng et al. (2016) argue that during dynamic processes, freezing is delayed as the ice-phase is not in equilibrium with the water phase. This non-equilibrium is most often ignored for freezing soil, which is further discussed in chapter 5. This ice-phase non-equilibrium approach separates the freezing rate from the coupled water and heat flow, and creates an additional equation that is coupled back to the water and heat flow using zero and first-order terms. Instead of two unknowns, three unknowns are then solved, which requires more computational resources.

In addition, researchers suggested that in soil, water does not begin to freeze at 0 °C, but that a

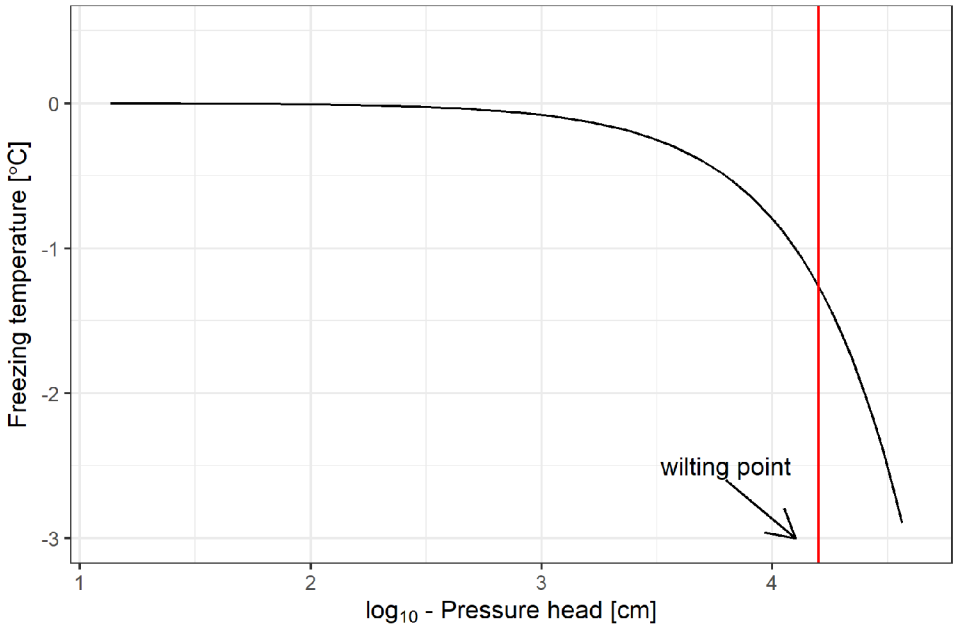

Figure 3.3: Freezing point depression, where the freezing temperature is reduced dependent on the pressure head. Red marks the wilting point, a common reference pressure for plant available water. The effect of this depression is negligible for soils with high water content, but becomes significant for drier soils.

freezing point depression exists, which decreases the freezing point depending on the pressure head of the soil (Fig. 3.3) (Dall'Amico et al. 2011).

Two non-linear constitutive functions are of importance here, the unsaturated conductivity curve and the retention curve. The relationship between soil water content and temperature below 0 °C is called the freezing characteristic curve (Koopmans and Miller 1966). This is a relation between unfrozen water and temperature. Kurylyk and Watanabe (2013) reviewed mathematical representations of freezing and thawing processes. One major difference between models is the question whether unfrozen water in freezing soil is dependent on the total amount of water present. For instance Watanabe and Wake (2009) found that frozen sandy soils with different total water content had the same amount of unfrozen water content for temperatures colder than -1 °C. The Clausius-Clapeyron equation predicts that the pressure head falls about 120 m/K, or 12000 cm/K. The effect of the differences in the initial condition is therefore extremely difficult to measure. For instance, using the retention curve parameterization according to Genuchten (1980), for a typical sand ($\alpha = 1$ [m^{-1}], $n = 3$ [-], $\theta_r = 0.02$ [-], $\theta_s = 0.45$ [-]) the volumetric water content before freezing is 0.42 at a pressure head of -0.5 m, 0.29 at a pressure head of -1 m and 0.18 at a pressure head of -1.5 m. This is a large difference for the water content, but is quite a narrow pressure head range.

Now at a temperature of -1 °C, the corresponding volumetric water content to pressure heads of -120.5 m, -121 m and -121.5 m differ less than 1×10^{-6} from each other and are therefore indistinguishable to each other. Even for soils with less steep retention properties, the volumetric water content will be close to the residual water content. Therefore, in the author's opinion, it would be a much more interesting question to investigate if the pressure head corresponding to the unfrozen water is independent of the initial water content. In this thesis, it is assumed that the pressure head and the unfrozen water content is dependent on the initial water content.

The decline in hydraulic conductivity with temperature has been experimentally investigated (Burt and Williams 1976; McCauley et al. 2002). McCauley et al. (2002) identified an exponential decline of the saturated hydraulic conductivity. Lundin (1990) introduced an impedance factor, which exponentially decreases the hydraulic conductivity. Most implementations increase impedance when more ice is present. This is because ice is thought to be blocking pores, and with greater ice content, more pores are blocked. Some researchers questioned the need for such a term (Kurylyk and Watanabe 2013), and argue that better constitutive relations are needed, but the impedance approach is still widely used and no functional parsimonious alternative has been presented so far.

Relevant theory and background regarding coupled water and heat flow for freezing soil was summarized. Latent heat tightly couples the water and heat flow and can moderate temperature change while freezing or melting is on-going. Although, in effect the soil might then be iso-thermal, this effect requires the consideration of a coupled water and heat flow system. Additional important aspects include cryo-suction, which is based on the assumption that freezing is equal to drying. A relevant framework for water to be present in a porous medium below the freezing temperature can be derived with the Clausius-Clapeyron equation. In addition, some models include a freezing point depression, where the temperature when freezing begins is reduced respective to the pressure head in the soil. It is under debate whether the cryo-suction is dependent on the soil's water content. Impedance to the hydraulic conductivity curve may occur due to the blockage of pores by ice, but is also often debated.

3.3 Coupled water and heat flow theory for snow

Snow is a complicated medium with non-conservative hydraulic and thermal properties. Liquid water occurs in snowpacks during rain-on-snow (ROS) events and during the ablation phase. ROS has been known to cause mid-winter and spring avalanches (Conway and Raymond 1993) as well as flooding (Pradhanang et al. 2013). These natural disasters depend on precedent snow conditions and complex hydrodynamics.

Liquid water transport models in snow can be found as part of avalanche forecasting services, because liquid water movement is important for wet snow avalanches (Hirashima et al. 2010). Examples include the Swiss SNOWPACK model used for avalanche warning (Bartelt and Lehning 2002; Lehning et al. 2002), which is also used in Japan, and the French CROCUS model (D'Amboise et al. 2017). To this day, snow is often modelled with a simplified bucket approach with limited physical representation. A large number of snow models exist, but they depend on a relatively small number of different process parameterizations. This was thoroughly reviewed in Essery et al. (2013). Essery et al. (2013) concluded that the most consistent results were found in models accounting for storage and refreezing of liquid water within snow. The first numerical models of coupled water and heat flow date back to the 70s. Water movement in snow has long been thought of as being driven only by gravity and water vapor flow due to a temperature gradient. The first to describe water flow through snow theoretically was S. C. Colbeck, who developed a one dimensional water flow model through snow based on Darcian flow to estimate the distribution of volume flux and water saturation in the snow (Colbeck 1971; Colbeck and Davidson 1973; Colbeck 1974). Only recently, not only gravitational but also capillary forces were included in models when simulating water fluxes through snow. According to early studies of Colbeck (1974) capillary forces in homogeneous snow only account for about 10% of the liquid flux. Even though capillary gradients may not drive most of the water flow, the consideration of capillary action can be very important, because they explain capillary barriers, which in turn can create ice crusts after refreezing and change the water flow significantly. Capillary barriers have often been observed during rain and dye tracer infiltration experiments into snow. A capillary barrier occurs under unsaturated conditions when two pore systems exhibit different capillary action, because of different pore sizes, e.g. when a layer of fine-grained snow is on top of a coarse-grained snow under unsaturated conditions. The use of the Richards equation started roughly a decade ago as available models did not yield an adequate simulation of the water content profile and the lack of model skill (Hirashima et al. 2010). Model skill in this context, often refers to recreating outflow from snowpacks. Wever et al. (2014) stressed that bucket models do not adequately represent outflow mechanisms on a subdaily scale, therefore the temporal scale is very important for model evaluation (Heilig et al. 2015). Daanen and Nieber (2009) developed a coupled water and heat model based on the generalized Clapeyron equation, but provided little validation. Wever et al. (2014) was the first to implement the Richards equation based model into a major snow model framework SNOWPACK. However, the implementation is often described to conduct water too fast (Würzer et al. 2017). Although capillary forces are known to be important for capillary barriers, even recent model developments often only consider gravitational forces,

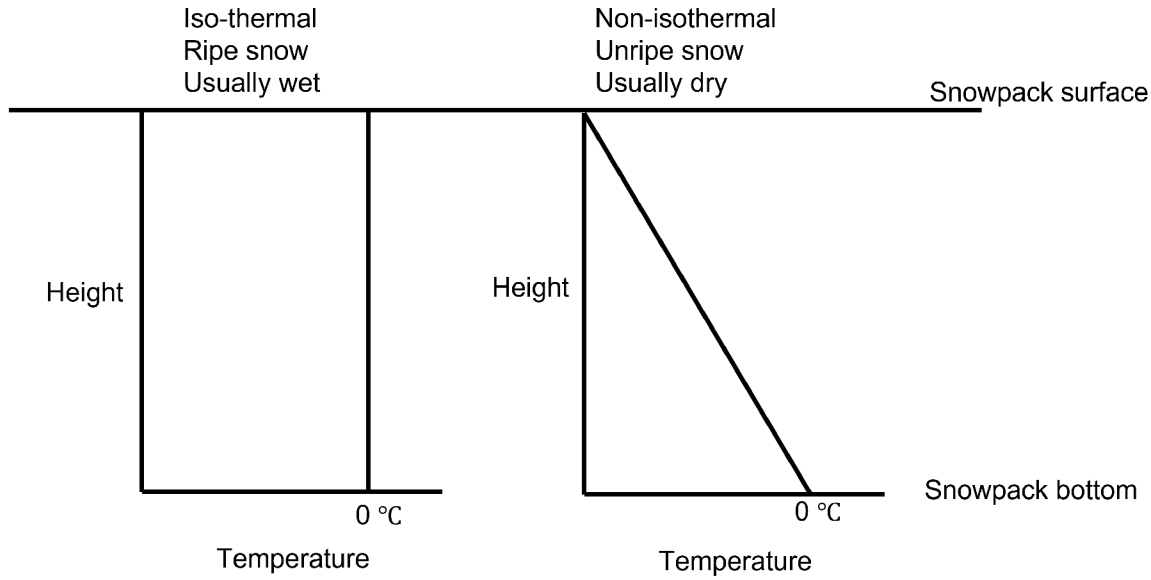

Figure 3.4: Schematic description of left: wet *warm* snow, which is usually ripe with an iso-thermal temperature distribution and a non-zero moisture content and right: dry cold snow with a linear temperature distribution.

i.e. Kelleners et al. (2016). How to best represent water flow, and what processes govern its movement in snow, is still up for debate.

Simulations of rain-on-snow events often focus on the outflow behaviour (Würzer et al. 2017). The reasons are two-fold, first water propagation may not seem homogeneous on the smaller scale (Fig. 3.5 b), and it is difficult to monitor liquid water content in the snowpack continuously, which limits validation data sets. Very generalized, two states of snow exist, which exhibit different thermal properties. On the one hand, there iso-thermal wet snow, which can be often found during snow ablation period (Fig. 3.4 left) and cold dry snow, which exhibits a vertical temperature distribution. This type of snow is usually coldest at the air-snow surface interface. Note, that the bottom temperature for both snow states is usually 0 °C. For field experiments, rain-on-snow sprinkling experiments can be used to generate data used for model validation with examples of snowpack after the experiments in Fig. 3.5. These photos are the result of brilliant blue dye tracer experiments that are often used in soil as well. Both preferential flow patterns as well as homogeneous flow patterns can be generated from rain or sprinkling events depending on the state of the snow. Fig. 3.5 a) shows homogeneous distribution of water flow without preferential flow. This type of flow can be observed in ripe snowpacks that have an isothermal vertical temperature distribution (Fig. 3.4 left), which can already contain moisture. Fig. 3.5 b) shows lateral flow barriers causing the

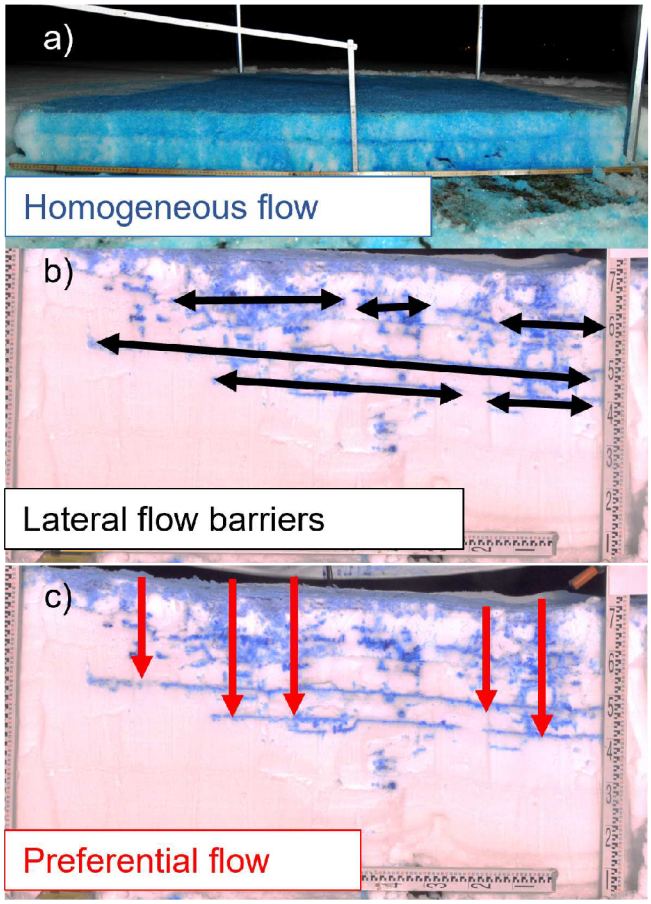

Figure 3.5: Different flow patterns snow after rain-on-snow experiments. a) Homogeneous flow where barriers and preferential flow are negligible. b) Lateral flow barriers that inhibit downward movement of snow. c) Vertical preferential flow or fingering flow that allow water to bypass section of the snow.

Table 3.1: Terminology used for grain size range for snow according to Fierz et al. (2009).

Term	Size range [mm]
Very fine	< 0.2
fine	$0.2 - 0.5$
medium	$0.5 - 1.0$
coarse	$1.0 - 2.0$
very coarse	$2.0 - 5.0$
extreme	> 5

snow to significantly flow laterally. These barriers can be due to denser ice or freeze-melt crusts, which are significantly less permeable, or capillary barriers. Fig. 3.5 c) shows preferential fingering flow. Katsushima et al. (2013) conducted laboratory experiments on dry snow with the aim to improve understanding of when preferential flow becomes important. The flow patterns generated showed preferential flow as well as the existence of capillary barriers. Katsushima et al. (2013) suggested that the tendency to generate preferential flow may be dependent on the mean grain size and even suggested an empirical relationship based on their experiments. Hirashima et al. (2014) created a 3-dimensional model that can recreate these flow paths. However, their model neglected freezing and only focused on fingering flow (Fig. 3.5 c) and still struggles to adequately represents lateral flow.

Snow hydraulic and thermal properties

To simulate water flow in snow, knowledge of hydraulic and thermal properties are essential. These include two functions, the hydraulic conductivity and the retention curve and serve as constitutive functions to the set of partial differential equations. Although for soil novel formulations of these properties are tested and developed, i.e. Iden et al. (2021), most snow simulations use more simplistic van Genuchten-Mualem Genuchten (1980) and Mualem (1976) formulations. Snow hydraulic properties are extremely difficult to measure. Standard procedures to obtain retention and hydraulic conductivity data, for instance with the laboratory evaporation method (Iden et al. 2019) are not feasible, because snow is a strongly non-conservative medium. A common tool to avoid measuring these properties directly are transfer functions. For soil these are called pedo-transfer functions, therefore here, for snow, they will be called cryo-transfer functions. These functions are commonly dependent on grain size and snow density (see Tab. 3.3). Tab. 3.1 summarizes commonly used terms for grain size range. Snow grains are therefore similar in size to sand and gravel assuming European soil reference size classification.

Shimizu (1970) first derived an empirical function for the saturated hydraulic conductivty dependent

Table 3.2: Typical densities for different snow types according to Muskett (2012) and ice.

Term	Density [kg m^{-3}]
New snow	$50 - 70$
Settled snow	$200 - 300$
Depth Hoar	$100 - 300$
Wind Packed Snow	$350 - 400$
Ice	≈ 917

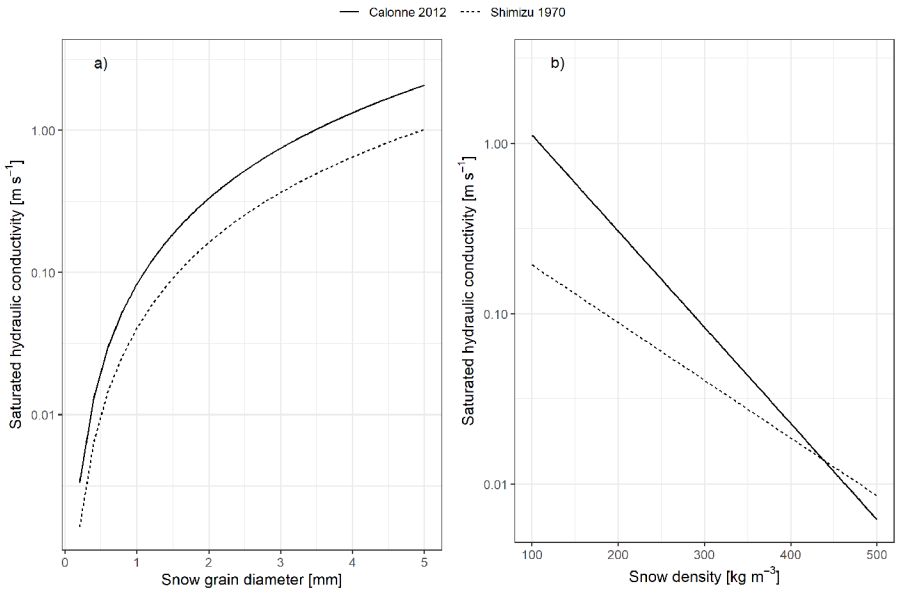

Figure 3.6: Comparison of saturated hydraulic conductivity estimates using Shimizu (1970) and Calonne et al. (2012) parameterization.

on grain size and density using experimental data from a permeameter. This parameterization is still widely used. Calonne et al. (2012) derived a new parameters, but using the same equation, based on 3D image processing. The saturated conductivity of snow with these parameterizations can be several orders higher than that of sand (Fig. 3.3). Although the resulting dependency of saturated hydraulic conductivity curves have similar shapes in both Shimizu (1970) and Calonne et al. (2012), Calonne et al. (2012) parameterization results in greater conductivity values. Shimizu (1970) is said to be only valid up to snow grains of 1 mm, but can be extended to 2 mm following Colbeck (1978).

Daanen and Nieber (2009), Yamaguchi et al. (2010), Hirashima et al. (2010), and Yamaguchi et al. (2012) developed cryo-transfer functions for the shape parameters of the van Genuchten function α, which is often referred to as the inverse of the air entry value and n, which determines the steepness of the retention curve. Together, they determine the pore size distribution of the given medium. Whereas Daanen and

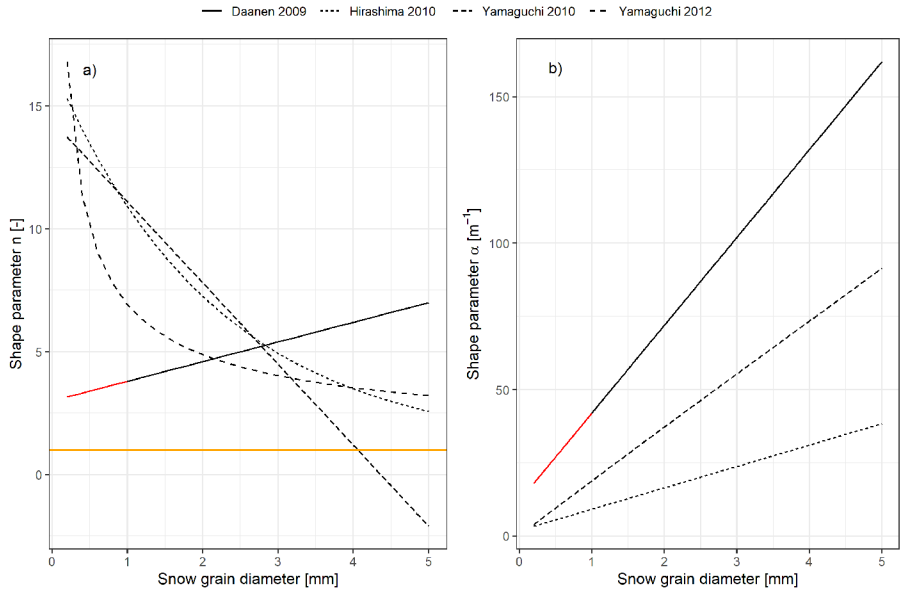

Figure 3.7: Comparison of van Genuchten shape parameters α and n from Daanen and Nieber (2009), Yamaguchi et al. (2010), Hirashima et al. (2010), and Yamaguchi et al. (2012). The red line indicates the validity for Daanen and Nieber (2009). The orange line indicates when n is below 1, as per definition n values below 1 are impossible.

Nieber (2009), Yamaguchi et al. (2010), and Hirashima et al. (2010) equations are only dependent on grain size diameter, the equation by Yamaguchi et al. (2012) is dependent on grain size diameter and snow density. Daanen and Nieber (2009) based their paramterizations on a limited experimental data set from Marsh and Woo (1985a) and only have a validity for grain size between 0.1-1 mm. Yamaguchi et al. (2010), Hirashima et al. (2010), and Yamaguchi et al. (2012) used a gravity drainage method to derive their parameterizations, mainly using rounded grains and melt forms. Here, a 30 cm snow column was packed and submerged in water at 0 °C. Whereas Daanen and Nieber (2009) parameterization predicts n to increase with grain size, Yamaguchi et al. (2010), Hirashima et al. (2010), and Yamaguchi et al. (2012) predict n to decrease with grain size. This means that Daanen and Nieber (2009) assumed that pore size distribution narrows with increasing grain size as the pore size distribution narrows with greater n, while Yamaguchi et al. (2010), Hirashima et al. (2010), and Yamaguchi et al. (2012) assume that the pores size distribution become wider with increasing grain diameter. Yamaguchi et al. (2010) derived a parameterization that does not hold for grain sizes greater than 4 mm as indicated by the orange line in Fig. 3.3, as n becomes smaller than 1 and thereby becomes non-physical.

For soil, n values are usually greater for coarser soil textures, such as sand. This is because sandy soils are usually more sorted, whereas clayey and loamy soils have a wider pore size distribution. Similarly, α

values are also greater for coarser textures, because it represents the inverse to the air entry value in the retention curves. This air entry in coarser textures occurs at lower suction (absolute pressure head). This can also be seen in all three cryo-transfer models, as α increases with snow grain diameter, assuming that these, on average, create greater pore spaces. Yamaguchi et al. (2012) concluded that melt forms of the water retention curve can be described with their model, but that the fit was not sufficient for rounded non-uniform grains. They suggest that sphericity might be another promising angle to be tested to develop better parameterization, but so far no cryo-transfer function exists to take into account sphericity.

Katsushima et al. (2013) fitted α and n using RETC software (Van Genuchten et al. 1991) for four grain sizes ranging from 0.25-1.4 mm. The fitted n values ranged between 9-14, and are greater than coarse soil and comparable to what is predicted by the models, whereas α parameters (7-16 m^{-1}) are in the lower range compared to the models. Similarly, the measured saturated conductivity values of 4.0×10^{-4} to 5.3×10^{-3} m/s (3468-46416 cm d^{-1}) are significantly smaller than what is predicted by Calonne et al. (2012) and Shimizu (1970).

Common cryo-transfer functions produce extremely steep retention properties with very high values of hydraulic conductivity. Already small changes in pressure head will cause snow to drain. This already indicates that capillary forces indeed do not play a major role in snow.

Illangasekare et al. (1990) calculated thermal conductivity with a linear and quadratic function depending on density. Calonne et al. (2011) conducted numerical simulations of the thermal conductivity of snow using microtomographic images and developed an empirical relationship (quadratic function) between effective thermal conductivity λ_{eff} and snow density ρ [kg m^{-3}]. The comparison in Fig. 3.8 shows that they are quite similar with similar assumptions on the effects of density on the thermal conductivity.

Depending on model assumptions, the saturated water content θ_s is defined differently (Fig. 3.9). In the context of the Clausius-Clapeyron equation, we define a total water content, which includes liquid and frozen water. In that respect, the pore space equals 1. Examples include Kelleners et al. (2016). Alternatively, one could assume that the θ_s is equal to the initial pore space not occupied by ice. Freezing and melting could occur in that space, in which case the assumptions of the Clausius-Clapeyron equation would then be limited to less space and total melt would be avoided. Thirdly, one could assume that θ_s changes and is always equal to the pore space not occupied by ice, e.g. Leroux and Pomeroy (2017) and D'Amboise et al. (2017). The third approach is difficult to combine with the Clausius-Clapeyron, as it would change the total pressure head artificially. It is also difficult to implement with the Clausius-

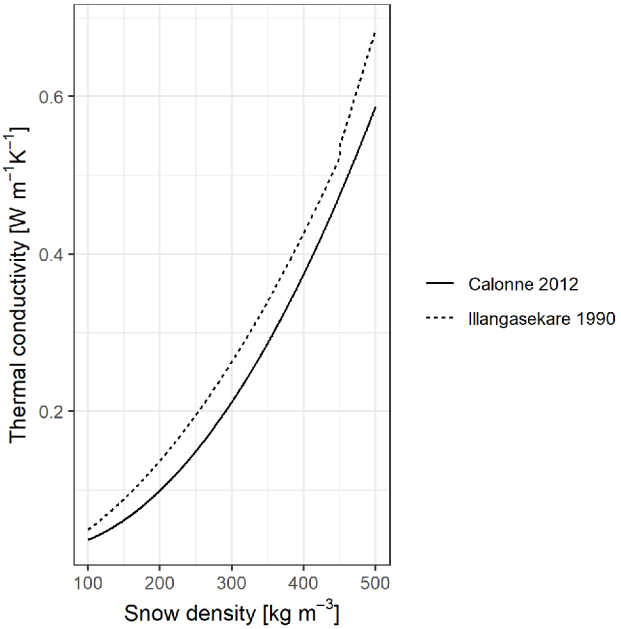

Figure 3.8: Comparison of two thermal conductivity cryo-functions for snow based on snow density by Illangasekare et al. (1990) and Calonne et al. (2011).

Clapeyron as it requires a separate solution of θ_i, whereas the advantage with Clausius-Clapeyron is the possibility to solve the total pressure head as its unknown, and then based retention curve parameters and the temperature, θ_i and θ_l are calculated.

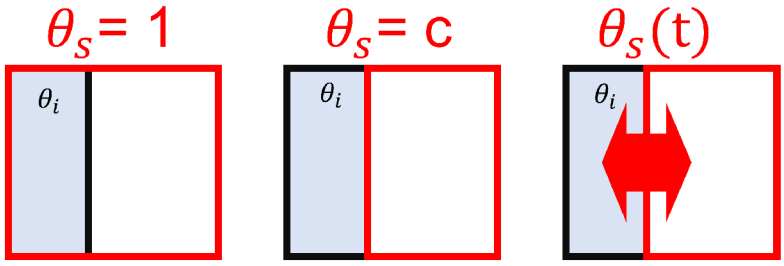

Figure 3.9: Conceptualizations of how to define saturated water content for snow. The first option sets it to 1, and the entire space can be understood as pore space. Second, the pore space not occupied by the initial snow is considered. Third, the saturated water content is variable and increases and decreases with pore space.

To recapitulate, theory regarding coupled water and heat flow for snow has been presented including a review on hydraulic properties. Using Richards equation based models is still new and the importance of certain flow phenomena unclear. In contrast to freezing soil, the retention curve and hydraulic conductivity

Table 3.3: Overview of cryo-transfer functions.

Process	Equation	Variables	Publication
Saturated conductivity	$K_s = \frac{g\rho_l}{\nu} 0.077 d^2 exp(-0.0078\rho_s)$	d: = snow grain diameter [m], g: gravitational acceleration [L T^{-2}], ρ_s: snow density [M L^{-3}], ν: dynamic viscosity of water at 0 °C, ρ_l: liquid water density [M L^{-3}]	Shimizu (1970)
	$K_s = \frac{g\rho_l}{\nu}\left[3 r_{es}^2 exp(-0.013\rho_s)\right]$	r_{es}: equivalent snow grain sphere radius [m]	Calonne et al. (2012)
shape parameter α	$\alpha = 30d + 12$	d: = snow grain diameter [mm]	Daanen and Nieber (2009)
	$\alpha = 7.3d + 1.9$	d: = snow grain diameter [mm]	Yamaguchi et al. (2010)
	$\alpha = 4.4 \cdot 10^6 (\frac{\rho_{db}}{d})^{-0.98}$	d: = snow grain diameter [m], ρ_{db}: bulk dry density of snow [kg m^{-3}]	Yamaguchi et al. (2012)
shape parameter n	$n = 0.8d + 3$	d: = snow grain diameter [mm]	Daanen and Nieber (2009)
	$n = -3.3d + 14.4$	d: = snow grain diameter [mm]	Yamaguchi et al. (2010)
	$n = 15.68 exp(-0.46d) + 1$	d: = snow grain diameter [mm]	Hirashima et al. (2010)
	$n = 1 + 2.7 \cdot 10^{-3} (\frac{\rho_{db}}{d})^{0.61}$	d: = snow grain diameter [m],ρ_{db}: bulk dry density of snow [kg m^{-3}	Yamaguchi et al. (2012)
Thermal conductivity	$\lambda_{eff} = 2.5 \cdot 10^{-6} \rho_s^2 - 1.23 \cdot 10^{-4} \rho_s + 0.024$	ρ_s: density of snow [kg m^{-3}]	Calonne et al. (2011)
	$\lambda = 0.307\rho_s + 1.964\rho_s^2$ for $\rho_s <$ 450 kg m^{-3}	ρ_s: density of snow [Mg m^{-3}]	Illangasekare et al. (1990)
	$\lambda = 2.98\rho_s - 0.805$ for $\rho_s >$ 450 kg m^{-3}		

curves obtained from cryo-transfer functions are much steeper and drainage occurs at a higher pressure head over a smaller pressure head range. Also in contrast to freezing soil, models of snow do not usually make use of an impedance factor for hydraulic conductivity, or the use a freezing point depression.

3.4 Numerical solver and implementation

The models were implemented in the Dual Richards' Unsaturated Equation Solver (DRUtES) (Kuraz et al. 2020). DRUtES can solve coupled advection-diffusion-reaction equations and is still being expanded with recent additions including coupled water, heat and vapor flow considering evaporation and the freezing module presented in this thesis. DRUtES's modularity allows the implementation of additional problems of advection-diffusion-reaction type. DRUtES is an object oriented library written in Fortran 2003/2008, which can be compiled on any unix based system, and even windows using Windows Subsystem for Linux with readily available gfortran compiler. For wide accessibility DRUtES is hosted on github with the main development repository on https://github.com/michalkuraz/drutes-dev, and was also selected as part of the Arctic Code Vault, an initiative that archived popular open-source code in the Svalbard archipelago. DRUtES is free software and can be redistributed and modified under the terms of the GNU General Public v3 License.

In DRUtES the spatial derivatives are approximated by the continuous linear Galerkin finite element method and the temporal derivatives are approximated by the implicit Rothe method. An adaptive time step scheme is implemented in DRUtES, where the time step is controlled by the convergence rate of the Picard iteration. DRUtES has been successfully applied to a range of real world and theoretical cases combining the Richards equation and the advection-dispersion-reaction equation (Kuraz et al. 2013b; Kuraz et al. 2013a; Kuraz et al. 2015).

DRUtES is a command-line software and takes input from configuration files. A model considering local thermal non-equilibrium was also implemented, but is still under development. In this thesis the model considering thermal local equilibrium (LTE) and ice-phase non-equilibrium (ICENE) are presented. The models were implemented with the following file structure. The configuration files for the models are listed under drutes.conf/freeze. The user can define hydraulic properties and thermal properties with different parameterizations available for freezing soil or snow. The source code can be found in the folder src, which requires compilation. The source file $freeze\_pointers.f90$ links governing equations to pre-defined modular constructions for diffusion, elasticity, advection and reaction terms defined in $freeze\_fnc.f90$ and $freeze\_helper.f90$. $freeze\_fnc.f90$ and $freeze\_helper.f90$ also contain functions to read initial

conditions, boundary conditions and constitutive functions. Global variables as well as additional necessary structures are defined in $freeze\_globs.f90$. Configuration files are read in $freeze\_reader.f90$.

```
DRUtES
├── bin
├── drutes_conf
│   ├── other
│   ├── global.conf
│   ├── solver.conf
│   ├── mesh
│   └── freeze
│       ├── freeze.conf
│       ├── freeze_heat_LTE.conf
│       ├── freeze_heat_LTNE.conf
│       └── freeze_ICENE.conf
├── out
│   ├── Files of observation points
│   └── Files of observation times
└── src
    ├── other
    └── soilfreeze
        ├── freeze_pointers
        ├── freeze_reader
        ├── freeze_globs
        ├── freeze_fnc
        └── freeze_helper
```

The LTE model results in a system of equations where two unknowns are solved, the stiffness matrix is schematically represented in 3.3. The ICENE model results in a system of equations where three unknowns are solved, the stiffness matrix is schematically represented in 3.4. For one-dimensional problems the discrete represention of the LTE model defined in Eq. (4.33) is a 2×2 block matrix, where each block is a 3-diagonal matrix. The ICENE model defined in Eq. (5.19) is a 3×3 block matrix, where each block in the water and heat terms is a 3-diagonal matrix, and the block in the ice term is 1-diagonal.

$$\left(\begin{array}{c|c} \text{Water terms in Water operator} & \text{Heat terms in Water operator} \\ \hline \text{Water terms in Heat operator} & \text{Heat terms in Heat operator} \end{array}\right) \tag{3.3}$$

$$\left(\begin{array}{c|c|c} \text{Water terms in Water operator} & \text{Heat terms in Water operator} & \text{Ice terms in Water operator} \\ \hline \text{Water terms in Heat operator} & \text{Heat terms in Heat operator} & \text{Ice terms in Heat operator} \\ \hline \text{Water terms in Ice operator} & \text{Heat terms in Ice operator} & \text{Ice terms in Ice operator} \end{array}\right) \tag{3.4}$$

For one-dimensional problems, LU decomposition is used. For the LTE model a row-balancing algorithm was developed, which is detailed in the appendix (B). For two-dimensional problems finding an efficient solver is still on-going work.

Chapter 4

Regularization strategy for discontinuity when modeling coupled water and heat flow in freezing unsaturated soil

4.1 Introduction

Freezing and thawing in soil occur in high altitude regions and in boreal regions with seasonally frozen soil as well as in regions with permafrost and therefore affects a large region. Permafrost thawing in particular can release carbon and methane and could act as a positive feedback mechanism to climate change (Kurylyk and Watanabe 2013). An accurate model of freezing and thawing in soil is required for many applications including simulation of land surface processes, hydrology and degrading permafrost (Frampton et al. 2013; Dall'Amico et al. 2011; Painter et al. 2013). The use of these models have even been extended to model the hydrological evolution of Mars (Painter et al. 2013) with the software MarsFlo. Freezing tightly couples water and heat flow, where temperature and temperature gradients influence the water flow through the soret effect (Tan et al. 2011), while phase change, water content and flow influence the temperature distribution.

In most porous media, the interface between liquid and frozen water is not sharp and a slushy zone is present (Amiri et al. 2018). In soil, unfrozen water can exist at sub-zero temperatures. A common observation of freezing soil is water accumulation towards the freezing front due to *Cryo-suction*. The soil freezing reduces the liquid pressure head and thereby initiates water flux towards the freezing front. Soil freezing is in fact similar to soil drying, which is an analogy that was first introduced by Harlan

(1973). Most mathematical models of freezing use the Clausius-Clapeyron equation, and by assuming the ice pressure to be zero, the pressure head and subsequently the unfrozen water content can be related to temperature with soil freezing curves. Examples of numerical implementations can be found in Hansson et al. (2004), Dall'Amico et al. (2011), Kelleners (2013), Karra et al. (2014), Kelleners et al. (2016), and Arzanfudi and Al-Khoury (2018). Kurylyk and Watanabe (2013) reviewed mathematical models of freezing and thawing with an overview on physical processes and appropriate model parameterization. Grenier et al. (2018) undertook a model comparison for freezing test cases for water saturated soils and Lamontagne-Hallé et al. (2020) developed numerical guidelines and provides an overview over available cryohydrogeological models and their capabilities. Many of these models still lack certain features such as cryosuction. We believe that this may be due to numerical issues that model developers face with their current solver and discretization setup. Implementing the freezing rate is not straight-forward. Using the Clausius-Clapeyron equation creates a discontinuity at the freezing temperature in the freezing rate term in the water transport equation and latent heat term in the heat transport equation, and little attention has been paid to the adequate description of their numerical treatment and computational challenges. Examples were described in Painter et al. (2016), where some of the numerical issues to be solved are convergence issues of the non-linear solver near the freezing and thawing front. Discretizing this discontinuous system with standard finite element methods (standard Galerkin type) can cause spurious oscillations (Arzanfudi and Al-Khoury 2018), because the standard finite element method uses continuous base and shape functions that are incapable of handling discontinuities within an element (Amiri et al. 2018). Modeling freezing is additionally difficult, as near the freezing front small changes in the solution (temperature) yield large changes in model parameters. This is a similar issue as observed with steep soil hydraulic properties. In addition, freezing decreases the liquid water content, essentially drying out the soil, causing steep gradients similar to that of infiltration into dry soil. This contribution aims to 1. revisit the theory and derivation of model formulations including the discontinuity; 2. investigate the application of regularization of the discontinuous term to create continuity; 3. develop a method to obtain optimal regularization parameters as the degree of the regularization may depend on the problem setup; 4. validate the model on various freeze column experiments conducted by Jame (1977) and Mizoguchi (1990). In addition, the model is also validated on melt and synthetic infiltration experiments to reproduce the freezing curtain effect.

4.2 Coupled Water and Heat Flow Model

In the following we present derivations for soil freezing, water flow, and heat flow, followed by the regularization approach. In this model implementation the primarily solved variables, or unknowns, are the total hydraulic head related to the total water content (frozen and unfrozen) H_w [m] and temperature T [K].

4.2.1 Soil freezing

To obtain the relationship between unfrozen water content and temperature, we assume that freezing is an analogy to drying (Dall'Amico et al. 2011). This common "freezing=drying" assumption allows the use of retention curve functions for freezing. For this, a pressure head is derived that is dependent on temperature using the generalized Clausius-Clapeyron equation. A detailed review of its use can be found in Kurylyk and Watanabe (2013). It is common to assume that the ice pressure differential over temperature is null, i.e. the ice pressure is constant, and so the generalized Clapeyron equation becomes:

$$\frac{\mathrm{d}p}{\mathrm{d}T} = \frac{Lf\rho_l}{T}, \tag{4.1}$$

where p is the capillary pressure [Pa], Lf is the latent heat of fusion $336{\cdot}10^3$ [J kg^{-1}] and T is temperature [K]. The pressure head for liquid unfrozen water under freezing conditions can be derived by converting p to pressure head by using $p = h\rho_l g$ and integrating Eq. (4.1) over the bounds of T_f to T and h_w to h_l (Dall'Amico et al. 2011) as follows

$$h_l = \begin{cases} h_w + \frac{Lf}{g} \ln \frac{T}{T_f}, & \text{for} \quad T < T_f, \\ h_w, & \text{for} \quad T \geq T_f, \end{cases} \tag{4.2}$$

where h_l is the pressure head of the unfrozen liquid water content [m], h_w is the pressure head of the total (frozen+unfrozen) liquid water content [m], g is gravitational acceleration (9.81 m s^{-2}) and T_f is the freezing temperature (0 °C or 273.15 K). This mimics findings that a significant amount of unfrozen water can exist in soil at subzero temperatures.

Equation (4.2) is a very handy expression, as it allows the use of well-established retention curve functions for the estimate of mobile unfrozen water. This concept allows the calculation of the volumetric ice content θ_i [-] as the difference of the total volumetric water content θ_w and the volumetric liquid water content θ_l as follows:

$$\begin{aligned} \theta_w &= \theta(h_w), \\ \theta_l &= \theta(h_l), \\ \theta_i &= \theta_w(h_w) - \theta_l(h_l). \end{aligned} \tag{4.3}$$

4.2.2 Water Transport

The extended Richards equation (Hansson et al. 2004) describes the variable saturated water flow for unfrozen and freezing temperatures where the liquid flux q_l includes a temperature driven liquid water flux. This allows water to redistribute along a temperature gradient. This phenomenon is also often called the Soret effect.

$$\frac{\partial \theta_l}{\partial t} + \frac{\rho_i}{\rho_l}\frac{\partial \theta_i}{\partial t} = \overbrace{\boldsymbol{\nabla} \cdot K_{lh}\boldsymbol{\nabla}(h_l + z) + \boldsymbol{\nabla} \cdot K_{lT}\boldsymbol{\nabla}T}^{-\boldsymbol{\nabla}\cdot\vec{q}l}, \tag{4.4}$$

where $\theta_{l,i}$ are the volumetric liquid water and ice contents [-], t is the time [s], $\rho_{i,l}$ are the density of ice and liquid water [kg m^{-3}], K_{lh} is the liquid hydraulic conductivity [m s^{-1}], z is the geodetic head [m], K_{lT} is the temperature hydraulic conductivity [m^2 s^{-1} K^{-1}] and T is the temperature [K].

In the following all terms are expanded using product and chain rules in respect to the unknown H_w [m] or T [K]. The solution component H_w is the total hydraulic head defined as

$$H_w = h_w + z. \tag{4.5}$$

Formulating the water flow equation in hydraulic head instead of pressure head removes the need to estimate $\frac{\partial K(h)}{\partial z}$ at material boundaries of two soil layers.

Given the density differences of ice and water, and following the derivation in Dall'Amico et al. (2011) (Appendix A therein), we can derive a total liquid-water-equivalent θ_{weq} [-] content as follows:

$$\theta_{weq} = \theta_w + \left(\frac{\rho_i}{\rho_l} - 1\right)\theta_i, \tag{4.6}$$

and in the capacity form:

$$\frac{\partial \theta_{weq}}{\partial t} = C(h_w)\frac{\partial hw}{\partial t} + \left(\frac{\rho_i}{\rho_l} - 1\right)\frac{\partial \theta_i}{\partial t}. \tag{4.7}$$

Following Eq. 4.2, 4.4 and 4.5, θ_i is a function of both unknowns $\theta_i(h_w, T)$ and the term $\frac{\partial \theta_i}{\partial t}$ can be

expanded as follows:

$$\frac{\partial \theta_i}{\partial t} = \frac{\mathrm{d}\theta_i}{\mathrm{d}h_w}\frac{\partial h_w}{\partial t} + \frac{\mathrm{d}\theta_i}{\mathrm{d}T}\frac{\partial T}{\partial t}. \tag{4.8}$$

We can further replace the dependence on h_w with H_w in the time derivative, because $\frac{\partial z}{\partial t} = 0$, and therefore

$$\frac{\partial h_w}{\partial t} = \frac{\partial h_w}{\partial t} + 0 = \frac{\partial h_w}{\partial t} + \frac{\partial z}{\partial t} = \frac{\partial H_w}{\partial t}. \tag{4.9}$$

Equation (4.7) becomes

$$\frac{\partial \theta_{weq}}{\partial t} = \left(C(h_w) + (\frac{\rho_i}{\rho_l} - 1)\frac{\mathrm{d}\theta_i}{\mathrm{d}h_w}\right)\frac{\partial Hw}{\partial t} + \left(\frac{\rho_i}{\rho_l} - 1\right)\frac{\mathrm{d}\theta_i}{\mathrm{d}T}\frac{\partial T}{\partial t}, \tag{4.10}$$

where the total derivative $\frac{\mathrm{d}\theta_i}{\mathrm{d}h_w}$ is

$$\frac{\mathrm{d}\theta_i}{\mathrm{d}h_w} = \frac{\mathrm{d}(\theta_w - \theta_l)}{\mathrm{d}h_w} = \left(C(h_w) - C(h_l)\frac{\mathrm{d}h_l}{\mathrm{d}h_w}\right), \tag{4.11}$$

and where $\frac{\mathrm{d}h_l}{\mathrm{d}h_w} = 1$. It becomes evident that $\frac{\mathrm{d}\theta_i}{\mathrm{d}h_w} = 0$ for temperatures above the freezing point. The total derivative $\frac{\mathrm{d}\theta_i}{\mathrm{d}T}$ is

$$\frac{\mathrm{d}\theta_i}{\mathrm{d}T} = \frac{\mathrm{d}(\theta_w - \theta_l)}{\mathrm{d}T} = -C(h_l)\frac{\mathrm{d}h_l}{\mathrm{d}T}, \tag{4.12}$$

which contains the total differential $\frac{\mathrm{d}h_l}{\mathrm{d}T}$, which is defined such that:

$$\frac{\mathrm{d}h_l}{\mathrm{d}T} = \begin{cases} \frac{Lf}{Tg} & \text{for} \quad T < T_f, \\ 0 & \text{for} \quad T \geq T_f, \end{cases} \tag{4.13}$$

where it becomes evident that we obtain a discontinuity at T_f. This discontinuity is relatively strong (120 m/K, Fig 4.1) and the numerical treatment of this term is discussed in section 4.3.

Following (4.2) we can expand the term ∇h_l as follows:

$$\boldsymbol{\nabla} h_l = \begin{cases} \boldsymbol{\nabla} h_w + \frac{\mathrm{d}h_l}{\mathrm{d}T}\boldsymbol{\nabla} T, & \text{for} \;\; T < T_f, \\ \boldsymbol{\nabla} h_w, & \text{for} \;\; T \geq T_f. \end{cases} \tag{4.14}$$

The right side of the Richards equation dependent on the primarily solved variables can then be expanded as follows:

$$\begin{aligned} -\boldsymbol{\nabla}\cdot\vec{q}_l &= \boldsymbol{\nabla}\cdot K_{lh}\boldsymbol{\nabla}(h_w+z) + \boldsymbol{\nabla}\cdot K_{lh}\frac{\mathrm{d}h_l}{\mathrm{d}T}\boldsymbol{\nabla}T + \boldsymbol{\nabla}\cdot(K_{lT})\,\boldsymbol{\nabla}T \\ &= \boldsymbol{\nabla}\cdot K_{lh}\boldsymbol{\nabla}H_w + \boldsymbol{\nabla}\cdot\left(K_{lh}\frac{\mathrm{d}h_l}{\mathrm{d}T} + K_{lT}\right)\boldsymbol{\nabla}T. \end{aligned} \tag{4.15}$$

Note, that the discontinuity $\frac{\mathrm{d}h_l}{\mathrm{d}T}$ is also present as a constitutive function in the diffusion term.

4.2.3 Heat Transport

The heat equation accounts for diffusion, advection and latent heat of freezing and melting:

$$\frac{\partial C_p T}{\partial t} - Lf\rho_i\frac{\partial\theta_i}{\partial t} = \boldsymbol{\nabla}\cdot\lambda\boldsymbol{\nabla}T - \boldsymbol{\nabla}\cdot C_l\vec{q}_l T, \tag{4.16}$$

where C_p is the heat capacity of the porous medium defined such that,

$$C_p = C_l\theta_l + C_n\theta_n + C_a\theta_a + C_i\theta_i, \tag{4.17}$$

which is the sum of volumetric heat capacities of liquid $C_l\theta_l$, soil matrix $C_n\theta_n$, air $C_a\theta_a$ and ice $C_i\theta_i$ [J m^{-3} K^{-1}], and λ is the heat conductivity [W m^{-1} K^{-1}]. In the following all terms are expanded using the chain rule in respect to H_w [m] or T [K], where $\frac{\partial h_w}{\partial t}$ expanded as $\frac{\partial H_w}{\partial t}$ with the same logic used in Eq. (4.9). $\frac{\partial\theta_i}{\partial t}$ is replaced according to Eq. (4.11) and (4.12).

$$Lf\rho_i\frac{\partial\theta_i}{\partial t} = Lf\rho_i\frac{\mathrm{d}\theta_i}{\mathrm{d}h_w}\frac{\partial H_w}{\partial t} + Lf\rho_i\frac{\mathrm{d}\theta_i}{\mathrm{d}T}\frac{\partial T}{\partial t} \tag{4.18}$$

C_p is a function of T and H_w, we expand the heat capacity term using the product and then the chain rule as follows:

$$\frac{\partial C_p T}{\partial t} = T\frac{\partial C_p}{\partial t} + C_p\frac{\partial T}{\partial t} = T\frac{\mathrm{d}C_p}{\mathrm{d}h_w}\frac{\partial H_w}{\partial t} + T\frac{\mathrm{d}C_p}{\mathrm{d}T}\frac{\partial T}{\partial t} + C_p\frac{\partial T}{\partial t}. \tag{4.19}$$

The soil matrix is independent on h_w, so $\frac{\mathrm{d}C_p}{\mathrm{d}h_w}$ is

$$\begin{aligned} \frac{\mathrm{d}C_p}{\mathrm{d}h_w} &= \frac{\mathrm{d}C_l\theta_l}{\mathrm{d}h_w} + \frac{\mathrm{d}C_i\theta_i}{\mathrm{d}h_w} + \frac{\mathrm{d}C_a(\theta_s-\theta_w)}{\mathrm{d}h_w} \\ &= C_l C(h_l)\frac{\mathrm{d}h_l}{\mathrm{d}h_w} + C_i(C(h_w) - C(h_l)\frac{\mathrm{d}h_l}{\mathrm{d}h_w}) - C_a C(h_w) \\ &= C_l C(h_l) + C_i(C(h_w) - C(h_l)) - C_a C(h_w). \end{aligned} \tag{4.20}$$

The soil matrix is independent on T, so then $\frac{\mathrm{d}Cp}{\mathrm{d}T}$ is

$$\frac{\mathrm{d}C_p}{\mathrm{d}T} = (C_l - C_i)C(h_l)\frac{\mathrm{d}h_l}{\mathrm{d}T}. \tag{4.21}$$

where the discontinuous term $\frac{\mathrm{d}h_l}{\mathrm{d}T}$ is also present.

The advection term is

$$\boldsymbol{\nabla} \cdot C_l \vec{q}_l T = C_l \vec{q}l \boldsymbol{\nabla} T + C_l T \boldsymbol{\nabla} \cdot \vec{q}l, \tag{4.22}$$

where$\boldsymbol{\nabla} \cdot \vec{q}_l$ is the right side of the Richards equation, and thus also discontinuous due to $\frac{\mathrm{d}h_l}{\mathrm{d}T}$ with

$$-C_l T \boldsymbol{\nabla} \cdot \vec{q}l = C_l T \boldsymbol{\nabla} \cdot K_{lh} \boldsymbol{\nabla} H_w + C_l T (\boldsymbol{\nabla} \cdot K_{lh} \frac{\mathrm{d}h_l}{\mathrm{d}T} + \boldsymbol{\nabla} \cdot K_{lT}) \boldsymbol{\nabla} T, \tag{4.23}$$

As shown above, the heat transport equation is also affected by the strongly discontinuous term $\frac{\mathrm{d}h_l}{\mathrm{d}T}$ as defined in (4.13), exacerbating the need to provide an efficient and reliable computational procedure.

4.2.4 Soil hydraulic and thermal properties

To describe the water retention curve, we use the commonly used parameterization of Genuchten (1980) and Mualem (1976), where the retention curve is

$$\theta(h) = \theta_r + (\theta_s - \theta_r)\left[1 + (-\alpha h_l)^n\right]^{-m} \text{ for } h \leq 0. \tag{4.24}$$

The hydraulic conductivity function (Genuchten 1980; Mualem 1976) is commonly expressed as

$$K_{lh,u} = K_s \cdot S^{1/2}[1 - (1 - S^{1/m})^m]^2, \tag{4.25}$$

where S is effective saturation defined as follows:

$$S = \frac{\theta(h_l) - \theta_r}{\theta_s - \theta_r}(1 + (-\alpha h_l)^n)^{-m} \text{ for } h \leq 0, \tag{4.26}$$

where θ_s is the saturated water content [-], θ_r is the residual water content [-], α is related to the inverse of the air entry value [m^{-1}] and n and m are shape parameters determining the pore size distribution with m usually defined as $m = 1 - \frac{1}{n}$[-]. When the soil is frozen, it has been reported that the resistance to flow is dramatically increased, which lead to the development of a reduced hydraulic conductivity as described in

Harlan (1973), which is commonly dependent on an empirical impedance factor Ω [-] and thermal quality α_{th} [-] Lundin (1990):

$$K_{lh} = 10^{-\Omega\alpha_{th}} K_{lh,u}, \tag{4.27}$$

where α_{th} is a multiplier consisting of either ice content or a ratio of ice content θ_i and total water content. Here, we use the following after (Hansson et al. 2004):

$$\alpha_{th} = \frac{\theta_i}{\theta_i + \theta_l - \theta_r}. \tag{4.28}$$

The hydraulic conductivity K_{lT} due to a gradient in temperature T is defined as Hansson et al. (2004):

$$K_{lT} = K_{lh,u} h_l G_{wT} \frac{1}{\gamma_0} \frac{\mathrm{d}\gamma}{\mathrm{d}T}, \tag{4.29}$$

where G_{wT} is gain factor which quantifies the temperature dependence of the soil water retention curve (Saito et al. 2006) [-],γ is the surface tension of soil water [kg s^{-2}] and $\gamma_0(25°\mathrm{C}) = 71.89$ g s^{-1}.

The apparent thermal conductivity combines the thermal conductivity λ_0 and macrodispersivity, which is a linear function of velocity:

$$\lambda = \lambda_0 + \beta C_l |q_l|, \tag{4.30}$$

where β is the thermal dispersivity [m]. For the thermal conductivity, we implemented an extension of Campbell (1985) model according to Hansson et al. (2004). Hansson et al. (2004) expanded Campbell (1985) expression of λ_0 to account for higher heat conduction of ice as follows:

$$\lambda_0 = C1 + C2(\theta_l + F\theta_i) - (C1 - C4) \exp\left(-[C3(\theta_l + F\theta_i)]^{C5}\right), \tag{4.31}$$

where Ci $(i = 1, ...5)$ are constants that can either be measured experimentally or derived from material properties, Campbell (1985) suggested $C5 = 4$ with F accounting for the difference in thermal conductivities of ice and water such that

$$F = 1 + F1\theta_i^{F2}. \tag{4.32}$$

4.2.5 Model assumptions

The following assumptions are made in the development of this model and the use of soil hydraulic and thermal properties:

- The solid and liquid phases are in thermal equilibrium
- Water freezes instantaneously, and ice melts instantaneously within a given time step (numerically).
- A total pressure head can be used to include both liquid and ice content. Volumetric liquid and volumetric ice content can be calculated with the retention curve.
- A freezing point depression can be neglected and a constant freezing temperature of 0 °C can be assumed.
- Regularization if used appropriately does not affect the physics.
- Water redistributes according to gravity, capillary action and temperature.
- The freezing curve can be used to derive retention curve properties following cryo-scution of the Clausius-Clapeyron equation.
- The solid matrix is immobile.
- Vapor flow can be neglected as sublimation is not considered a dominant process in the simulated experiments.
- The effect of hysteresis can be neglected for the examples.

4.3 Regularization

To understand the extent of the discontinuity, here is a summary of the system of equations governing the water and heat flow considering freezing, fully expanded with the discontinuity in red:

$$\left(C(h_w)+(\frac{\rho_i}{\rho_l}-1)(C(h_w)-C(h_l))\right)\frac{\partial H_w}{\partial t}-\left(\frac{\rho_i}{\rho_l}-1\right)C(h_l)\boxed{\frac{\mathrm{d}h_l}{\mathrm{d}T}}\frac{\partial T}{\partial t}=$$
$$\boldsymbol{\nabla}\cdot K_{lh}\boldsymbol{\nabla}H_w+\boldsymbol{\nabla}\cdot\left(K_{lh}\boxed{\frac{\mathrm{d}h_l}{\mathrm{d}T}}+K_{lT}\right)\boldsymbol{\nabla}T,$$

$$\left(T\left(C_lC(h_l)+C_i(C(h_w)-C(h_l))-C_aC(h_w)\right)-\left(C(h_w)-C(h_l)\right)Lf\rho_i\right)\frac{\partial H_w}{\partial t} \tag{4.33}$$
$$+\left(Cp+T(C_l-C_i)C(h_l)\boxed{\frac{\mathrm{d}h_l}{\mathrm{d}T}}+C(h_l)\boxed{\frac{\mathrm{d}h_l}{\mathrm{d}T}}Lf\rho_i\right)\frac{\partial T}{\partial t}=$$
$$\boldsymbol{\nabla}\cdot\lambda\boldsymbol{\nabla}T-C_l\vec{q}_l\boldsymbol{\nabla}T+C_lT\boldsymbol{\nabla}\cdot\left(K_{lh}\boxed{\frac{\mathrm{d}h_l}{\mathrm{d}T}}+K_{lT}\right)\boldsymbol{\nabla}T+C_lT\boldsymbol{\nabla}\cdot K_{lh}\boldsymbol{\nabla}H_w.$$

The discontinuity of $\frac{\mathrm{d}h_l}{\mathrm{d}T}$ (4.13) is depicted in Fig 4.1 a. The discontinuity can be smoothed over using a regularization factor with a continuous scaling function. In this contribution, part of the sine function was selected to create a continuous function. The regularization value is dependent on the freezing intensity of the system and a user-defined regularization temperature T_r. The closer T_r is to to the T_f the steeper the regularization curve:

$$\bar{\Phi}r=\begin{cases}\frac{sin(\frac{T_r-T}{T-T_f}\Pi+\frac{\Pi}{2})}{2}+0.5, & \text{for} \quad T_r\leq T\leq T_f,\\ 1, & \text{for} \quad T<T_r.\end{cases} \tag{4.34}$$

Although it is common to handle discontinuities with approximations from both sides, this is not the case here to avoid freezing above the freezing temperature and to avoid residual jumps at T_f. Our approximation decreases the freezing rate near the freezing temperature. With this, we obtain a regularized term defined as:

$$\frac{\mathrm{d}h_l}{\mathrm{d}T}=\begin{cases}\bar{\Phi}r\cdot\frac{Lf}{Tg}, & \text{for} \quad T<T_f,\\ 0, & \text{for} \quad T\geq T_f.\end{cases} \tag{4.35}$$

Function $\bar{\Phi}r$ is the regularizing term. With a proper setup of T_r, it can deliver computational reliability to the discontinuous model. For the selection of an optimal regularization parameter, we propose comparison

of parameters to a proxy for oscillation and a proxy for the steepness of the freezing front.

This regularized model was implemented into the open-source code DRUtES (www.drutes.org). More details on the implementation are in Appendix B.

4.4 Model validation: Freezing columns experiments

4.4.1 Laboratory Column Experiments and Model Setup

We simulate freezing soil column experiments conducted by Jame (1977) and Jame and Norum (1980) and Mizoguchi (1990), which have been widely used to verify and compare models (e.g Hansson et al. 2004; Daanen and Nieber 2009; Dall'Amico et al. 2011; Painter 2011; Peng et al. 2016).

Mizoguchi (1990) used four identically packed Kangawa sandy loam cylinders, which were 20 cm in length and 8 cm in diameter. These four columns contained the same initial water content of 0.33-0.35 [m^3 m^{-3}]. The columns were thermally insulated and cooled to a temperature of 6.7 °C. The first cylinder was used for the initial conditions, whereas the top of the three other cylinders were exposed to a circulating cooling fluid of -6 °C to obtain water content after 12 h, 24 h and 50 h, respectively. To obtain the water content, each soil column was sliced in 1 cm thickness and oven-dried. The volumetric water content data thus represent 1 cm averaged values in liquid water equivalent. The soil hydraulic and soil thermal properties for the Mizoguchi (1990) experiment were fitted by Hansson et al. (2004) using Hydrus-1D (Tab. 4.1). However, many reproductions of this experiment use different values for the impedance term Ω, the relation of n and m of the soil hydraulic properties, different soil thermal property descriptions and boundary conditions. We found a better agreement with a higher heat transfer coefficient (Tab. 4.1).

Jame (1977) investigated the effect of initial water content and temperature gradient on the freezing behaviour. Meshed silica flour in 30 cm soil tubes of 10 cm diameter were used. The columns were thermally insulated with rock wool and Styrofoam. The temperature was measured by 12 pre-installed thermocouples and the water content was measured by gamma-ray attenuation, which cannot distinguish between frozen and unfrozen water. Whereas Mizoguchi (1990) columns were upright, Jame (1977) columns were horizontal. We use experiments 8, 9 used in Peng et al. (2016) and 13 (test 1 in Jame and Norum (1980)) in this contribution. For experiments 8 and 9, the columns were cooled to 5 °C and one end was further cooled to -6 °C. For experiment 13, the column was cooled to 20 °C and one end was further cooled to -10 °C thereby creating a relatively strong temperature gradient. The initial water content of experiments 8 and 13 was 0.2 [m^3 m^{-3}] and for experiment 9 the initial water content was 0.134 [m^3 m^{-3}].

The same hydraulic and thermal properties were used to reproduce the three experiments (Tab. 4.1). The soil hydraulic properties were fitted to a soil freezing curve Jame and Norum (1980) (Fig. B.1 a). The thermal conductivity (unfrozen) was fitted to data provided in Jame and Norum (1980) to the Campbell (1985) model (Fig. B.1 b). We obtained parameters F1 and F2 for the extended Campbell model (Hansson et al. 2004) from calibrating the model manually. The saturated hydraulic conductivity and impedance factor were manually calibrated to match the experiments, all other data was independently fitted. All observations were digitized using the software Engauge digitizer. Water content was only reported in % dry weight and recalculated to volumetric water content for further comparison.

For the cold end, the boundary condition was defined by a flux or Neumann type as follows

$$q_n = h_c(T_c - T_{end}), \tag{4.36}$$

where h_c [W m^{-2} K^{-1}] is a heat transfer coefficient, T_c is the temperature of the coolant and T_{end} is the temperature of the respective end of the system under cooling. The same h_c value was used for all three Jame experiments. To model the heat leak reported in Hansson et al. (2004), a similar boundary condition was used for the warm end for the Mizoguchi experiment:

$$q_n = h_{lab}(T_{lab} - T_{bot}), \tag{4.37}$$

where h_{lab} [W m^{-2} $^{-1}$] is the heat transfer coefficient, T_{lab} is the lab temperature of 6.7 °C and T_{bot} is the temperature of the soil column at the bottom. The numerical setup is briefly described in Tab. 4.2. Note, that the regularization parameters are not the same across the Jame experiments. This is because the regularization is dependent on the problem to be modelled and not the soil itself, as it is not a soil hydraulic property.

4.4.2 Effect of regularization on freezing column experiments

The effect of the regularization on freezing column experiments conducted by Mizoguchi (1990) and Jame and Norum (1980) is depicted in Fig. 4.1. In these experiments one side of an unfrozen column is cooled, which induces freezing. As the cooling continues, a freezing front propagates through the soil column. Fig. 4.1 shows the distribution of h_w after 24 h. The decrease in liquid water causes a water flux towards the freezing front, which in turn causes a difference in h_w. We integrated the difference between the unregularized $\frac{\mathrm{d}h_l}{\mathrm{d}T}$ and the regularized $\frac{\mathrm{d}h_l}{\mathrm{d}T}$ as a proxy for regularization intensity (Int_R),

Table 4.1: Hydraulic and thermal parameter values used in the numerical simulation for model verification.

Parameter	Mizoguchi	Jame
θ_r	0.05	0.02
θ_s	0.535	0.49
K_s (m s^{-1})	$3.2 \cdot 10^{-6}$	$1 \cdot 10^{-6}$
α (m^{-1})	1.11	0.115
n	1.48	2.3
ω	5	1.5
ρ_d (g cm^{-3})	-	1.33
Cs (J kg^{-1} K^{-1})	840	839
$C1$ (W m^{-1} K^{-1})	0.55	0.85
$C2$ (W m^{-1} K^{-1})	0.80	3.7
$C3$	3.07	50
$C4$ (W m^{-1} K^{-1})	0.13	0.24
$C5$	4.00	4.00
$F1$	13.05	20
$F2$	1.06	2.43
h_c (W m^{-2} K-1)	90	350
h_l (W m^{-2} K-1)	30	-

Table 4.2: Numerical setup used in the numerical simulation for model verification.

	Parameter	Mizoguchi	Jame		
			8	9	13
Regularization	T_r (K)	272.67	272.83	272.99	272.83
Space discretization	L (m)	0.2		0.3	
	dx (m)	0.001		0.005	
Time discretization	t (s)	180000		259200	
	dt_{min} (s)	1		1	
	dt_{max} (s)	200		200	
Picard method	iteration criterion	1×10^{-2}		1×10^{-2}	
	max. iterations	10		10	

where larger values indicate greater regularization. We used the number of gradient sign changes as a proxy for oscillation, where a high number of sign changes indicates oscillation. Note, that the example in Fig 4.1 shows an extreme case of regularization to visualize the integral difference. We compared the intensity of regularization with this proxy for oscillation and the maximum gradient of $\frac{\mathrm{d}h_w}{\mathrm{d}z}$. Fig. 4.1 indicates that the number of sign changes is significantly reduced with increasing regularization. Similarly, the steepness at the freezing front is also reduced. Red is not regularized and results in oscillations. Dark blue is over-regularized and resulted in a reduced maximum gradient, because the cryosuction is reduced too intensely, which causes a markedly different distribution in pressure head. Teal is optimal, as the gradient at the freezing front is maintained without oscillations. The teal parameter set results in similar

simulation as red, however without causing oscillations. Note that the optimal regularization is quite low with a T_r of -0.15-0.3 °C. The advantage of the regularization term is that it can be easily included into any code. Furthermore, the regularization can be adapted to suit different freezing problems that may need stricter or looser regularization. In theory, it could also be easily applied to other discontinuities for a given solution variable p, where T_f should be replaced by the position of the discontinuity, and T by the parameter p. A challenge with this approach is choosing sensible parameters. We recommend setting the terms so the effect of the regularization becomes as great as necessary, but as small as possible. This means that an optimal regularization setup is such that the change in the gradient sign of $\frac{\mathrm{d}h_w}{\mathrm{d}z}$ is significantly reduced (no oscillations) without significant reduction in the solution gradient $\frac{\mathrm{d}h_w}{\mathrm{d}z}$ at the freezing front. This is because the treatment was introduced as a numerical strategy and should not be considered as a constitutive function. A problem can be *overregularized* as seen in the example for the blue set. In that example, we can see that the solution can change dramatically even though the soil hydraulic and thermal properties, and initial and boundary conditions have not changed. Therefore, we would not recommend fitting T_r together with other parameters defining soil hydraulic or thermal properties. Alternatively, if the user wishes to accept the discontinuity, more complex finite methods which can represent the discontinuity must be used. Examples include the work of Arzanfudi and Al-Khoury (2018), who implemented an extended finite element solution for soil freezing and thawing.

4.4.3 Comparison of Simulation Results to Experiments

The redistribution of water towards the cold end can be clearly seen in Fig. 4.2 for the Mizoguchi experiment and in Fig. 4.3 for the three Jame experiments and simulations. A steep drop in water content can be identified at the freezing front. This effect can be explained through the strong reduction of the liquid pressure head when freezing starts. This creates a strong gradient in h_l, which induces liquid water flow towards the freezing front. Over the course of the experiment, the freezing front propagates more slowly as the temperature distribution reaches steady state and water accumulates at the front until the gradient in H_l becomes zero. In the Jame experiments, the difference in initial condition and temperature gradient produces different water content distributions. For the Jame experiments, given that the only difference among the simulations is the temperature of the cool end and the laboratory temperature, the model predicts the volumetric water content and temperature distribution well. We do note, that the simulations predict higher water contents near the cool end compared to the experiments. This effect is less pronounced for the Mizoguchi experiment, because the water content was averaged over 1 cm slices

to match the experimental data. The overestimation near the cool end is greatest for the experiment with the largest freezing intensity and temperature gradient (Jame experiment 13). This experiment was also the most difficult to simulate and required the strongest regularization.

In experiments with lower water content (Jame 9) or steep temperature gradients (Jame 13), water accumulates at the freezing front causing the freezing front to grow over time and resulting in a U shape, whereas experiments with higher initial water and a moderate temperature gradient (Mizoguchi and Jame 8) produce an almost constant water distribution between the cool end and the freezing front. How far the freezing front propagates, how the water redistributes and whether water accumulates near the cool end or at the propagating freezing front, depends on the initial water content as well as the freezing intensity of the system, because they change the hydraulic conductivity as well as the available mobile water. In the model, the hydraulic conductivity is a result of both the unfrozen hydraulic conductivity and the impedance factor. We note that it was difficult to reproduce all Jame experiments equally with a single set of soil hydraulic properties. One potential issue may be that the soil hydraulic properties were derived from the soil-freezing curve. Kurylyk and Watanabe (2013) suggested that additional adjustment parameters may be necessary to scale hydraulic retention properties from soil freezing curves to account for different interface energies.

Similar to our results, Jame and Norum (1980), Hansson et al. (2004), Daanen and Nieber (2009), Painter (2011), and Karra et al. (2014) reported an overestimation of the water content near the cold end for both the Mizoguchi and Jame experiments. Painter (2011) suggested that this is indicative of a missing process not commonly included in models. One possibility is the existence of a thermodynamic non-equilibrium between the ice and water phase in the freezing process. This has been explored by Peng et al. (2016). In their work, the non-equilibrium approach delays the freezing by reducing the freezing rate and therefore the cryosuction is less pronounced and the liquid flux towards the cold end is reduced. Kurylyk and Watanabe (2013) suggest that this disequilibrium should not be neglected if the rate of temperature change exceeds 0.1 °C h^{-1} in the range of 0 to -0.5 °C. Note, that despite the consideration of non-equilibrium, Peng et al. (2016) also overestimate the water towards the cool end somewhat.

We note that a stronger regularization could have decreased the overestimation for Jame experiment 13. However, we chose the regularization parameter to handle oscillatory behavior, while affecting the actual shape of the solution as little as possible. This is because the regularization should be a numerical tool, and should not be seen as an additional constitutive function that should be used for curve fitting. Note, we assume that the temperature of the water, ice, air and soil are equal. For the test cases this is

an appropriate assumption. However, local thermal non-equilibrium (Heinze and Blöcher 2019) may have to be considered when water enters the medium and infiltrates the soil.

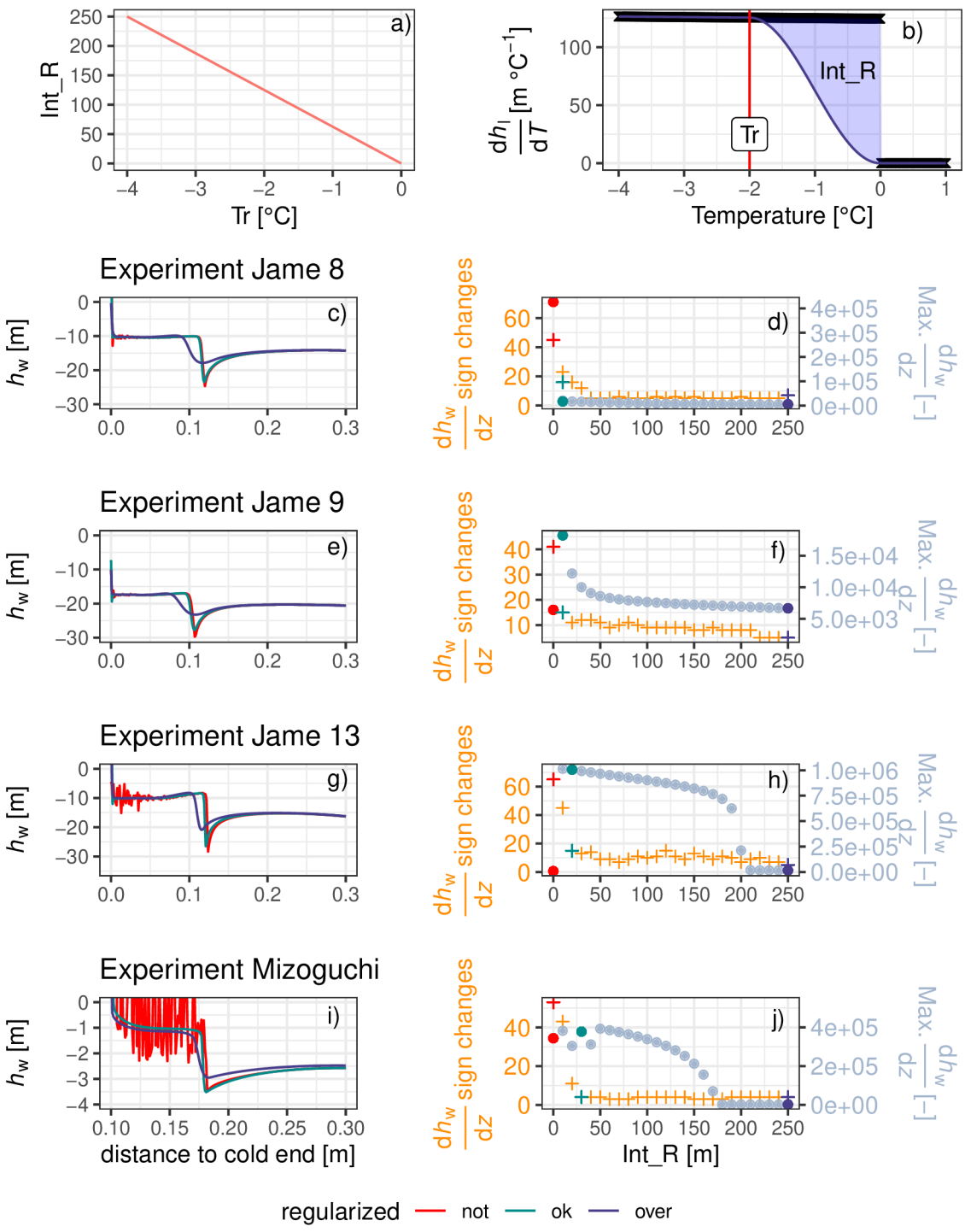

Figure 4.1: a: Int_R calculated for a range of regularization temperatures T_r [K] b: Discontinuous $\frac{\mathrm{d}h_l}{\mathrm{d}T}$ (4.13) and Int_R $= \int_{-\infty}^{T_f} (\frac{\mathrm{d}h_l}{\mathrm{d}T} - R)\mathrm{d}T$ where R is the regularization. c, e, g, i: Effect of regularization on h_w after 24 h. d, f, h, j: sign changes (+) of and max. (o) $\frac{dh_w}{\mathrm{d}z}$ over Int_R .

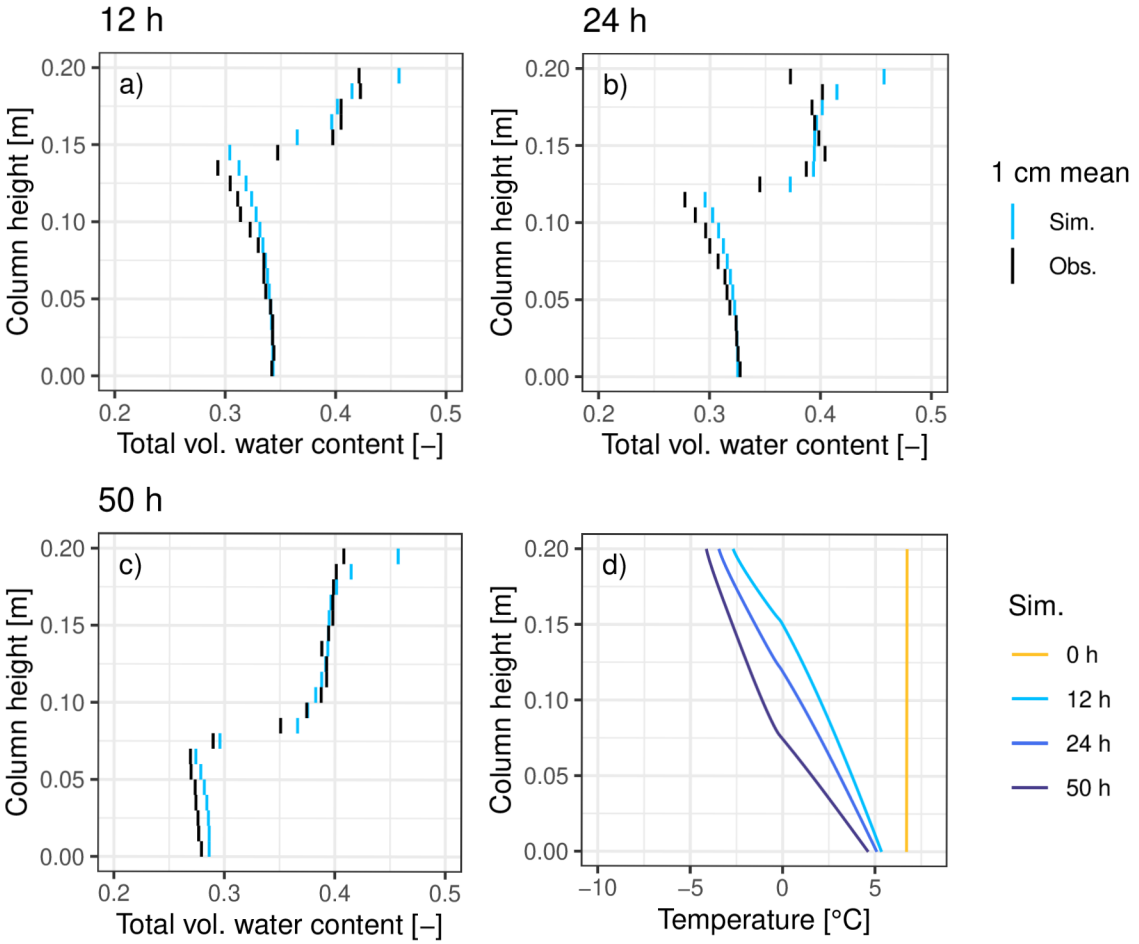

Figure 4.2: Observations and simulations of the total (ice + liquid) volumetric water content (in liquid water equivalent) after a) 12 h, b) 24 h and c) 50 h, and d) simulated temperatures for the Mizoguchi experiment (Mizoguchi 1990; Hansson et al. 2004). The simulated values of the volumetric water content were averaged over 1 cm.

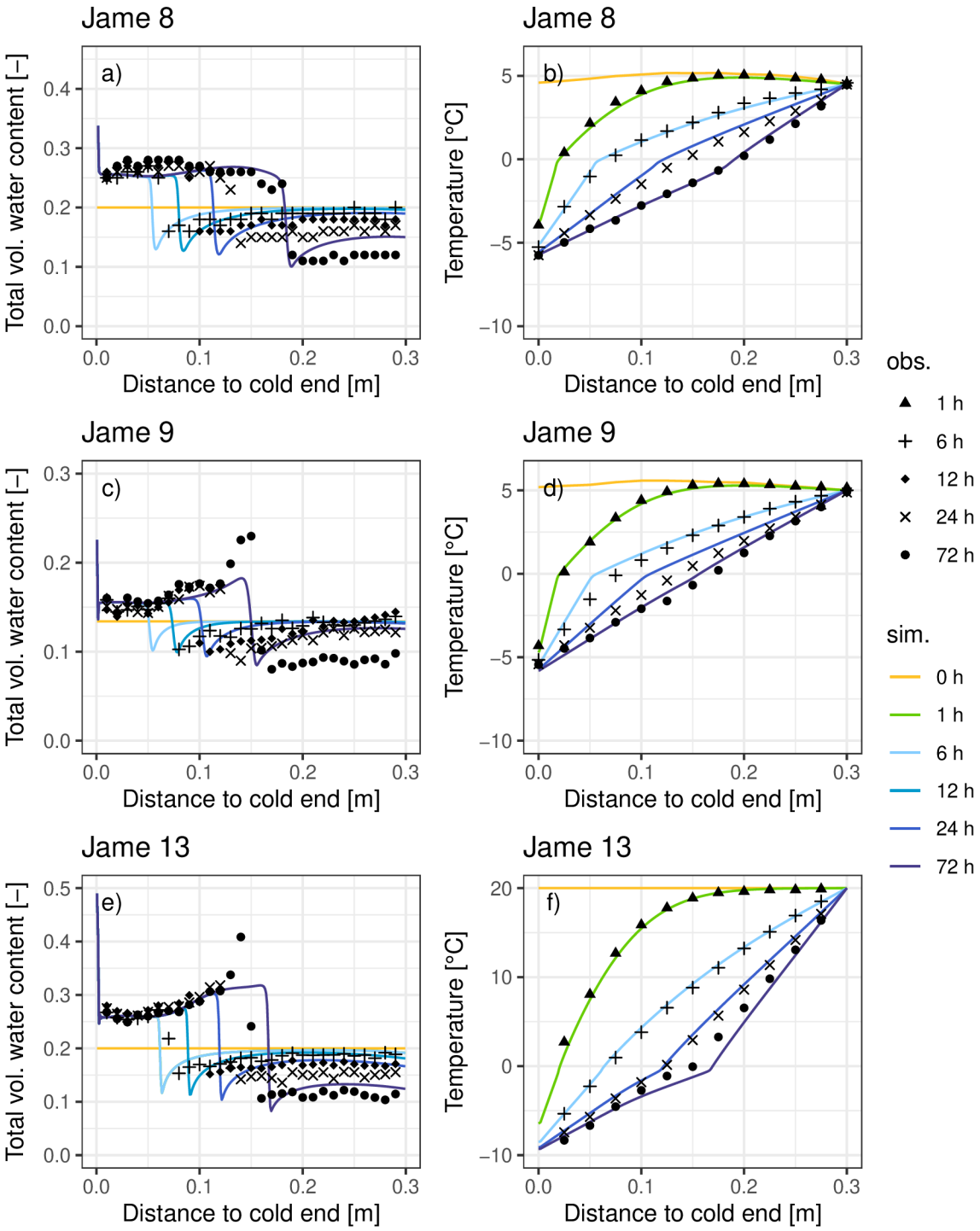

Figure 4.3: Observations and simulations of the total (ice + liquid) volumetric water content and temperature distribution for Jame experiment 8, experiment 9 and experiment 13 (Jame 1977).

4.5 Model validation: Freezing curtain

The freezing curtain or zero-curtain effect occurs in freezing or melting soil due to the consumption or release of heat due to phase change. This effect is often called the zero-curtain effect, because as long as freezing or melting occurs the temperature will remain around 0 °C. To study this effect several synthetic examples were setup, some of which are comparable to those in Dall'Amico et al. (2011).

4.5.1 Model Setup

In the first set of experiments, a 20 cm frozen soil column is warmed at the top to induce melt. Zero flux Neumann boundaries are set for the water flow and the bottom of the heat flow equation. The melting at the top boundary is simulated using a 50 W m^{-2} flux condition. Three experiments with different initial water content were conducted to observe water content dependent effects. The soil hydraulic and thermal properties used are that of the Mizoguchi experiment, which can be found in Tab. 4.1. For the second set of experiments, water ponding of 1 mm was simulated by applying a Dirichlet boundary condition at the top boundary for the water flow equation.

4.5.2 Simulation results and discussion

In the first set of synthetic experiments, melt was simulated without additional rain. Fig. 4.4 shows the surface pressure head corresponding to the liquid water (h_l) (top) and temperature (bottom) of the three experiments for three regularization setups, where $T_r = 273.15$ K is unregularized, and $T_r = 272.15$ K represents the strongest regularization of the three. Unregularized ($T_r = 273.15$ K) simulations only give satisfactory results for experiment 1, where the initial ice content was only about 0.04 [-]. It is evident that the duration of melt is dependent on the initial ice content. In the third experiment, the most ice was present and the regularization required is the strongest. Interestingly, lack of regularization does not only lead to oscillations and unphysical jumps, but also very different temperature and pressure head

Table 4.3: Model setup for melt and infiltration experiments

Experiment		1	2	3
T_{init}	[K]	263.15	263.15	263.15
$\theta_{tot,init}$	[-]	0.1	0.2	0.3
$\theta_{i,init}$	[-]	0.4	0.14	0.24
$\theta_{l,init}$	[-]	0.06	0.06	0.06
Simulation time	[d]	14	14	14

profiles. This is because even slight oscillations in the temperature near the freezing temperature causes h_l to change dramatically. This will also cause oscillatory behavior in the calculated ice and liquid water contents, which in turn creates oscillations in the release and consumption of latent heat. The temperature in the first experiment increases the most as least energy has to be invested into phase transition. No significant curtain effect is evident at the surface, as the ice content at the surface melts rapidly. Fig. 4.5 shows the effect of initial water content for adequately regularized experiments on the freezing curtain effect. The results are shown for temperature, liquid water content and ice content at the surface, at 1 cm deep, at 10 cm deep and at 20 cm deep. As expected, the third experiment with the most ice content shows the longest duration of a freezing curtain. The effect is strongest at 20 cm, as water melted from the top infiltrates downwards, refreezes and then melts. The consumption of latent heat time taken to melt are therefore largest. Note, that the movement of water is due to the liquid pressure head and gravity. The gradient in liquid pressure head becomes much stronger. One interesting effect can be observed at 20 cm, where a peak can be observed in the liquid water content. This is because liquid water accumulates at the bottom, and simultaneously ice melts. This causes the gradient in total head to reverse so that water moves upward again. Additionally, we can see in the third experiment, how melt water infiltrates into the colder soil where it refreezes, causing a peak in ice content. This shows that the model adequately recreates common features associated with freezing soil.

Fig. 4.6 depicts melt experiments with additional ponding. Here, much stronger regularization was necessary to obtain oscillation free simulations. Again, the experiment 3 required strongest regularization. In the ponding experiments, water infiltrates the soil, and refreezing of the water occurs. The temperature in experiment 1 rises faster in the beginning, because less of the initial ice content melts, which would mitigate the temperature increase. Note, that the freezing curtain does not actually occur exactly at 273.15 K (0 °C), as under current model assumptions ice can melt at sub-zero temperatures. Because the temperature decreases h_l, it follows that how melt occurs is dependent on the retention curve of a given soil. For most soils, most phase change will still occur between 272.15-273.15 K.

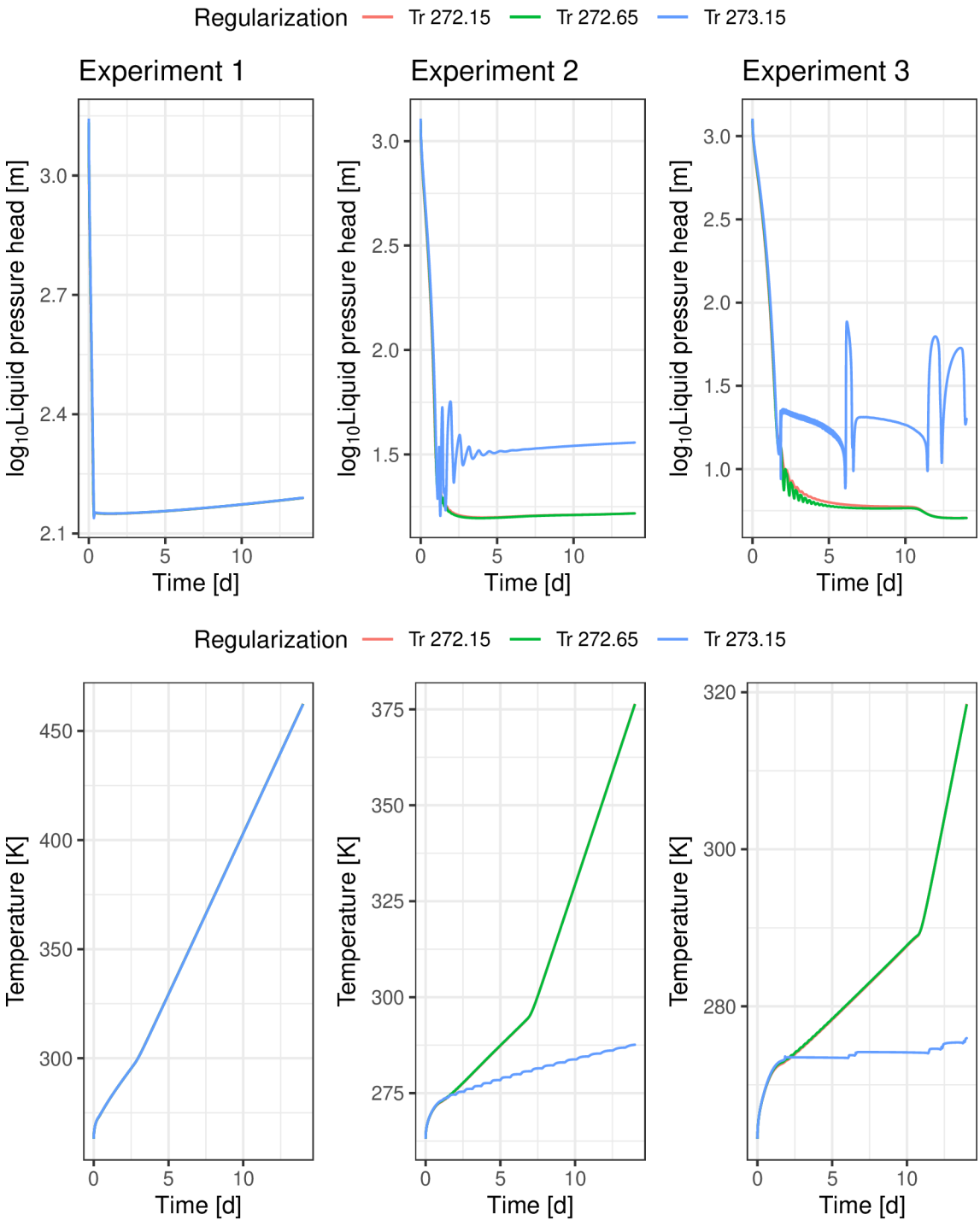

Figure 4.4: Effect of regularization on melt experiments on the surface pressure head and temperature.

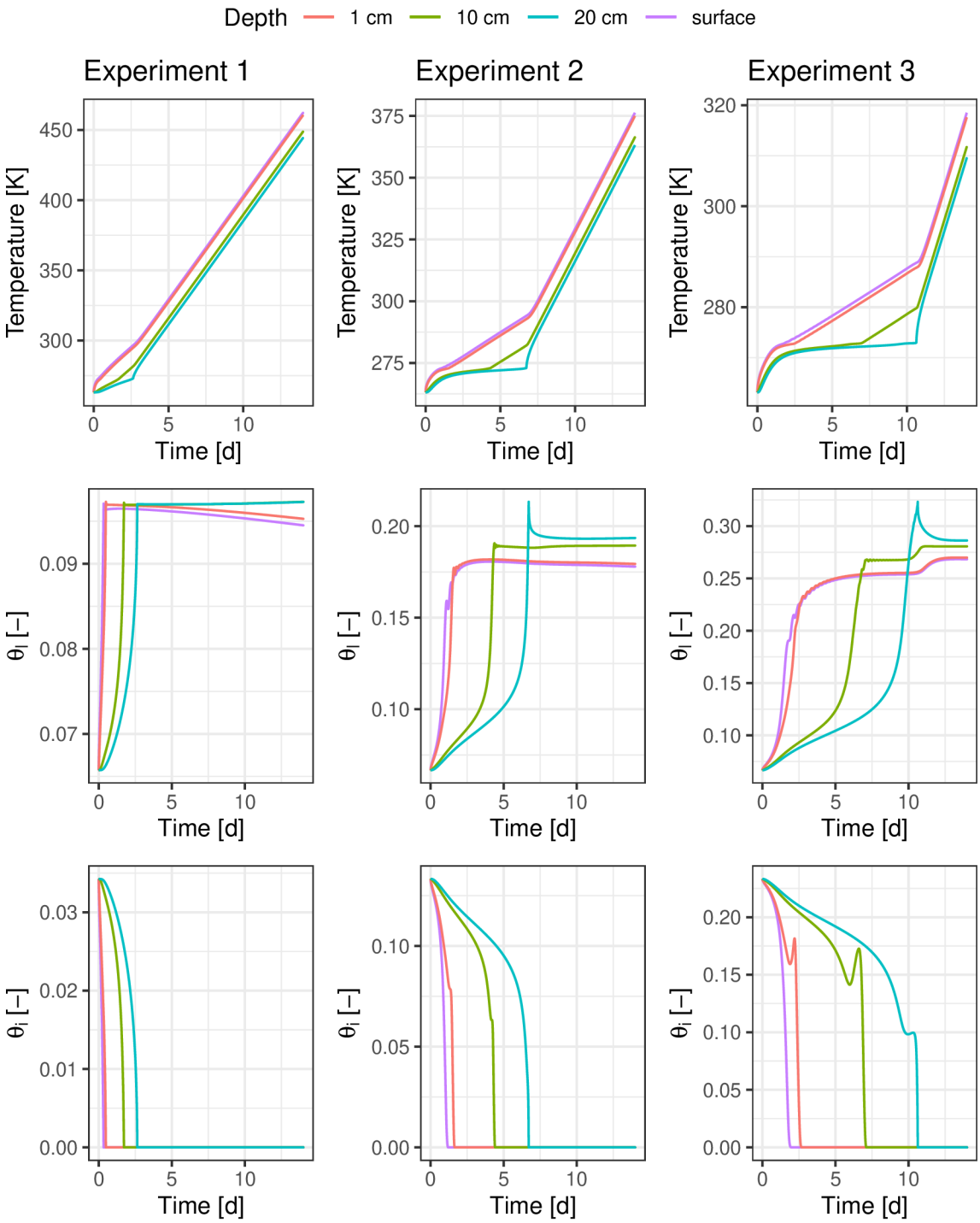

Figure 4.5: Effect of initial water content on the freezing curtain effect for melt experiments.

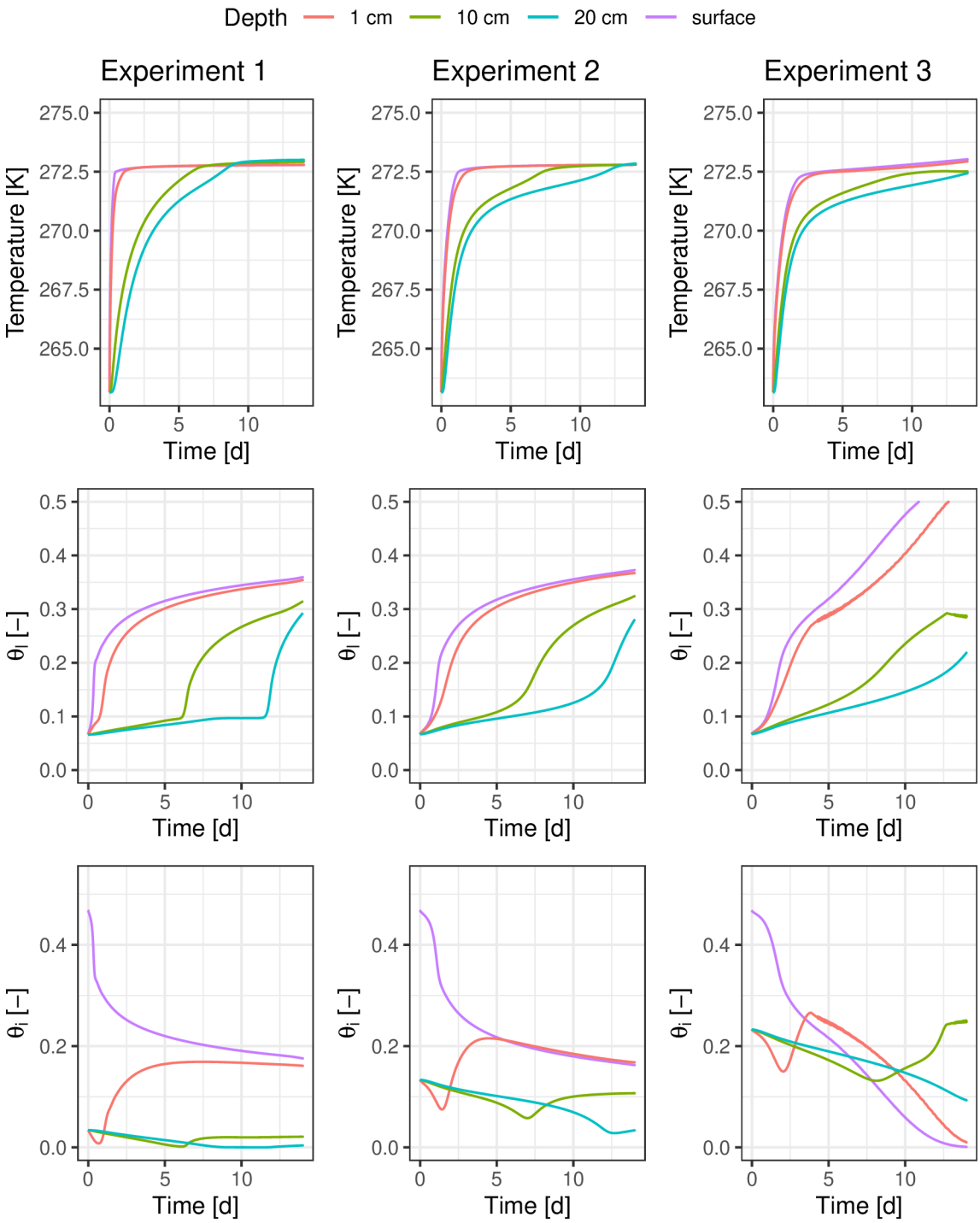

Figure 4.6: Effect of initial water content on the freezing curtain effect for melt experiments with ponding.

4.6 Conclusion

In this contribution, we show that regularization is a relatively simple tool to deal with oscillations when simulating freezing soils. We used a one-parametric regularization approach using a section of the sine function that can be used for a wide range of freezing examples and synthetic melt examples. The regularization temperature governing the regularization should be chosen carefully to avoid over-regularising the problem. We recommend testing several regularization sets while plotting the maximum gradient of $\frac{\mathrm{d}h_w}{\mathrm{d}z}$ and the number of sign changes of $\frac{\mathrm{d}h_w}{\mathrm{d}z}$. Although in the presented examples the regularization temperatures were similar, different regularization may be necessary for different problem setups particularly with stronger freezing and with water content closer to saturation.

We tested our model on freezing column experiments commonly used in model verification with most soil hydraulic and soil thermal properties derived from secondary information and not the experiments themselves. We particularly recommend testing models on the range of experiments provided in Jame (1977), where temperature, water content and soil hydraulic and thermal properties data are available.

As with other implementations, we also report an overestimation of the water content near the freezing front, which is greatest for experiments with larger temperature gradients. The mathematical formulation based on the Clausius-Clapeyron equation results in a strong flux towards the freezing front. The non-equilibrium assumption presented in Peng et al. (2016) and briefly discussed in Kurylyk and Watanabe (2013) should be explored further to determine when equilibrium between the ice and water phase does not hold true and what parameterization can effectively describe this assumption.

Chapter 5

Considering non-equilibrium between the liquid water and ice phase in soil-freezing

5.1 Introduction

Freezing soil column tests are a popular method to validate numerical model implementations. In these experiments, a soil column is cooled below freezing using a cooling agent, which induces a freezing front, while the column itself is sealed. The movement of water is thereby induced by the process of freezing. Most models are able to recreate the temperature distribution as well as the propagation of the freezing front. Freezing column experiments result in various water content distributions, where water is moving towards the cool-end due to cryosuction. The greatest mismatch between most models and these freezing column experiments is the overestimation of the water content near the cool end (Jame and Norum 1980; Hansson et al. 2004; Daanen and Nieber 2009; Painter 2011; Karra et al. 2014). This indicates that the cryosuction, which causes the water to move towards the freezing front is overestimated. Painter (2011) suggested that this is indicative of a missing process not commonly included in models. The Clausius-Clapeyron equation assumes instantaneous freezing and instant equilibrium between the ice-water interface. Research suggested that this equilibrium assumption may not always be valid. One possibility is the existence of a thermodynamic non-equilibrium between the ice and water phase in the freezing process. This has been explored by Peng et al. (2016). In their work, the non-equilibrium approach delays the freezing by reducing the freezing rate and thereby the cryosuction is less pronounced and the liquid flux towards the cold end is reduced. Kurylyk and Watanabe (2013) suggests that this disequilibrium should not be neglected if the rate of temperature change exceeds 0.1 °C h^{-1} in the range of 0 to -0.5 °C. Liu et al. (2012) suggested that

for rapid transient transport processes one needs to be careful in applying the Clausius-Clapeyron equation to every point. Spaans and Baker (1996) suggested that the thermodynamic equilibrium assumption of the Clausius-Clapeyron equation may never be reached, or may take a very long time to establish. Peng et al. (2016) concluded that the Clausius-Clapeyron equation may not sufficiently describe the ice-water interfaces in freezing soils, because the Clausius-Clapeyron equation was derived from a "static" ice-water interface. This contradicts the continuous and significant water redistribution found in freezing soils, and because the freezing rate of water is limited, which means time is required for the ice-water interface to reach thermal equilibrium from a prefreezing status, during which the transient process is likely to be in a state of non-equilibrium.

Despite the importance of non-equilibrium, model implementations are scarce and none are open-source. To the best of our knowledge the only contribution was in Peng et al. (2016), who performed limited validation on freezing column examples without considering melting. This becomes further evident as their freezing rate formulation has serious short-comings when considering melt. Therefore, a new one-dimensional numeric model was developed that deals with coupled water and heat transport in partially frozen soils assuming that the ice-water interfaces in freezing soil are not necessarily defined by equilibrium. This model was evaluated using experimental laboratory column freezing experiments and synthetic infiltration experiments that cover both freezing and melting.

5.2 Coupled water and heat flow with freezing rate

In this section, we derive a set of partial differential equations that govern the liquid water flow, heat flow and the freezing rate. In this approach the liquid and ice water are not in phase-equilibrium and the change of ice is explicitly modelled in a separate PDE. We first derive a parameterization for the freezing rate, followed by the coupled system of equations.

5.2.1 Freezing rate

The change of the ice content is assumed to depend on the freezing rate v_f

$$\frac{\partial \theta_i}{\partial t} = v_f \tag{5.1}$$

Peng et al. (2016) developed a parameterization of v_f considering that according to Voytkovskiy and Golubev (1973) the freezing rate of water is proportional to the cubic root of the extent of supercooling.

The freezing rate decreases and becomes zero when the ice-water interface reaches equilibrium:

$$v_f = \begin{cases} \beta(\theta_l - \theta_{l,cl})(T_f - T)^{1/3} & \text{for} \quad T < T_f, \\ 0 \quad \text{for} \quad T \geq T_f, \end{cases} \tag{5.2}$$

where β is a calibration factor [s^{-1} $K^{\frac{1}{3}}$], θ_l is the liquid water content, $\theta_{l,cl}$ is the equilibrium liquid water content calculated with the Clausius-Clapeyron equation as $\theta(h_{cl})$ with

$$h_{cl} = h_w + \frac{L_f}{g} \ln \frac{T}{T_f} \quad \text{for} \quad T < T_f, \tag{5.3}$$

where h_w is the pressure head corresponding to liquid and frozen water [m], T_f is the freezing temperature, g is gravitational acceleration (9.81 m s^{-2}), and T_f is the freezing temperature of 0°C, which is assumed to be constant. When $\theta_l > \theta_{l,cl}$, v_f is positive and freezing occurs, and if $\theta_l < \theta_{l,cl}$, v_f becomes negative and melting can occur. v_f is therefore, not only a freezing rate, but also a melting rate. The issue with this approach is that it does not assure all ice is melted before the temperature reaches T_f, and as v_f is forced to 0, the system is not permitted to melt further. This approach is therefore acceptable for freezing, but not for melting.

Here, a new parameterization is proposed based on the equilibrium ice content.

$$v_f = \frac{\theta_{i,eq} - \theta_i}{\beta}, \tag{5.4}$$

where v_f will be smaller when the system is closer to equilibrium and larger when the system is not in equilibrium, with

$$\theta_{i,eq} = \begin{cases} \theta_l + \theta_i - \theta_{l,cl} & \text{for} \quad T < T_f, \\ 0 \quad \text{for} \quad T \geq T_f, \end{cases} \tag{5.5}$$

and

$$\beta = \begin{cases} \beta_f & \text{for} \quad T < T_f, \\ \beta_m & \text{for} \quad T \geq T_f. \end{cases} \tag{5.6}$$

β_f and β_m are equilibrium time constants for freezing and melting [s]. They describe the time it takes to reach equilibrium. This approach allows melting even if equilibrium has not been reached at T_f. Mathematically, this approach is quite similar to the approach of dynamic non-equilibrium proposed

by Ross and Smettem (2000) and thoroughly discussed in Diamantopoulos and Durner (2012). Dynamic non-equilibrium can occur because the redistribution of the air-water configuration does not occur instantaneously and instabilities at the interface can cause the measured pressure head to be smaller while in disequilibrium. Following Peng et al. (2016), β can be expanded by the effect of super-cooling, which suggests greater non-equilibrium near T_f, which is in correspondence with the assumption of Kurylyk and Watanabe (2013). However, this changes the units of β_f to [s^{-1} $K^{\frac{1}{3}}$] and the physical meaning becomes more difficult to define.

$$\beta = \begin{cases} \frac{\beta_f}{(T-T_f)^{1/3}} & \text{for} \quad T < T_f, \\ \beta_m & \text{for} \quad T \geq T_f. \end{cases} \tag{5.7}$$

Furthermore, $(T - T_f)^{1/3}$ causes β to go towards infinity when T reaches T_f. The freezing rate will go towards zero and freezing or melting will stop. The rate can become so low, that no melting will occur until temperatures more positive than T_f are reached. The author considers $(T - T_f)^{1/3}$ too strong. Therefore, the effect of $(T - T_f)^{1/3}$ is minimized using a threshold, which is somewhat arbitrarily set to 0.1.

5.2.2 Coupled water and heat flow model

The extended Richards equation (Hansson et al. 2004) describes the variable saturated water flow for unfrozen and freezing temperatures where the liquid flux q_l includes a temperature driven liquid water flux:

$$\frac{\partial \theta_l}{\partial t} + \frac{\rho_i}{\rho_l}\frac{\partial \theta_i}{\partial t} = \overbrace{\boldsymbol{\nabla} \cdot K_{lh} \boldsymbol{\nabla}(h_l + z) + \boldsymbol{\nabla} \cdot K_{lT} \boldsymbol{\nabla} T}^{-\boldsymbol{\nabla} \cdot \vec{q}_l}, \tag{5.8}$$

where $\theta_{l,i}$ are the volumetric liquid water and ice contents [-], t is the time [s], $\rho_{i,l}$ are the density of ice and liquid water [kg m^{-3}], K_{lh} is the liquid hydraulic conductivity [m s^{-1}], h_l is the pressure head corresponding to liquid water [m], z is the geodetic head [m], K_{lT} is the temperature hydraulic conductivity [m^2 s^{-1} K^{-1}] and T is the temperature [K]. The heat equation accounts for diffusion, advection and latent heat of freezing and melting:

$$\frac{\partial C_p T}{\partial t} - L_f \rho_i \frac{\partial \theta_i}{\partial t} = \boldsymbol{\nabla} \cdot \lambda \boldsymbol{\nabla} T - \boldsymbol{\nabla} \cdot C_l \vec{q}_l T, \tag{5.9}$$

where C_p is the heat capacity of the porous medium, L_f is the latent heat of fusion $336{\cdot}10^3$ [J kg^{-1}], C_l is the volumetric heat capacity of liquid water, and λ is the apparent heat conductivity [W m^{-1} K^{-1}]. In the following we first expand all terms to be dependent on our three solution components, namely the total head $H_l = h_l + z$ [m], temperature T [K], and ice content θ_i. For the time derivative of h_w we can use H_l , because $\frac{\partial z}{\partial t} = 0$, and therefore

$$\frac{\partial h_l}{\partial t} = \frac{\partial h_l}{\partial t} + 0 = \frac{\partial h_l}{\partial t} + \frac{\partial z}{\partial t} = \frac{\partial H_l}{\partial t}. \tag{5.10}$$

The left side of the Richards equation can then be rewritten in its capacity form as

$$\frac{\partial \theta_l}{\partial t} = C(h_l)\frac{\partial h_l}{\partial t} = C(h_l)\frac{\partial H_l}{\partial t}. \tag{5.11}$$

We expand the heat capacity term using the product and then the chain rule as follows:

$$\frac{\partial C_p T}{\partial t} = T\frac{\partial C_p}{\partial t} + C_p\frac{\partial T}{\partial t}. \tag{5.12}$$

$T\frac{\partial C_p}{\partial t}$ can be expanded on the solution components as follows:

$$T\frac{\partial C_p}{\partial t} = T\frac{\mathrm{d}C_p}{\mathrm{d}h_l}\frac{\partial H_l}{\partial t} + T\frac{\mathrm{d}C_p}{\mathrm{d}T}\frac{\partial T}{\partial t} + T\frac{\mathrm{d}C_p}{\mathrm{d}\theta_i}\frac{\partial \theta_i}{\partial t}. \tag{5.13}$$

The solid soil matrix and ice are independent on h_l, so $\frac{\mathrm{d}C_p}{\mathrm{d}h_l}$ becomes

$$\frac{\mathrm{d}C_p}{\mathrm{d}h_l} = \frac{\mathrm{d}C_l\theta_l}{\mathrm{d}h_l} + \frac{\mathrm{d}C_a(\theta_s - \theta_l - \theta_i)}{\mathrm{d}h_l} = C_l C(h_l) - C_a C(h_l). \tag{5.14}$$

where $C_{l,i,a}$ are heat capacities of liquid water, ice and air respectively [J m^{-3} K^{-1}]. We assume that $\frac{\mathrm{d}C_p}{\mathrm{d}T}$ is negligible:

$$\frac{\mathrm{d}C_p}{\mathrm{d}T} = 0. \tag{5.15}$$

$\frac{\mathrm{d}C_p}{\mathrm{d}\theta_i}$ reduces to the following

$$\frac{\mathrm{d}C_p}{\mathrm{d}\theta_i} = C_i - C_a. \tag{5.16}$$

The heat advection term becomes

$$\boldsymbol{\nabla} \cdot C_l \vec{q}_l T = C_l \vec{q}_l \boldsymbol{\nabla} T + C_l T \boldsymbol{\nabla} \cdot \vec{q}_l, \tag{5.17}$$

with

$$C_l T \boldsymbol{\nabla} \cdot \vec{q}_l = -C_l T \boldsymbol{\nabla} \cdot K_{lh} \boldsymbol{\nabla} H_l - C_l T \boldsymbol{\nabla} \cdot K_{lT} \boldsymbol{\nabla} T, \tag{5.18}$$

which is a non-linear term. The product of temperature was linearized here by the fixed point Picard iteration scheme.

This results in the following set of equations, where all capacity terms are on the right, and all diffusion, advection and reaction terms are on the left. $\frac{\partial \theta_i}{\partial t}$ in the water and heat flow equations is replaced with v_f and are implemented as zero-order or first-order reaction terms.

$$\begin{aligned}
&C(h_l)\frac{\partial H_l}{\partial t} = \boldsymbol{\nabla} \cdot K_{lh} \boldsymbol{\nabla} H_l + \boldsymbol{\nabla} \cdot K_{lT} \boldsymbol{\nabla} T - \frac{\rho_i}{\rho_l} v_f, \\
&C_p \frac{\partial T}{\partial t} + T(C_l C(h_l) - C_a C(h_l))\frac{\partial H_l}{\partial t} = \\
&\boldsymbol{\nabla} \cdot \lambda \boldsymbol{\nabla} T - C_l \vec{q}_l \boldsymbol{\nabla} T + C_l T \boldsymbol{\nabla} \cdot K_{lh} \boldsymbol{\nabla} H_l + C_l T \boldsymbol{\nabla} \cdot K_{lT} \boldsymbol{\nabla} T + L_f \rho_i v_f - (C_i - C_a) v_f T, \\
&\frac{\partial \theta_i}{\partial t} = v_f.
\end{aligned} \tag{5.19}$$

This system of equation solves three unknowns. For one-dimensional problems considered here, the discrete representation of Eq. 5.19 is a 3x3 block matrix, where the water and heat blocks are 3-diagonal matrices. We assume v_f to be independent of water and heat terms, therefore water and heat terms in the ice operator are 0. The ice term in the water and heat operator are not strictly 0, but in this work the coupling is implemented as zero-order terms, and therefore does not appear in the stiffness matrix.

$$\left(\begin{array}{c|c|c}
\text{Water terms in Water operator} & \text{Heat terms in Water operator} & \text{Ice terms in Water operator} \\
\hline
\text{Water terms in Heat operator} & \text{Heat terms in Heat operator} & \text{Ice terms in Heat operator} \\
\hline
\text{Water terms in Ice operator} & \text{Heat terms in Ice operator} & \text{Ice terms in Ice operator}
\end{array}\right) \tag{5.20}$$

5.2.3 Model assumptions

The following assumptions are made in the development of this model and the use of soil hydraulic and thermal properties:

- Freezing and thawing do not occur instantaneously, but are delayed due to a non-equilibrium in the ice-water interface.
- The Clausius-Clapeyron equation can be used to calculate equilibrium states of freezing.
- The freezing rate decreases near 0 °C.
- The solid and liquid phases are in thermal equilibrium.
- Freezing point depression can be neglected and a constant freezing temperature of 0 °C can be assumed.
- Water redistributes according to gravity, capillary action and temperature.
- The freezing curve can be used to derive retention curve properties following cryo-suction of the Clausius-Clapeyron equation.
- The solid matrix is immobile.
- Vapor flow can be neglected as sublimation is not considered a dominant process in the simulated experiments.
- The effect of hysteresis can be neglected for the examples.

5.3 Model validation: Freezing column experiments

Model comparisons between the ICENE and regularized LTE model for the means of model verification were also conducted and can be found in the Appendix C.2. These included simple experiments to reach thermal static states or infiltration of water, and a freezing example Fig. C.1 and Fig. C.2. Without phase change, simulations of the two models are identical for temperature and infiltration experiments.

5.3.1 Model Setup

We simulate freezing soil column experiments conducted by Jame (1977) and Jame and Norum (1980) and Mizoguchi (1990), which have been widely used to verify and compare models (e.g Hansson et al. 2004;

Daanen and Nieber 2009; Dall'Amico et al. 2011; Painter 2011; Peng et al. 2016). The soil hydraulic and thermal properties to reproduce the Jame and Mizoguchi experiments were identical to that found in Tab. 4.1 in the previous chapter. The model setup was also largely identical to that in Tab. 4.2. Differences are listed in Tab. 5.1. As small differences in ice content can have larger implications, a smaller Picard iteration criterion was necessary.

Table 5.1: Difference in numerical setup and parameterization used in the numerical simulation for model testing of the Mizoguchi and Jame experiments (Jame 1977; Jame and Norum 1980; Mizoguchi 1990).

	Parameter	Mizoguchi	Jame		
			8	9	13
	$\mathrm{d}t_{max}$ (s)	5	5		
Picard method	iteration criterion	1×10^{-4}	1×10^{-4}		
Equilibrium time constant	β_f	1000	1000		

5.3.2 Effect of the equilibrium parameter on freezing column experiments

The Jame and Mizoguchi experiments were simulated for a simulation time of 24 h to show-case the effect of different β_f values. Lower β_f values indicate that the system freezes more rapidly, whereas greater β_f values delay freezing. Lower β_f values also cause greater accumulation of water near the cold end for all experiments. A higher β_f can successfully reduce the overestimation, but also decreases the decrease in water content at the freezing front and can delay a propagation of the freezing front into the soil. The Mizoguchi example nicely exemplifies the difficulty of solving the system of equations together in combination with solving θ_i with a zero-order reaction term. For the lowest β_f value, the ice content increases so dramatically that the total water content exceeds θ_s. It is likely that the Picard iteration criterion of 1×10^{-4} was not sufficient and caused errors to accumulate. Setting a reasonable Picard iteration criterion is challenging when taking into account three different physical properties, i.e. pressure head, temperature and volumetric ice content, as their magnitude and acceptable error differ. For freezing soil, the volumetric ice content is most sensitive to these errors. A stricter iteration criterion would have dramatically increased the simulation time, as either very small time steps or more iterations would be necessary.

5.3.3 Comparison of simulation results to experiments

The redistribution of water towards the cold end can be clearly seen in Fig. 5.2 for the Mizoguchi experiment and Fig. 5.3 for the three Jame experiments and simulations. Similar to experiments with the

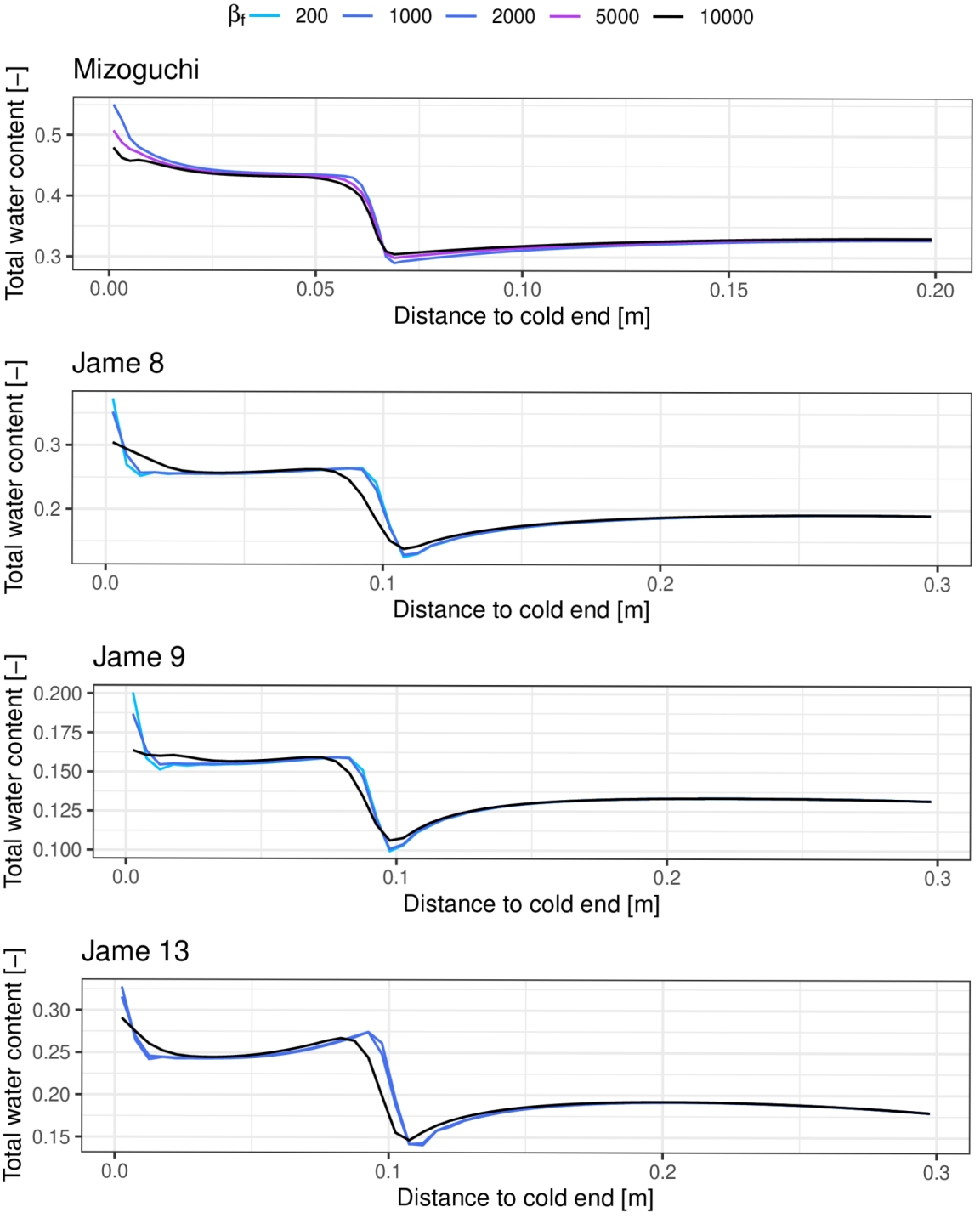

Figure 5.1: Influence of β_f values on the distribution of total water content for Jame and Mizoguchi experiments for a simulation time of 24 h.

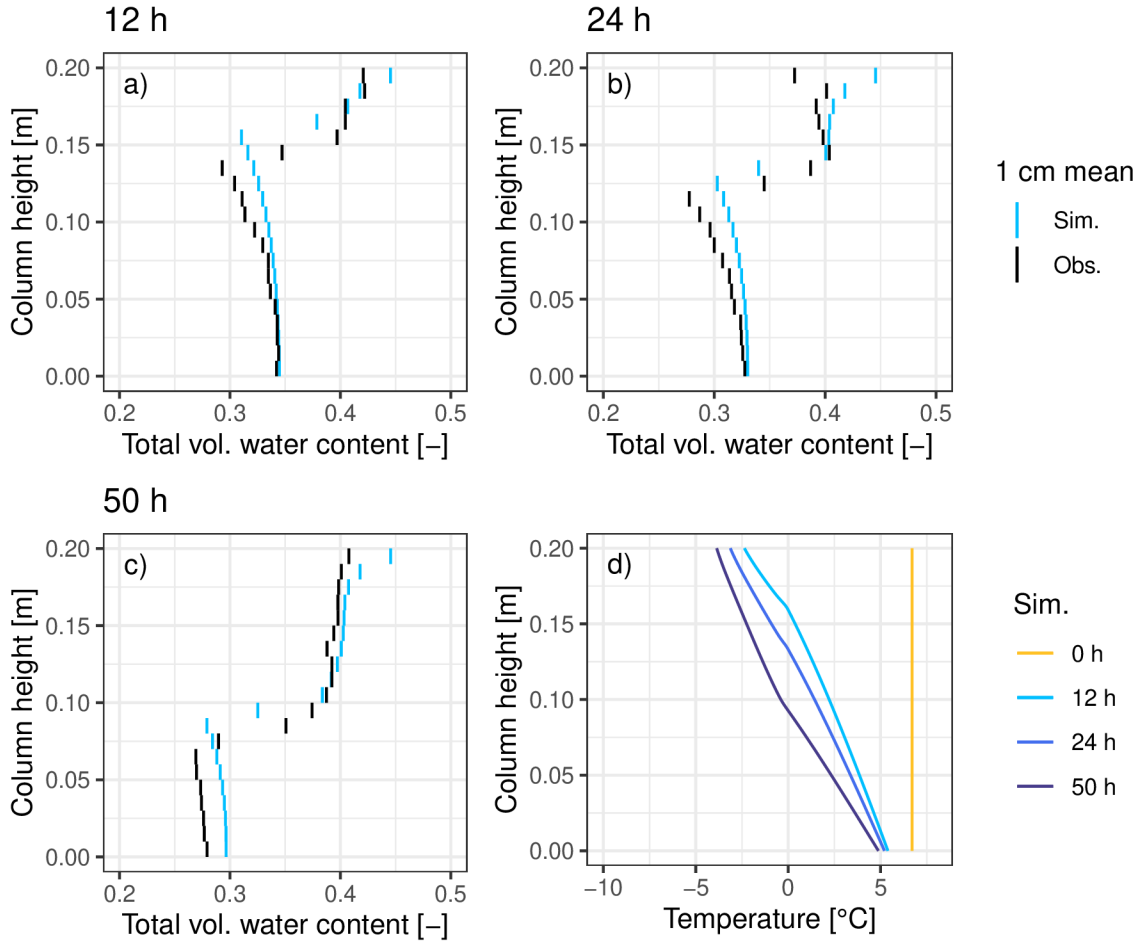

Figure 5.2: Observations and simulations of the total (ice + liquid) volumetric water content (in liquid water equivalent) after a) 12 h, b) 24 h and c) 50 h; d) simulated temperatures for the Mizoguchi experiment (Mizoguchi 1990; Hansson et al. 2004) using a non-equilibrium time constant of 5000 s. The simulated values of the volumetric water content were averaged over 1 cm.

equilibrium model, a steep drop in water content can be identified at the freezing front. The ice-phase non-equilibrium nicely reduces the overestimation at the cold end, however the freezing front clearly does not propagate sufficiently into the soil. Only the prediction of the Jame experiment 13 has improved.

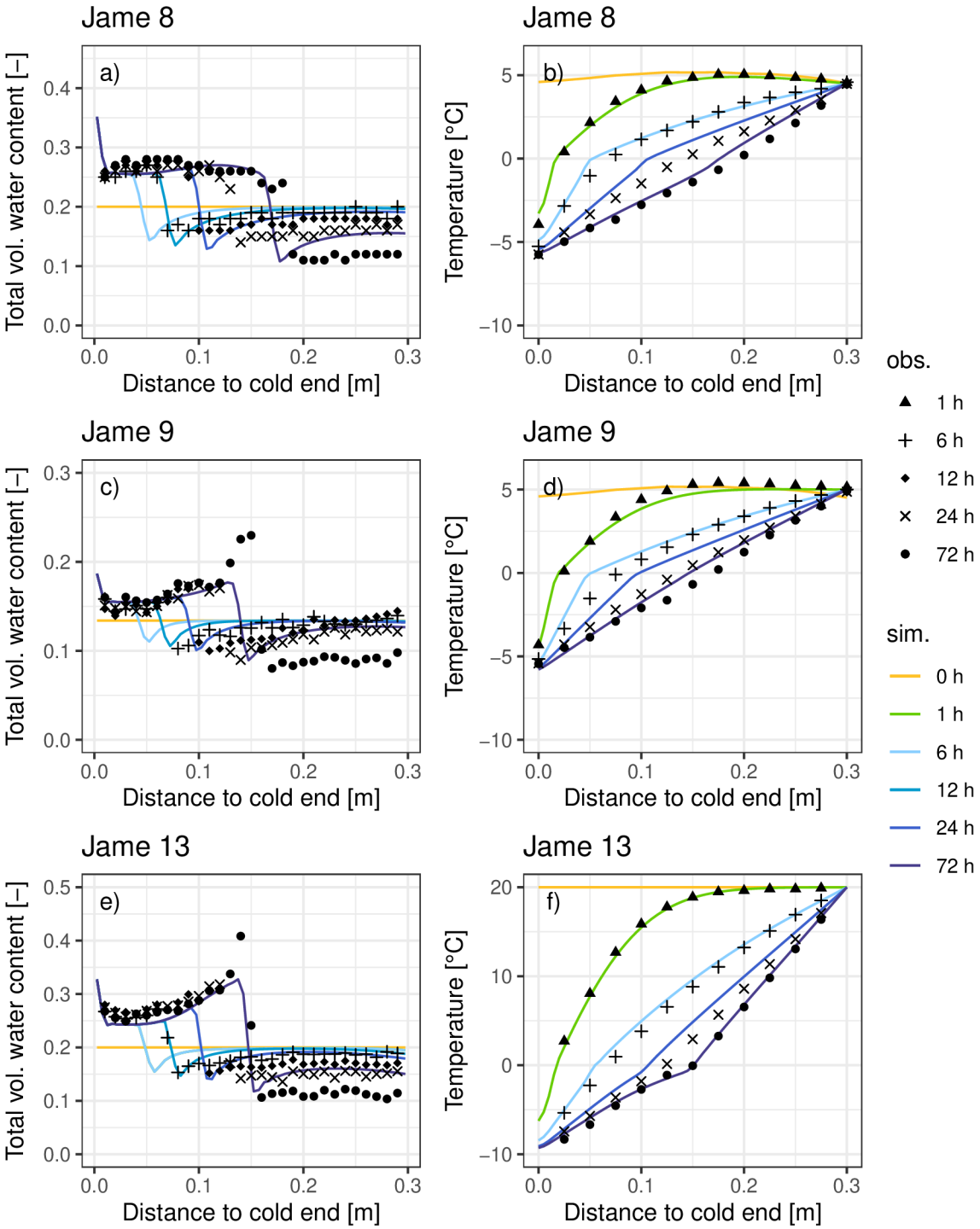

Figure 5.3: Observations and simulations of the total (ice + liquid) volumetric water content and temperature distribution for Jame experiment 8, experiment 9 and experiment 13 (Jame 1977) with a non-equilibrium time constant of 1000 s.

5.4 Model validation: Freezing curtain

5.4.1 Model Setup

To see if the model can successfully reproduce a freezing curtain, three melt experiments were conducted with different initial water content. The simulation setup for the freezing curtain experiments was identical to that listed in Tab. 4.3. The maximum time step was reduced to 10 s, and the Picard iteration criterion reduced to 1×10^{-4}.

5.4.2 Simulation results

Fig. 5.4 shows the effect of the β_f and β_m on the distribution of the volumetric ice and liquid water content over time. Note, that in contrast to the previous section, melting also occurs, and therefore β_m is also necessary. As expected, lower β values speed up the melt process. For lower β values, oscillations are present that are nicely pronounced in the ice content. These oscillations are a combination of the Picard criterion, spatial discretization and model features. The Picard criterion will also affect time discretization. Even with a freezing rate of 0, the ice content sometimes continues melting and can even create slightly negative ice contents. This creates a feedback loop due to the consumption of latent heat, which cools the system and causes melt water to refreeze. We can see that slower freezing reduces the feedback loop dramatically. They are greatest for experiment three, where due to higher initial total water and ice content, a higher melt rate is generated for a given temperature.

Fig. 5.5 shows the three melt examples. The ice-phase non-equilibrium model is clearly capable of reproducing a freezing curtain as indicated by the almost constant temperature at 20 cm depth. The freezing curtain effect is also longest for the experiment with the most initial ice content. Refreezing of melt water is evident in the third experiment. In comparison to the model assuming instant freezing depicted in Fig. 4.5, the ice has melted completely significantly later and less steeply. This is in accordance with model assumptions, as the non-equilibrium model induces delays in melting. Further, the maximum temperatures reached at the end of the simulations are significantly different for the third experiment, but very comparable when comparing the temperature of the system once the entire ice is molten.

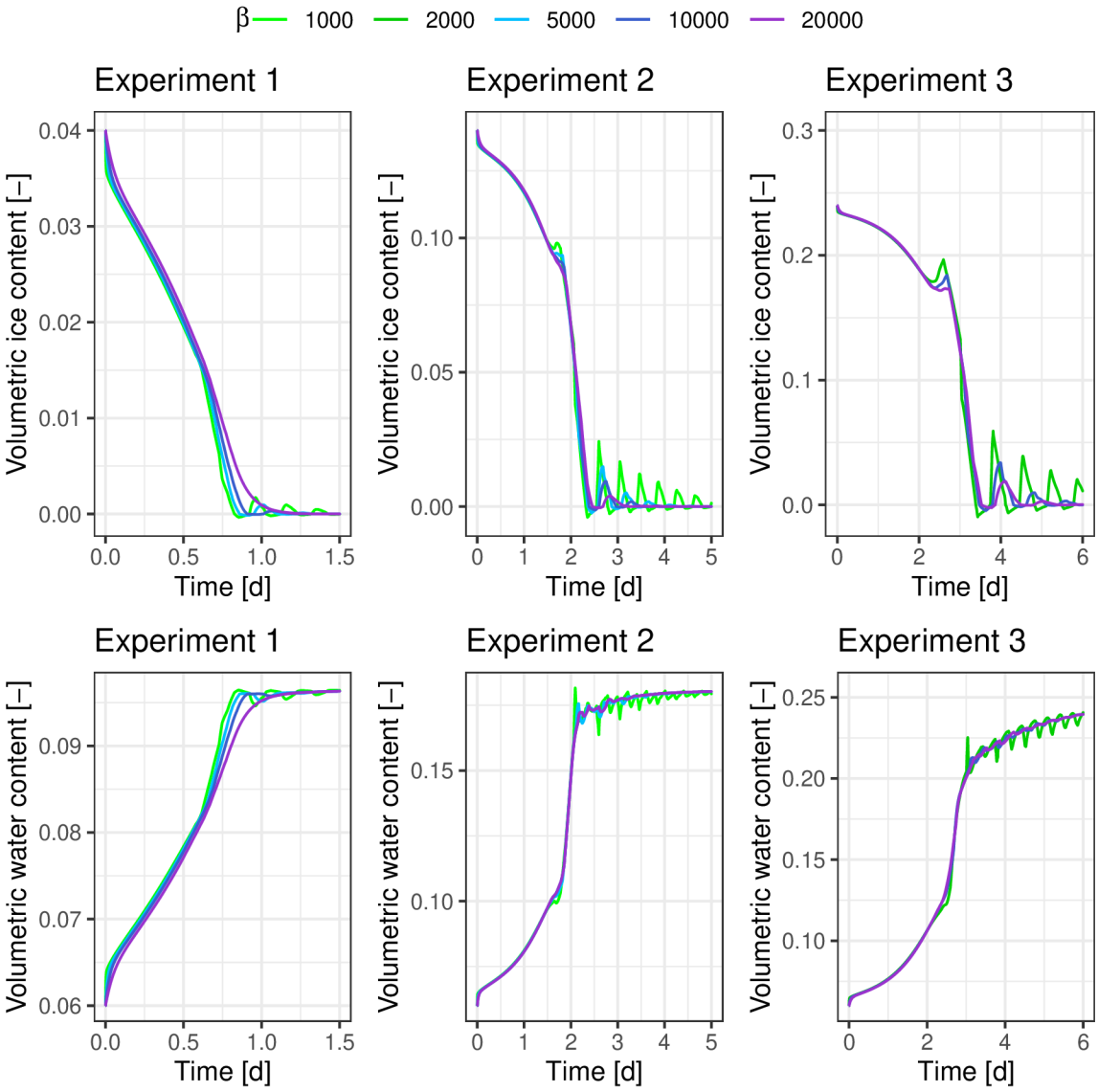

Figure 5.4: Effect of various equilibrium time constant on freezing curtain effect for melt experiments. Simulated volumetric ice and liquid water content at the soil surface.

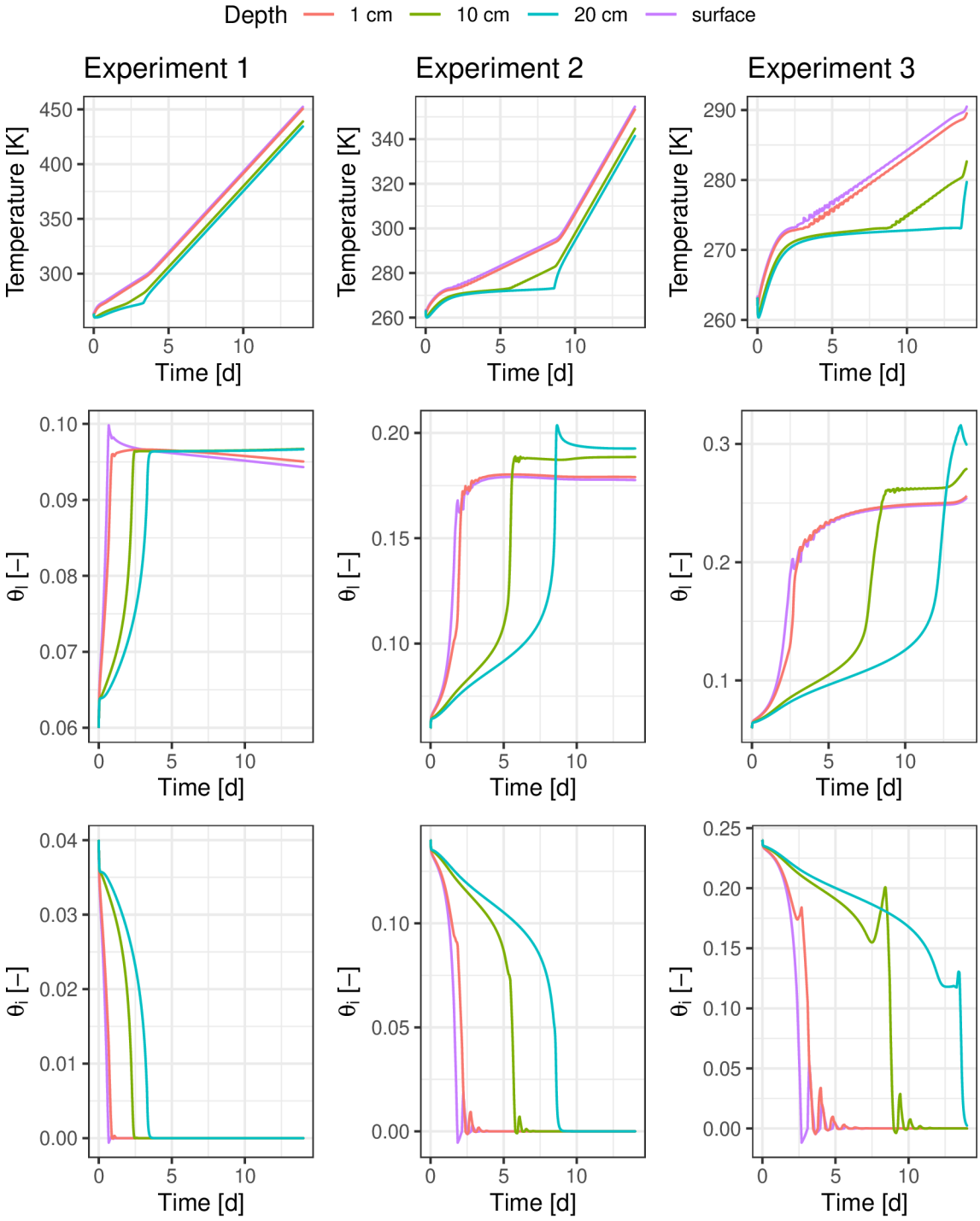

Figure 5.5: Simulated temperature, volumetric liquid water content and volumetric ice content of melt experiments with a non-equilibrium time constant of $\beta_f = 10000$ s and $\beta_m = 10000$ s.

5.5 Conclusion

Models based on the Clausius-Clapeyron equation often report an overestimation of the water content near the freezing front, because the mathematical formulation based on the Clausius-Clapeyron equation results in a strong flux towards the freezing front. Some researchers such as Painter (2011) suggested that this is indicative of a missing process not commonly included in models. This overestimation is hypothized to be due to non-equilibrium at the ice-water interface. In this contribution, we developed a novel ice-phase non-equilibrium approach that works for both freezing and melting in freezing and thawing soils. This has been first explored by Peng et al. (2016) and has now been extended. We tested our model on freezing column experiments commonly used in model verification, with most soil hydraulic and soil thermal properties derived from secondary information and not from the experiments themselves. The parameters that had to be manually fitted were taken from the regularized LTE model. Some oscillations near the freezing temperature were observed, which can occur when the Picard criterion is not set low enough and the problem is not sufficiently discretized spatially for a given v_f. These oscillations are amplified by reactions of latent heat. Under the assumption that v_f is independent of the water and heat operator, the ice block can be solved first and within the Picard iteration scheme. Furthermore, solutions could be rejected when non-physical θ_i values appear, which would trigger a decrease in dt. These values include negative values as well as values exceeding θ_s. In contrast to regularization, the equilibrium time constant is a physical parameter, so this model provides a tool to study the effects of different equilibrium assumptions on the speed of freezing for porous media. We show that the model successfully counteracts the overestimation observed. However, the propagation of the freezing front is also lessened. It might be fruitful to focus future research on non-equilibrium parameterizations, where the non-equilibrium time constant depends on the temporal change in temperature, as suggested in Kurylyk and Watanabe (2013). This could lead to a greater non-equilibrium at the cold end, and yet maintain the freezing front. More experiments are needed to understand the magnitude of equilibrium time constants, especially for melting frozen soils.

Chapter 6

Experimental investigation and mathematical modelling of hydraulic properties of snowpacks

6.1 Introduction

An accurate description of liquid water flow through snowpacks is essential to improve forecasting of disasters such as avalanches and floods, and is important for river and reservoir management (Yamaguchi et al. 2010; Yamaguchi et al. 2012; D'Amboise et al. 2017). Liquid water flow through snow does not only occur during snow-melt, but also during rain-on-snow (ROS) events (Juras et al. 2017; Würzer et al. 2017). There are, however, deficits in the understanding of processes governing snowpack runoff due to ROS (Rössler et al. 2014). To accurately forecast snowpack related disasters, adequate computer models are needed. However, many numerical snowpack models oversimplify liquid water movement (Hirashima et al. 2010) and there are still deficits in the knowledge of hydraulic properties of snowpacks (Wever et al. 2014). The porous system of snowpacks is very complex, including phase changes due to cyclic freezing and thawing. This causes time-dependent hysteretic changes in hydraulic properties, such as the retention curve and the unsaturated hydraulic conductivity. These are highly coupled to heat flux in the porous medium (D'Amboise et al. 2017; Würzer et al. 2017; Leroux and Pomeroy 2017). Recent model development included the use of the Richards equation to simulate the flow of liquid water through snow under unsaturated conditions, considering gravitational and capillary forces. For example the implementation into the SNOWPACK model by Wever et al. (2016) or the Crocus model by D'Amboise

et al. (2017), who implemented a hybrid Richards equation-bucket scheme. Some of these neglect heat flow and neglect freezing, e.g. Hirashima et al. (2014). Physical-based freezing routines can be derived using the Clausius-Clapeyron equation. As far as the author is aware, no snow model has so far tested a model based on the Clausius-Clapeyron equation for a coupled water and heat flow, where the the heat flow equation included convection as well. There are three groups of experiments that can be used to help validate snow models. First, synthetic experiments, where a simulation is designed to reproduce a specific concept, i.e. the freezing curtain effect. Second, laboratory experiments, which require a well equipped laboratory and a cold room, such as Katsushima et al. (2013), who conducted complex snow column drainage experiments to obtain flow patterns of preferential flow in snow for different snow. Third, field experiments, such as rain-on-snow sprinkling experiments, such as Juras et al. (2013), Juras et al. (2016), and Juras et al. (2017). These are extremely laborious experiments that mimic rain events with an artificial sprinkler. Most snow models have been validated using laboratory experiments. There is, however, a lack of model validation with experimental field data. Furthermore, little experimental field data exists from non-alpine areas, such as Czech mountain sites. This work addresses the lack of available field experiments and presents results of dye sprinkling experiments to extend the dataset that describe percolation of liquid water through different snow types.

In the two previous chapters, two models were presented. First, a regularized local-thermal-equilibrium model, which assumes instantaneous freezing, and second, a model assuming ice-phase non-equilibrium allowing the user to define equilibrium time constants to delay freezing. In this work these two mathematical models describing freezing and thawing in soils were adapted and implemented for snowpacks into DRUtES (Kuraz et al. 2020) using the standard finite element method. The models were first tested on synthetic infiltration experiments presented in Illangasekare et al. (1990). One question is to see how well these models do on field data, and to see to what extent these one-dimensional model setups can represent rain-on-snow experiments. To do this, the models were tested on selected rain-on-snow experiments. Simulations of rain-on-snow events often only focus on the outflow behaviour (Würzer et al. 2017). Whereas here, changes in density, liquid water content and temperature are also presented and observed mismatches are discussed.

6.2 Mathematical model for coupled water and heat flow for snow

6.2.1 Mathematical model for coupled water and heat flow for snow with regularization

The mathematical model considering regularization is identical to that presented in the previous chapter 4 and is only repeated for clarity. The main difference is in the parameterization of the constitutive functions. As for frozen soil, for snow the solutions are the temperature T [K] and the total pressure head H_w, namely,

$$H_w = h_w + z, \tag{6.1}$$

where h_w refers to the pressure head combining the liquid and frozen water content [m], and z is the spatial coordinate [m]. Similar to assumptions made by Kelleners et al. (2016), the saturated water content θ_s is assumed to be 1. For the full derivation, we refer the reader to Chapter 4. The complete set of equations for this model is as follows:

$$\begin{aligned}
&\left(C(h_w) + (\frac{\rho_i}{\rho_l} - 1)(C(h_w) - C(h_l))\right) \frac{\partial H_w}{\partial t} - \left(\frac{\rho_i}{\rho_l} - 1\right) C(h_l) \frac{\mathrm{d}h_l}{\mathrm{d}T} \frac{\partial T}{\partial t} = \\
&\boldsymbol{\nabla} \cdot K_{lh} \boldsymbol{\nabla} H_w + \boldsymbol{\nabla} \cdot \left(K_{lh} \frac{\mathrm{d}h_l}{\mathrm{d}T} + K_{lT}\right) \boldsymbol{\nabla} T, \\
&\left(T\left(C_l C(h_l) + C_i(C(h_w) - C(h_l)) - C_a C(h_w)\right) - \left(C(h_w) - C(h_l)\right) L f \rho_i\right) \frac{\partial H_w}{\partial t} \\
&+ \left(Cp + T(C_l - C_i) C(h_l) \frac{\mathrm{d}h_l}{\mathrm{d}T} + C(h_l) \frac{\mathrm{d}h_l}{\mathrm{d}T} L f \rho_i\right) \frac{\partial T}{\partial t} = \\
&\boldsymbol{\nabla} \cdot \lambda \boldsymbol{\nabla} T - C_l \vec{q_l} \boldsymbol{\nabla} T + C_l T \boldsymbol{\nabla} \cdot \left(K_{lh} \frac{\mathrm{d}h_l}{\mathrm{d}T} + K_{lT}\right) \boldsymbol{\nabla} T + C_l T \boldsymbol{\nabla} \cdot K_{lh} \boldsymbol{\nabla} H_w.
\end{aligned} \tag{6.2}$$

where C is the capacity term of the water retention curve, ρ_i is the density of ice [kg m^3], ρ_l is the density of liquid water [kg m^3], h_l is the pressure head of the liquid water [m], K_{lh} is the unsaturated hydraulic conductivity [m s^{-1}], K_{lT} is the thermal hydraulic conductivity [m^2 s^{-1} K^{-1}], $C_{p,l,i,a}$ are volumetric heat capacities of the porous medium, liquid water, ice and air [J m^{-3} K^{-1}], λ is the thermal conductivity [W m^{-1} K^{-1}].

The following assumptions are made in the development of this model and the use of snow hydraulic and thermal properties:

- No snow metamorphism takes place, i.e. grain diameter is constant.

- The effects of dry snow density on thermal retention curve parameters, saturated conductivity and thermal conductivity are neglected.
- A total pressure head can be used to include both liquid and ice content. Liquid and ice content can be calculated with the retention curve, which results in the saturated water content being 1.
- The solid and liquid phases are in thermal equilibrium.
- Water freezes instantaneously, and ice melts instantaneously within a given time step (numerically).
- A freezing point depression is not applicable for snow.
- Regularization if used appropriately does not affect the physics.
- Water redistributes according to gravity, capillary action and temperature.
- Vapor flow can be neglected as sublimation is not considered a dominant process in the simulated experiments.
- The effect of hysteresis can be neglected for the examples.

6.2.2 Mathematical model for coupled water and heat flow for snow with ice-phase non-equilibrium

The model assuming ice-phase non-equilibrium is largely identical to that presented in Chapter 5. Here also the total pressure head H_l [m], temperature T [K] and the ice content θ_i [-] are solved. The set of equations used for snow considering ice-phase non-equilibrium (ICENE) are as follows:

$$
\begin{aligned}
&C(h_l)\frac{\partial H_l}{\partial t} = \boldsymbol{\nabla}\cdot K_{lh}\boldsymbol{\nabla}H_l + \boldsymbol{\nabla}\cdot K_{lT}\boldsymbol{\nabla}T - \frac{\rho_i}{\rho_l}v_f,\\
&C_p\frac{\partial T}{\partial t} + T(C_l C(h_l) - C_a C(h_l))\frac{\partial H_l}{\partial t} =\\
&\boldsymbol{\nabla}\cdot\lambda\boldsymbol{\nabla}T - C_l\vec{q}_l\boldsymbol{\nabla}T + C_l T\boldsymbol{\nabla}\cdot K_{lh}\boldsymbol{\nabla}H_l + C_l T\boldsymbol{\nabla}\cdot K_{lT}\boldsymbol{\nabla}T + L_f\rho_i v_f - (C_i - C_a)v_f T,\\
&\frac{\partial\theta_i}{\partial t} = v_f.
\end{aligned}
\tag{6.3}
$$

For snow, the parameterization for the freezing rate v_f for the ice-phase non-equilibrium model was adjusted to better reflect melting and freezing observed in snow. This also means that this model does not

assume that the ice content calculated with the Clausius-Clapeyron equation represents the equilibrium ice content. More specifically this means that liquid water cannot exist without freezing at sub-zero temperatures. Therefore, the ICENE still assumes that there is a non-equilibrium in the ice-phase, but it is not the non-equilibrium counterpart to the rLTE model. This decision was also made because retention properties change rapidly with small changes in the pressure head due to steep retention functions in snow. This means that extremely small temperature changes can cause the entire snowpack to melt or freeze rapidly. This can cause non-physical oscillations, similar to that described in Fig. 5.4. Therefore, a heat-based approach was developed, as follows:

$$v_f = \frac{\theta_{i,eq} - \theta_i}{\beta}, \tag{6.4}$$

where $\theta_{i,eq}$ is the equilibrium ice content [-], θ_i is the volumetric ice content [-] and β is the equilibrium time constant [s]. vf will be smaller when the system is closer to equilibrium and larger when the system is further from equilibrium, with

$$\theta_{i,eq} = \begin{cases} min(\theta_i + \theta_{i,maxfreeze}, \theta_l) & \text{for} \quad T < T_f, \\ max(\theta_i - \theta_{i,maxmelt}, 0) & \text{for} \quad T \geq T_f, \end{cases} \tag{6.5}$$

where $\theta_{i,maxmelt}$ and $\theta_{i,maxfreeze}$ represent the maximum amount of ice that can be melted or frozen. $\theta_{i,maxmelt}$ can be calculated based on the melting factor of Illangasekare et al. (1990) as follows

$$\theta_{i,maxmelt} = \frac{C_p \rho_p (T - T_f)}{L_f \rho_i}, \tag{6.6}$$

and $\theta_{i,maxfreeze}$ can be adopted accordingly:

$$\theta_{i,maxfreeze} = \frac{C_p \rho_p (T_f - T)}{L_f \rho_l}, \tag{6.7}$$

where C_p is the volumetric heat capacity of the porous medium [J kg^{-1} K^{-1}], ρ_p is the density of the porous medium [kg m^{-3}], T is the temperature [K], T_f is the freezing temperature [K] and L_f is the latent heat of fusion [J kg^{-1}]. The term $C_p \rho_p (T - T_f)$ determines how much heat is available for melt when the temperature is brought down to T_f, and division by $L_f \rho_i$ converts this into a maximum amount of ice that can be melted. Similarly, $C_p \rho_p (T_f - T)$ is the energy that is released when freezing or refreezing liquid water, where division by $L_f \rho_l$ converts it into to maximum amount of liquid water that can be frozen.

β can be adjusted according to freezing and melting as follows:

$$\beta = \begin{cases} \beta_f & \text{for} \quad T < T_f, \\ \beta_m & \text{for} \quad T \geq T_f. \end{cases} \tag{6.8}$$

Note, that different to freezing soil the effect of supercooling using the third root of the temperature difference of the material and the freezing temperature is not taking into account in the non-equilibrium parameterization. This is because this heat approach already moves v_f towards 0 near the freezing temperature.

This model assumes a minimal form of hysteresis by scaling the retention curve according to the ice content, as $\theta_s = 1 - \theta_i$.

The following assumptions are made in the development of this model and the use of snow hydraulic and thermal properties:

- No snow metamorphism takes place, i.e. snow grain diameter are not allowed to change.
- Freezing and thawing do not occur instantaneously, but are delayed due to non-equilibrium at the ice-water interface.
- The equilibrium state only depends on available heat and not on the Clausius-Clapeyron equation. This means that at sub-zero temperatures all water will freeze, and at above-zero temperatures all ice will melt.
- The freezing rate is 0 at 0 °C, so no phase transition takes place at 0 °C.
- The saturated water content changes with the ice content, and therefore a simple hysteretic effect is included. Full hysteresis, however, is neglected for the examples.
- The ice and liquid phases are in thermal equilibrium.
- A freezing point depression is not applicable for snow.
- Water redistributes according to gravity, capillary action and temperature.
- Vapor flow can be neglected as sublimation is not considered a dominant process in the simulated experiments.

6.2.3 Snow hydraulic and thermal properties

The retention curve was parameterized by the van Genuchten model:

$$\theta(h) = \theta_r + (\theta_s - \theta_r)\,[1 + (-\alpha h_l)^n]^{-m} \text{ for } h \leq 0, \tag{6.9}$$

and the unsaturated hydraulic conductivity curve with the Mualem model:

$$K_l = K_s \cdot S^{1/2}[1 - (1 - S^{1/m})^m]^2, \tag{6.10}$$

where the saturated conductivity K_s was calculated according to the parameterization developed by Shimizu (1970):

$$K_s = \frac{g\rho_l}{\nu} 0.077 d^2 \Big[exp(-0.0078\rho_s) \Big], \tag{6.11}$$

where ρ_l is the density of water [kg m^{-3}], g is gravitational acceleration (9.81 m s^{-2}), ν is the kinematic viscosity [m^2 s^{-1}] of water at 0 °C , d is the grain size [m], ρ_s is the density of snow [kg m^{-3}].

S is effective saturation defined as follows:

$$S = \frac{\theta(h_l) - \theta_r}{\theta_s - \theta_r}(1 + (-\alpha h_l)^n)^{-m} \text{ for } h \leq 0, \tag{6.12}$$

where θ_s is the saturated water content [-], θ_r is the residual water content [-], α is related to the inverse of the air entry value [m^{-1}] and n and m are shape parameters determining the pore size distribution, with m usually defined as $m = 1 - \frac{1}{n}$[-]. $m = 1 - 1/n$ and n and α can be estimated from cryo-transfer functions.

As detailed in the introduction of this thesis and depicted in Fig. D.3 and D.4, the choice of cryo-transfer function dramatically changes the retention and unsaturated hydraulic conductivity curves. For this simulation, α and n were calculated with Yamaguchi et al. (2012). This decision was based on a study conducted by master student Čejková (2019), who tested different cryo-transfer functions on the outflow behavior of rain-on-snow experiments conducted by Juras et al. (2017). According to Yamaguchi et al. (2012) α and n are dependent on the bulk dry density ρ_{db} [kg m^{-3}] and grain size d [m] as follows:

$$\alpha = 4.4 \cdot 10^6 \big(\frac{\rho_{db}}{d}\big)^{-0.98} \tag{6.13}$$

and

$$n = 1 + 1.27 \cdot 10^{-3} \left(\frac{\rho_{db}}{d}\right)^{0.61}. \tag{6.14}$$

Calonne et al. (2011) conducted numerical simulations of the thermal conductivity of snow using microtomographic images and developed an empirical relationship between effective thermal conductivity λ_{eff} and snow density ρ [kg m^{-3}]:

$$\lambda_{eff} = 2.5 \cdot 10^{-6} \rho^2 - 1.23 \cdot 10^{-4} \rho + 0.024. \tag{6.15}$$

6.3 Model Testing

Illangasekare et al. (1990) performed several one-dimensional synthetic infiltration tests on snow to test meltwater infiltration. These tests were also partly recreated by Daanen and Nieber (2009) and can be used for model testing. We assume a 0.5 m snow column with a linear temperature gradient with 10 °C at the bottom and 0 °C at the top. Two different infiltration intensities were applied. For the regularized local thermal equilibrium (rLTE) model, different water temperatures close to 0 °C were explored. Shown is the test where the inflow was 0.05 °C. The overall tests setup, including dimension and experiments are taken from Illangasekare et al. (1990). However, since Illangasekare et al. (1990) did not use the van Genuchten-Mualem model, the snow hydraulic and thermal properties are taken from Daanen and Nieber (2009), where constant snow grain size of 1 mm and a snow density of 500 kg m^{-3} is assumed to estimate hydraulic and thermal properties, where $\alpha = 42$, $n = 3.8$, $\theta_r = 0$. These properties produce a rather steep retention curve with a high inverse of the air entry value, so temperatures a few tenths of a degree below freezing will create sufficient *cryosuction* to cause the medium to freeze-thaw under the Clausius-Clapeyron framework (rLTE). The model used in Illangasekare et al. (1990) and Daanen and Nieber (2009) neglect heat convection, which is the heat transported by the water flux. In their simulations, the heat only changes due to the phase change. Neglecting heat convection causes the water flux to travel "faster" than the heat. Therefore liquid water penetrates cold areas where freezing can occur, which changes the porosity. These changes in porosity are simply an artifact of their model assumptions, i.e. the neglect of heat convection. Although Illangasekare et al. (1990) acknowledge that it takes time for freezing to take place, for the simulations all available water was allowed to freeze within a given time step, which is essentially instantaneous freezing. Daanen and Nieber (2009) also assumed instantaneous freezing. In the rLTE and ICENE models here, heat is transported with the liquid. This causes the 0 °C to be transported

Table 6.1: Simulation setups for synthetic infiltration experiments for snow, based on Illangasekare et al. (1990).

Experiment	1	2
T_{in} [K]	273.2	273.2
q_{in} [mm h^{-1}]	1	0.5
T_r [mm h^{-1}]	272.15	272.15

into the snow profile without phase change. With the rLTE model, with a top boundary temperature 0 °C water does not infiltrate into the snow due to the steep retention curve, which causes ponding at the surface. To initialize the ICENE, a small water content needs to be assigned. This water slowly freezes, and the water penetrates until the snow becomes so dry that no water can be conducted. As the retention and hydraulic curves are very steep, no strong pressure head gradient develops that would induce a flux, so water accumulates. Once water accumulates, the liquid water freezes at the lower boundary of the accumulated water. The depth of this accumulation depends on the initial water content and the equilibrium time constant. The greater the constant, the further the water can penetrate into the snow as freezing is delayed. Interestingly, the non-equilibrium approach with a higher non-equilibrium constant is most similar to the simulations of Illangasekare et al. (1990) and Daanen and Nieber (2009), and shows that the lack of heat convection can have a similar effect as ice-phase non-equilibrium.

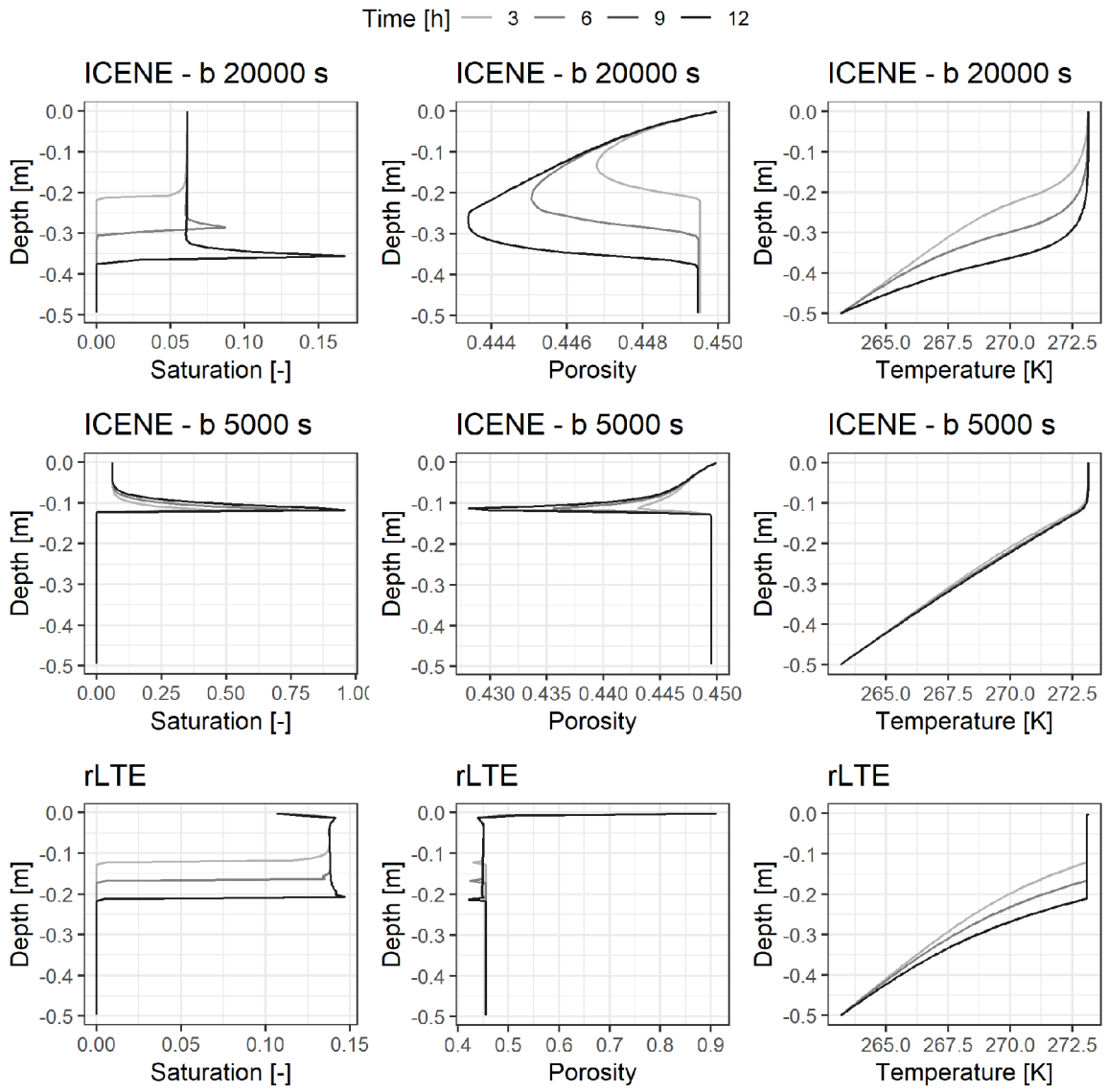

Figure 6.1: Simulated profiles of snow properties versus depth for an infiltration rate of 1 mm h^{-1}: saturation versus depth, porosity versus depth and temperature versus depth for the ICENE model with equilibrium time constants of 20000 s and 5000 s, and the regularized LTE model.

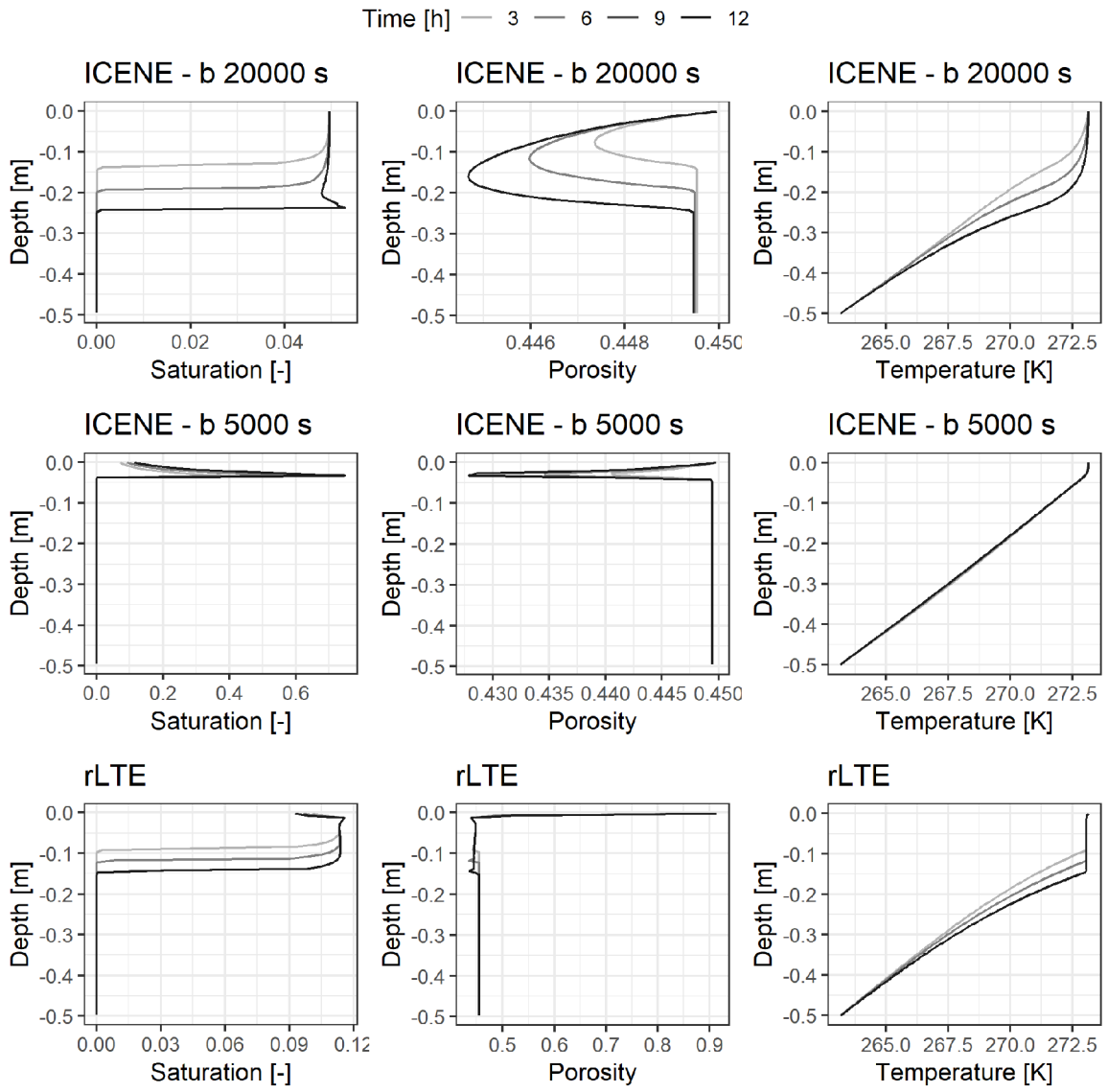

Figure 6.2: Simulated profiles of snow properties versus depth for an infiltration rate of 0.5 mm h^{-1}: saturation versus depth, porosity versus depth and temperature versus depth for the ICENE model with equilibrium time constants of 20000 s and 5000 s, and the regularized LTE model.

6.4 Rain-on-snow dye tracer experiments

Three sprinkling experiments were conducted at three Czech mountain sites in 2019. These sprinkling experiments mimicked rain-on-snow events. The experiments were conducted with a portable rain simulator, which was calibrated beforehand.

6.4.1 Site locations

Four sites were prepared prior to the experiments, two sites in Kubová Huť, one site in Luisino Údolí, and one in Horní Němčice (Fig. 6.3).

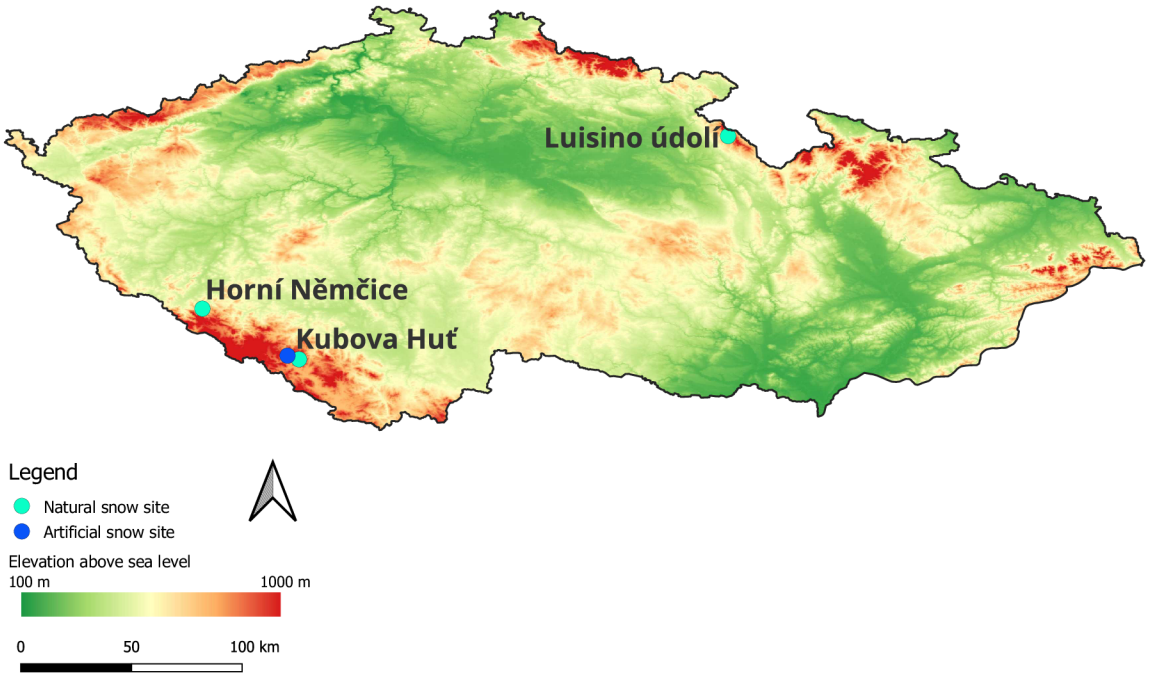

Figure 6.3: Experimental site locations indicating natural and artificial snow sites in Czechia. (Projection, WGS 84 with DGM from Tadono et al. (2014)). Credit: S. Blöcher.

6.4.2 Site Preparation

Prior to the experiments, each site had to be prepared. The preparation included leveling and cleaning fields, and digging and constructing drainage channels. At the end of the drainage channel, a shaft was

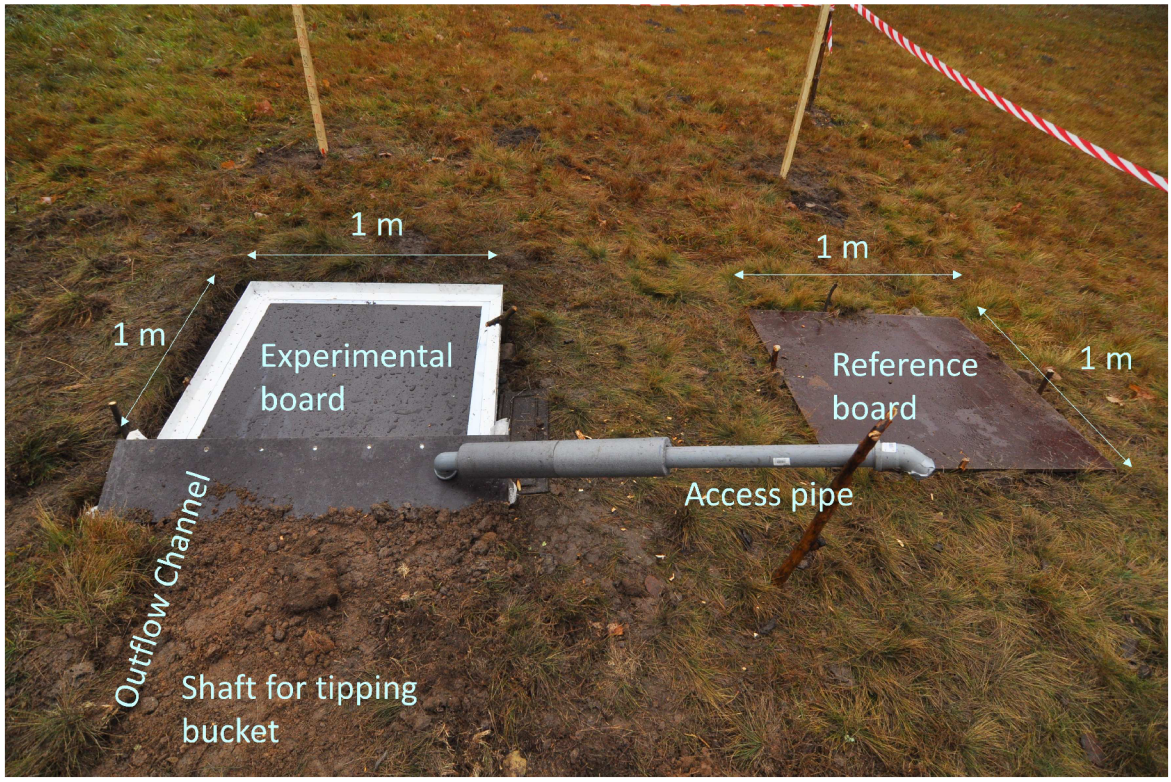

Figure 6.4: Annotated installation in Luisino Údolí with experimental board and reference board.

dug that could house a tipping bucket. At each site, poles and experimental and reference boards were installed. The poles were used as guides so the boards could be located before the experiments. The reference board was used to determine a snow profile with identical properties to the experimental boards. Both the reference and experimental boards measured 100 cm x 100 cm (Fig. 6.4). These boards were left at each site, in order for natural snow to accumulate. The measurement boards and the drainage channel were positioned on a slope, so that water flows downwards into the drainage channel. An additional access pipe was installed to ensure the outflow channel did not freeze and to allow unblocking the channel without disturbing the snow.

6.4.3 Rain-on-snow experiments

Conducting ROS experiments is labor intensive and was only possible with the help of committed master students and colleagues. Three ROS experiments were conducted in 2019. The first experiment was conducted in Kubová Huť (Forest site) on the 15th of January, followed by a second experiment conducted on the 1st of February in Luisino Údolí and a final third experiment in Kubová Huť (Ski School) on the

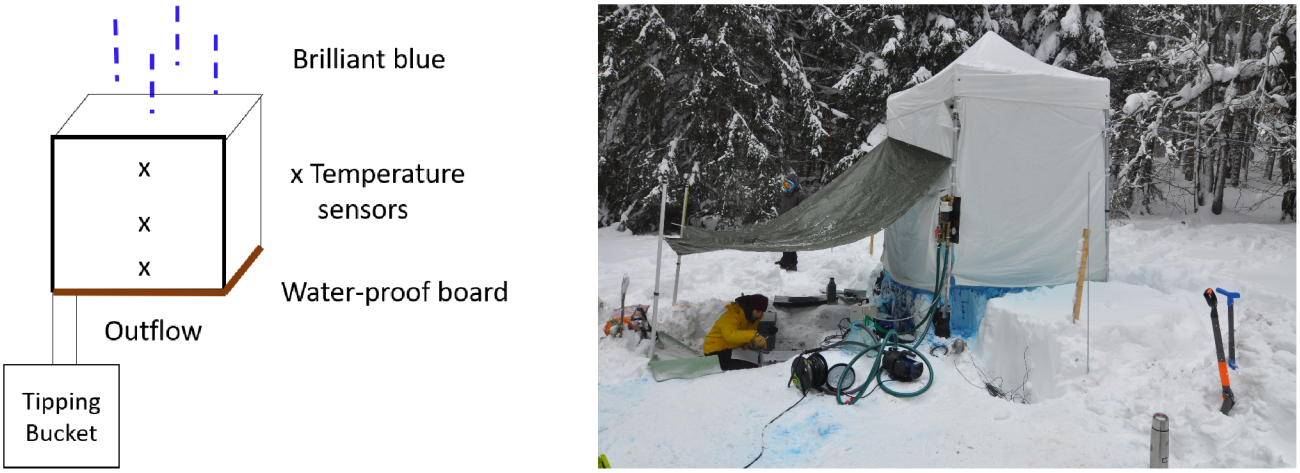

Figure 6.5: Left: Schematic of experimental setup. Right: Sprinkling experiment on the 15th of January in Kubová Huť (Forest site). Photo credit: R. Juras.

15th of March. No experiments were conducted in Horní Němčice due to insufficient snow. The water used for sprinkling was colored with brilliant blue, otherwise known as E133, a safe food coloring, with a concentration of 0.4 g l^{-1}. The advantage of food coloring as opposed to deuterium, is that flow paths become easily visible after the experiment. Its concentration can also be detected using a spectrometer. The portable rain simulator consisted of a metal construction covered by a tent covering an area of 200 cm x 200 cm. The tent was therefore significantly wider than the experimental board. The tent was inserted into the snow and fixed in place using heavy sand bags. The sprinkling system was pressurized at around 2-2.2 bar and distributed artificial rain through a nozzle, which was calibrated at a height of 160 cm above the snow surface. The target area of 1 m^2 was surrounded by at least 50 cm of natural undisturbed snow. This decreased the edge effect and allowed for natural flow behavior to occur. 50 l barrels were used to supply water to the pumping system. The rain intensity was 11 mm/h, or 22 l/h. Before the experiment started, the shaft for the tipping bucket had to be uncovered. At each location a snow wall on the side of the outflow was built and temperature sensors were inserted horizontally into the snow and fixed with insulation tape. During the experiments, outflow and temperature were logged using a Fiedler logger. A setup of the sprinkling device and a photograph of the Kubová Huť site can be seen in fig. 6.5, right. The outflow was manually monitored as well.

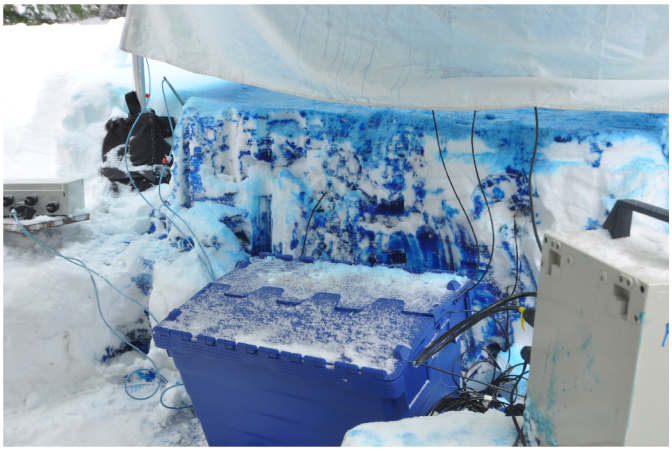
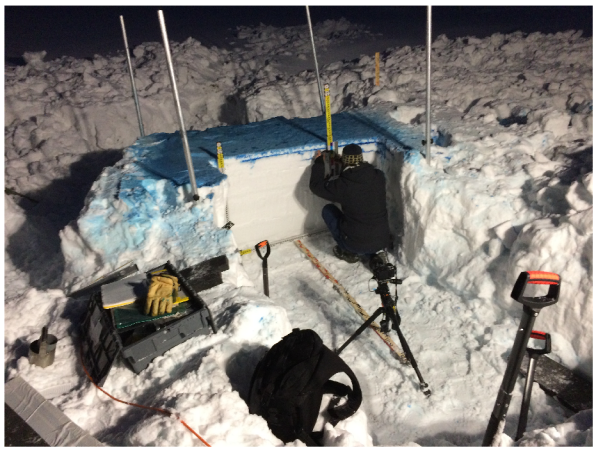

Figure 6.6: Left: Kubová Huť (Forest site) from outflow side with temperature sensors. The fiedler logger is located in the blue box. Photo credit: R. Juras. Right: Post experimental snow pit at the Luisino Údolí. Photo credit: J. Blöcher

Snowpack profile and measurements

Pre- and post-experimental snow pits were dug, and temperature, density and water content measurements were taken along the profile, and snow layering was determined according to snow structure and hardness changes. Two pre-experimental profiles were excavated that were both located on the reference board, which was placed near the experimental board. In addition, photos were taken of snow grain samples placed on a grid for later processing (see postprocessing). Temperature was also measured at the snow surface as well as in the air at roughly 2 m. Snow density was measured using the cylinder method and a scale as well as with the Denoth meter, a snow sensor from SLF, which estimates snow density of dry snow based on reference capacitance values. Water content was also (indirectly) measured with the Denoth meter, however, to obtain accurate water content estimates, postprocessing of emissivity values was required. All measurements were taken every 5 cm starting at the snow surface. The post-experimental snow pits were excavated on the experimental board at a 90 degree angle to the outflow direction at different distances to the edge of the experimental board.

6.4.4 Post-processing

Snow profile

After the experiments, the experimental site was excavated and pictures were taken to record the flow paths. The pictures were then processed in R (R Core Team 2021) to determine horizontal and vertical flow paths, as well as areas of light and dark blue. For this, a simple R package *"Bluesnow"* was developed

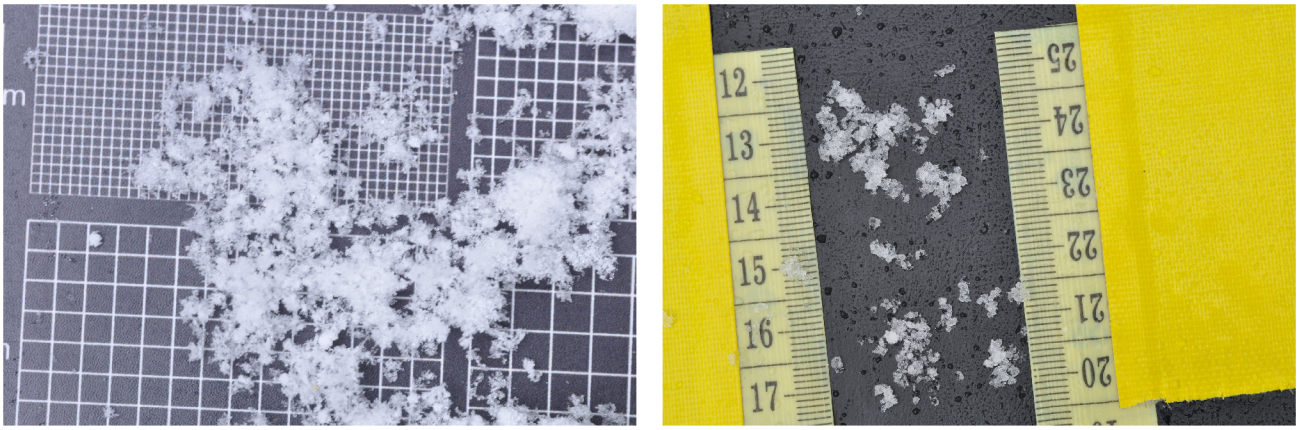

Figure 6.7: Photograph of snow grains to be post-processed. a) Kubová Huť in January. b) Kubová Huť in March. Photo credit: V. Cejkova, R. Juras

that first removes shadows and gray areas from the snow profile and then segregates the pictures into its color groups. The package was then used to determine the area fractions covered in light and dark blue. A first version of this package was co-developed by master student Ibrahim Bello and described in Bello (2019).

Grain size

Both snow hydraulic and thermal properties are based upon the concept of mean grain size. When recording a snow profile, the range of grain size and grain shape is recorded using a magnifier and a crystal card. This method is relatively quick, but also imprecise. Therefore, we designed a box where snow samples were photographed (Fig. 6.7) and later processed with the image processing software imageJ (Schneider et al. 2012) to obtain a more representative value of mean grain size. These photos were taken on a dark background with a ruler in view to allow setting of a scale. Manual and automatic detection were tested as part of the master thesis of Simon Audes (in preparation), where it was concluded that automatic detection is somewhat difficult. In the following, his grain size estimations using the manual method were used.

Liquid water content

The Denoth meter (SLF Snow Sensor, FPGA) was used to measure liquid water content. The Denoth meter measures dielectric properties with a capacity sensor. To obtain accurate values of the liquid water content, the dry snow density needs to be known, as the emissivity not only increases with increasing

liquid water content but also with snow density. If dry snow measurements are not available, estimates are needed. The total emissivity returned by the Denoth meter can change according to weather conditions, which is why the emissivity of air is always measured to compensate. The liquid water content was calculated by accounting for the dry snow density first, and then estimating the liquid water content with the regression parameters published by the company. First, the effect of the density of the dry snow on the emissivity measurement ϵ_{ρ_s} needs to be estimated, such that

$$\epsilon_{\rho_s} = \frac{-b_\rho + \sqrt{b_\rho^2 + 4\rho_s a_\rho}}{2a_\rho}, \tag{6.16}$$

where $a_\rho = 59.9$ and $b_\rho = 586.5$. ϵ_{ρ_s} represents $\epsilon_{\text{air}} - \epsilon_{\text{drysnow}}$.

The measured difference in emissivity for the wet snow is:

$$\Delta\epsilon = \epsilon_{\text{air}} - \epsilon_{\text{wetsnow}}, \tag{6.17}$$

and the density compensated emissivity is

$$\Delta\epsilon_{\text{corrected}} = \Delta\epsilon - \epsilon_{\rho_s}. \tag{6.18}$$

The liquid water was then calculated as:

$$LWC = a_{LWC}\Delta\epsilon^3_{corrected} - b_{LWC}\Delta\epsilon^2_{corrected} + c_{LWC}\Delta\epsilon_{corrected}, \tag{6.19}$$

where $a_{LWC} = 0.271$, $b_{LWC} = 2.688$ and $c_{LWC} = 10.337$.

6.4.5 Rain-on-snow experiment in Kubová Huť - Forest site

The first experiment was conducted in Kubová Huť on the 14th and 15th of January 2019 at a forested site, which the team was permitted to use thanks to the ski resort Kubová Huť. The air temperature was around -3 °C and it was snowing. The snow height was roughly 78 cm and layered. The initial snow was dry and no water could be observed.

Simulation setup

Setting up the simulation was not straight-forward due to the heterogeneity of the pre-experimental profiles. Fig. D.1 (Appendix) shows the layers identified from two pre-experimental profiles. These two profiles were located less than 1 m from each other and resulted in very different layering. The second profile was given preference, as an ice layer experimentalound in post-experimental profiles was present. In total 12 layers were identified and for each, specific hydraulic and thermal properties assigned.

Hydraulic and thermal parameters used for the simulation can be found in Tab. 6.2. With the regularized model, a saturated water content θ_s of 1 is assumed. For the regularized model, the initial condition for the water flow equation was the total water content (ice and liquid water). The model recalculated the water content input into H_w and, based on the temperature, to ice and liquid water content values. For the ICENE model, the initial condition for the water flow equation was a sufficiently low pressure head of $h_l = -1$ m. Measurements of the volumetric ice content values derived from the measured dry snow density along the height of the snow profile were used as an initial condition for the ice equation, which were linearly distributed between 2 measurement points. The initial temperature distribution was linear, coldest at the snow-air interface and warmest with 0°C at the snow-board interface. Temperature measurements of pre-experimental snowpack profiles were used as the initial condition for both models. The boundary conditions for both models were identical. The top boundary for the water flow equation was a time dependent Neumann condition, where the rain started after 60 s of simulation time with an intensity of 6.1×10^{-6} m s^{-1} lasting 3600 s. For the rest of the period, a zero-flux Neumann condition was assumed. For the bottom boundary a zero-flux boundary was assumed, because no outlfow was detected during the experiment. Due to misalignment of the experimental board, the board was not perfectly centered. This caused less of the target rain to infiltrate the target area. Therefore additional simulations were run with reduced inflow. A seepage face boundary would more adequately describe the bottom boundary, if outflow was present. For the heat flow equation a time dependent Dirichlet condition was set, where the temperature was set equal to the temperature in the tent before and after the rain, and set to 1 °C during the rain period. The bottom boundary for the temperature equation was a Dirichlet condition set to 0 °C. For the ICENE model, zero-flux conditions were used for the ice equation.

Results

Two post-experimental snow pits were analyzed after the experiment 16-17 cm from the edge of the experimental board and 80-83 cm from the edge of the experimental board (Fig.6.8), which resulted

Table 6.2: Hydraulic and thermal parameter values used in the numerical simulation of the rain-on-snow experiment conducted on the 14th and 15th of January 2019 in Kubová Huť at the forest site.

Height	K_s	α	n	m	θ_r	θ_s	θ_s (ICENE)
m	ms^{-1}	m^{-1}	-	-	-	-	-
0.00-0.08	0.12	32.6	5.2	0.8	0.0	1.0	0.63
0.08-0.11	0.06	23.4	6.2	0.8	0.0	1.0	0.61
0.11-0.15	0.05	21.7	6.4	0.8	0.0	1.0	0.65
0.15-0.21	0.30	51.2	4.2	0.8	0.0	1.0	0.65
0.21-0.26	0.09	27.5	5.7	0.8	0.0	1.0	0.67
0.26-0.30	1.07	93.5	3.2	0.7	0.0	1.0	0.68
0.30-0.31	2×10^{-4}	4.9	14.8	0.9	0.0	1.0	0.02
0.31-0.36	0.036	17.7	7.2	0.9	0.0	1.0	0.74
0.36-0.46	0.05	20.2	6.7	0.9	0.0	1.0	0.77
0.46-0.56	0.18	41.9	4.6	0.8	0.0	1.0	0.82
0.56-0.70	0.06	23.4	6.2	0.8	0.0	1.0	0.80
0.70-0.78	0.22	50.3	4.2	0.8	0.0	1.0	0.85

Table 6.3: Numerical setup used in the simulation for rain-on-snow experiments conducted on the 15th of January 2019 in Kubová Huť at the forest site

	Parameter	LTE	ICENE
Regularization	Tr (K)	268.75	-
Space discretization	L (m)	0.78	
	dx (m)	0.075-0.01	0.001-0.1
Time discretization	t (s)	9000	
	dt_{min} (s)	1×10^{-4}	
	dt_{max} (s)	0.2	5
Picard method	iteration criterion	1×10^{-2}	1×10^{-4}
	max. iterations	20	20

in very different liquid water and temperature profiles. Fig D.5 shows the processed snow profile 2, highlighting the vertical distribution of the blue fraction together with measured liquid water content. The area fraction of the dark blue corresponds well to the vertical distribution of the measured liquid water content. Both post-experimental profiles were several cm less high than the pre-experimental profiles. Profile 1 showed no liquid water content as the rain did not propagate into this section. The temperature profile remained similar to the initial condition for the lower 50 cm, however some temperature effects are visible. Profile 2 clearly shows preferential flow paths as well as barriers. Fig. 6.9 shows simulated and measured liquid water content, density and temperature over depth after the experiment (150 minutes after initial sprinkling). With the regularized LTE model (rLTE) water freezes instantly resulting in a temperature profile more closely resembling that of profile 1, where rain did not penetrate the snow. Assuming that the liquid water does not freeze instantaneously allows the water to penetrate deeper into

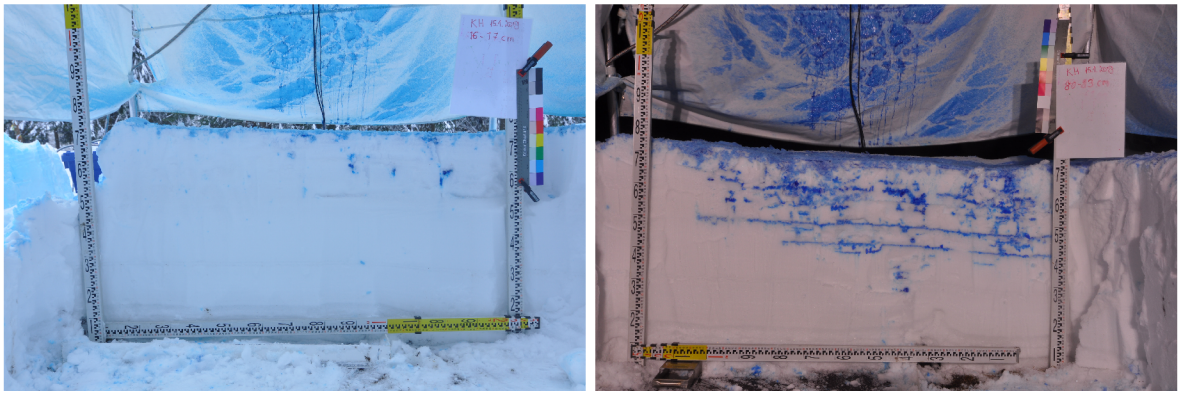

Figure 6.8: Profile pictures of post-experimental snowpits used for comparison. Profile 1 was dug 16-17 cm from the edge of the experimental board. Profile 2 was dug 80-83 cm from the edge of the experimental board. Photo credit: R. Juras.

the snowpack. The simulation with the full inflow of 11 mm h^{-1} results in a similar temperature profile to profile 2, which became completely iso-thermal during the experiment, and then started cooling again after the water inflow stopped. However, the measured liquid water content distribution was not presented well, as the ICENE model predicted more water to be in the snow and even reached the bottom of the snowpack and was thereby faster than the observations. The mismatch may be because snow properties derived from snow grain diameter and snow density measurements from the pre-experimental profiles used to setup the simulations did not cause capillary barriers. While taking measurements from the pre-experimental snow pits, the team took great care in trying to identify capillary barriers, as these were of great interest for the simulations. However, we did not identify significant changes in grain diameter and density between the upper snow layers, as such the retention and hydraulic properties remained similar. This might be an indication that lateral flow barriers are not traditionally capillary barriers, but perhaps due to changes in anisotropy of the hydraulic properties of snow. Further, the snow profile shows at least a two-dimensional flow, which may simply not be captured well by one-dimensional simulations.

Fig. 6.10 shows the liquid water content, ice content and temperature of the rLTE and ICENE simulations with full inflow of 11 mm h^{-1} over time in 10 minute stripes. For rLTE, in Fig. 6.10 a and c the liquid water accumulated at the surface and froze, which was indicated by an increased ice content at the very top. The initial temperature condition at the bottom of the profile was 0 °C at which no ice was present, which caused a significant amount of water to exist in the beginning of the simulation at the bottom of the profile. This is a strong indicator that Clausius-Clapeyron-based approaches may not yield accurate representation of the water-pressure-temperature relationship near 0 °C. In contrast, with

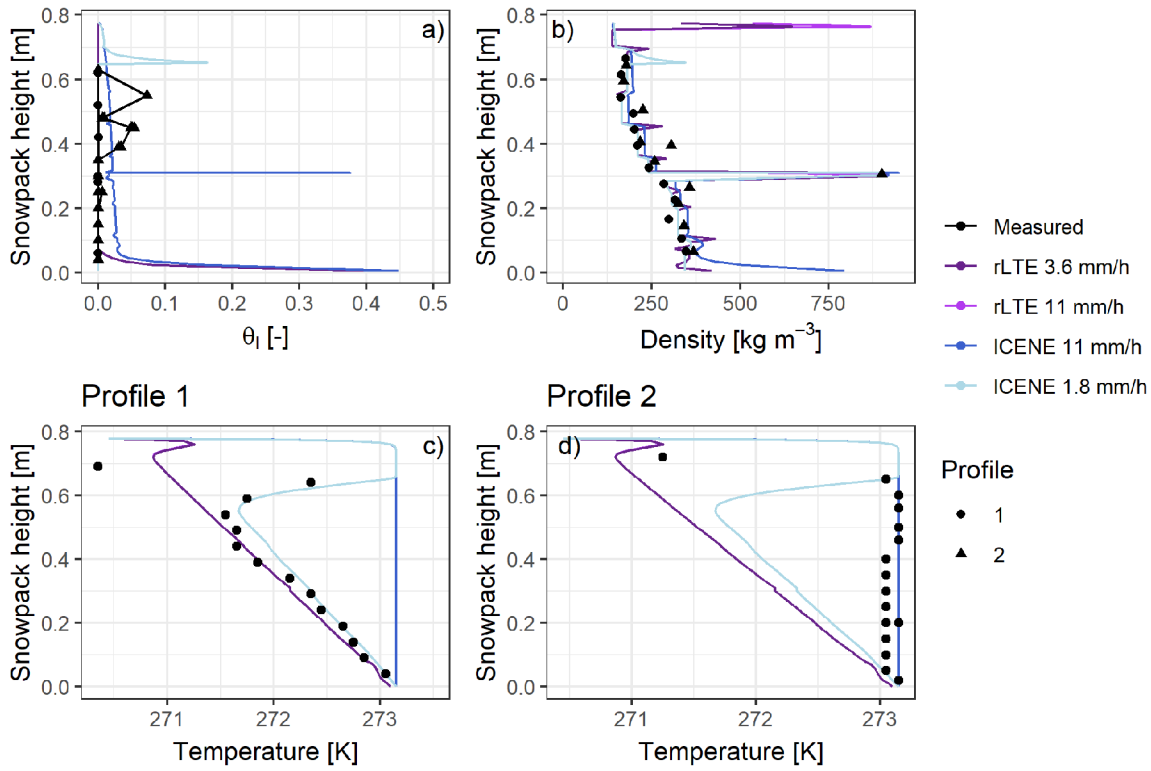

Figure 6.9: Simulations and measurements of liquid water content, density and temperature over snow height for two snow profiles of the rain-on-snow experiment conducted on the 15th of January 2019 in Kubová Huť (Forest site).

the ICENE model, the water infiltrates and accumulates at the ice layer at a snowpack height of 30 cm and at the bottom of the profile. Little thawing and freezing occurred because the initial temperature was already close to the freezing point, at which according to the formulation, no phase transition occurs. As soon as melt occured, the temperature decreased to 0 °C, which inhibited further melting.

6.4.6 Rain-on-snow experiment in Kubová Huť - Ski school site

The ROS experiment at the ski school in Kubová Huť was conducted on the 16th of March 2019. The site is close to the forest edge to avoid disturbance of the operation of the ski school. The interesting part about this site is that it receives natural as well as artificial snow from snow cannons. The snowpack height was only about 30 cm, and the temperature was around 0 °C and the snowpack was isothermal and moist. On the day of the experiment, slight sleet occurred.

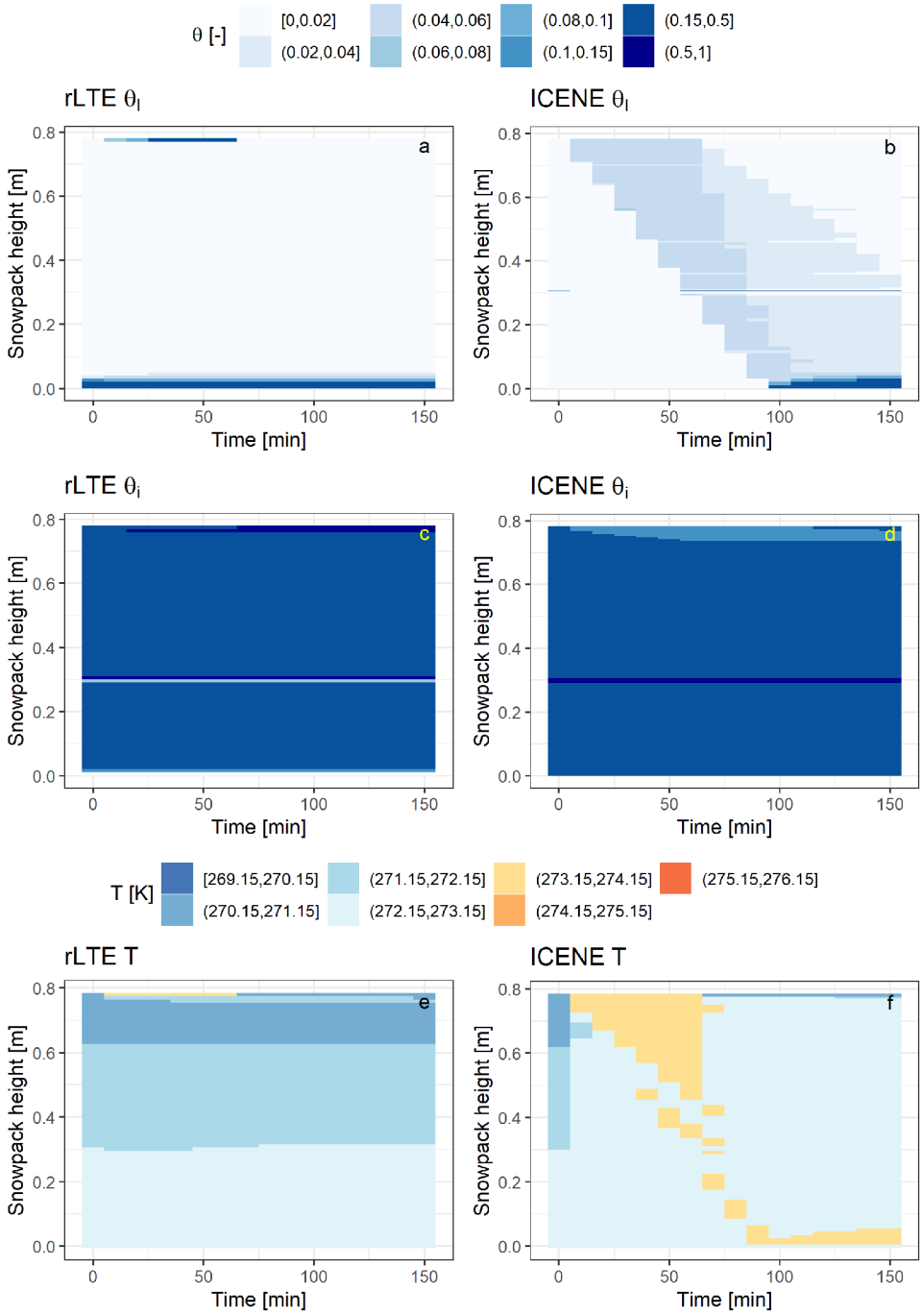

Figure 6.10: Simulated liquid water content, ice content and temperature over height in 10 minute stripes for the rLTE and ICENE models of the rain-on-snow experiment conducted on the 15th of January in Kubová Huť (Forest site).

Simulation setup

For the March experiment, only the ICENE model was used. This was because the snow was iso-thermal at 0 °C and the regularized LTE model would have predicted that no snow was present. Three materials were identified in the pre-experimental profiles. The hydraulic properties can be found in Tab. 6.4. The top boundary for the water flow equation was a time dependent Neumann condition, where the rain started after 60 s of simulation time with an intensity of 6.1×10^{-6} m s^{-1} (11 mm h^{-1}) lasting 1800 s (30 minutes). Outflow was first detected after 1260 s. For the rest of the period a zero-flux Neumann condition was assumed. Different boundary conditions for the bottom were selected in an attempt to recreate the outflow. First, a seepage face boundary was assumed, which switches from a zero-flux Neumann condition to a constant Dirichlet condition as soon as the snow is saturated. Second, a Neumann condition that switches from no-flow to a pre-defined flux at a pressure head threshold. Several different combinations of threshold and flux were tested. Presented are 1. No Outflow BC (seepage face switching at saturation). 2. Outflow BC 1, which switches at a pressure head of $h = -0.248$ m, and permits drainage of 11 mm h^{-1}. 3. Outflow BC 2, which switches at a pressure head of $h = -0.2$ m, and permits drainage of 5.5 mm h^{-1}. For the heat flow equation a constant Dirichlet condition of 0 °C for the top and bottom boundary was assumed. Zero-flux conditions were used as the bottom and top boundary condition for the ice equation, in order for ice to gain or lose mass through melt or thawing. The numerical setup is summarized in Tab. 6.5. The initial condition for temperature was iso-thermal at 0 °C. The initial condition for liquid water and density were more difficult to set due to the heterogeneity in the distribution. The density measurements of the snow already included liquid + dry snow and the dry snow density had to be estimated in order to calculate the liquid water content. For this, one dry snow density was assumed per layer, it was set in order for the liquid water content estimated from the measured emissivity values and the dry snow density to recreate the mean snow density (liquid + ice). The mean liquid water content at each height was then used to calculate a pressure head with the estimated cryo-functions that are also based on the dry snow density. The pressure head was then assigned as the initial condition to obtain liquid water content distribution matching the measurements (Fig. 6.12 a and b).

Results

Fig. 6.11 shows the post-experimental snow profile 45-48 cm from the edge of the experimental board. In addition, Fig. D.6 shows a processed snow profile picture, with the vertical distribution of the dark blue and the measured liquid water content. The flow pattern almost seems homogeneous, but is still

Table 6.4: Hydraulic and thermal parameter values used in the numerical simulation of the rain-on-snow experiment conducted on the 16th of March 2019 in Kubovka Hut at the ski school site.

Height	K_s	α	n	m	θ_r	θ_s
m	ms^{-1}	m^{-1}	-	-	-	-
0.00-0.15	0.0058	8.64	3.54	0.72	0	0.55
0.15-0.23	0.0161	13.13	3.72	0.73	0	0.62
0.23-0.30	0.0215	13.71	3.54	0.72	0	0.75

Table 6.5: Numerical setup used in the simulation for rain-on-snow experiments conducted on the 16th of March 2019 in Kubovka Hut at the ski school site.

	Parameter	ICENE
Space discretization	L (m)	0.3
	dx (m)	0.005
Time discretization	t (s)	10200
	d$tmin$ (s)	1×10^{-4}
	d$tmax$ (s)	0.2
Picard method	iteration criterion	1×10^{-4}
	max. iterations	10

dominated by wider preferential flow paths that bypass sections of the snow, which is also additionally highlighted in D.6. The top of the snow surface is clearly visible and also indicates that the rain did not enter the snow homogeneously. A clear barrier is visible between the most upper layer (0.23-0.30 m) and middle layer (0.15-0.23 m). The material barrier was also identified in the pre-experimental snow pit excavation. However, close inspection of the post-experimental snow pit photographs revealed minor lateral barriers not identified in the pre-experimental snow pit. Fig. 6.11 shows the temporal evolution of the liquid water content over depth. Ice content is not shown, as the temperature range did not allow for any phase change. The no-flow boundary condition predicted the greatest accumulation of liquid water at the bottom of the snowpack. Here, we can also clearly see the effect of the layering, as some water accumulated at a height of 0.23 m resulting from a clear difference in retention properties. Fig. 6.12 depicts the measured liquid water content and snow density prior to and after the experiment, and the measured and simulated liquid water content and snow density after the experiment, and the cumulative outflow over time. The measured liquid water content increased in the upper section of the snowpack, but also varied dramatically with measurements of water content ranging from 0 to 0.15 [-]. In the simulations, this was not recreated, instead the simulations indicate drainage of the two upper layers. This may be indicative that the hydraulic properties were not accurately estimated, as the retention ability of the middle layer was not captured well. This can have two reasons, either the cryo-functions used were not correct, or the input parameters (the grain diameter obtained from image processing and the estimated dry snow density)

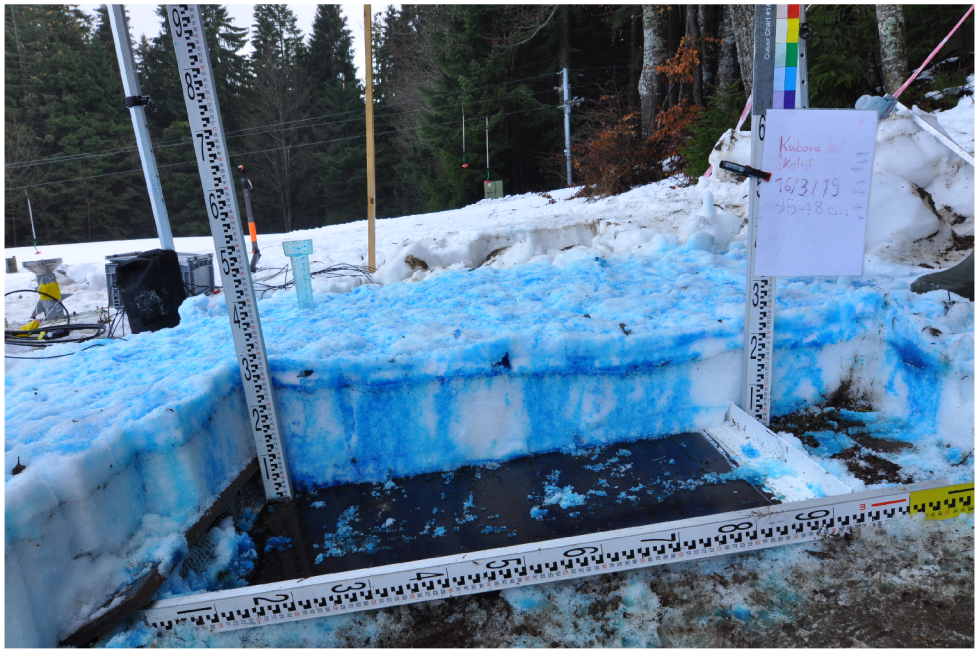

Figure 6.11: Photograph of snow profile after the rain-on-snow experiment on the 16th of March 2019 in Kubová Huť (Ski school site) taken 45-48 cm from the edge of the experimental board. Photo credit: R. Juras.

were incorrect. The estimates of the liquid water content values of the post-experimental snow pits also depend on the assumed dry snow density. Wet snow metamorphism may have caused the dry snow density to increase locally, which would have resulted in lower liquid water content calculations, as greater dry snow density would have increased the emissivity as well. The observed outflow was not simulated well by the simulations, even with the adapted boundary conditions. The observed outflow flux also never reached the input flux. This may be an indication that some of the water may have not propagated into the lowest snowpack layer. This is also supported by the lower liquid water content values around 10 cm height compared to the simulations. Instead, lateral flow may have left the area of interest, decreasing the vertical flux onto the experimental board. For outflow to occur, saturation should be present. The flow path is not strictly homogeneous, and water could have flown preferentially and the snow could thus have been saturated locally. This would have also caused the water to flow faster than predicted with the simulations. The large variation in measured emissivity and calculated liquid water contents also shows that large horizontal differences existed, which supports this theory.

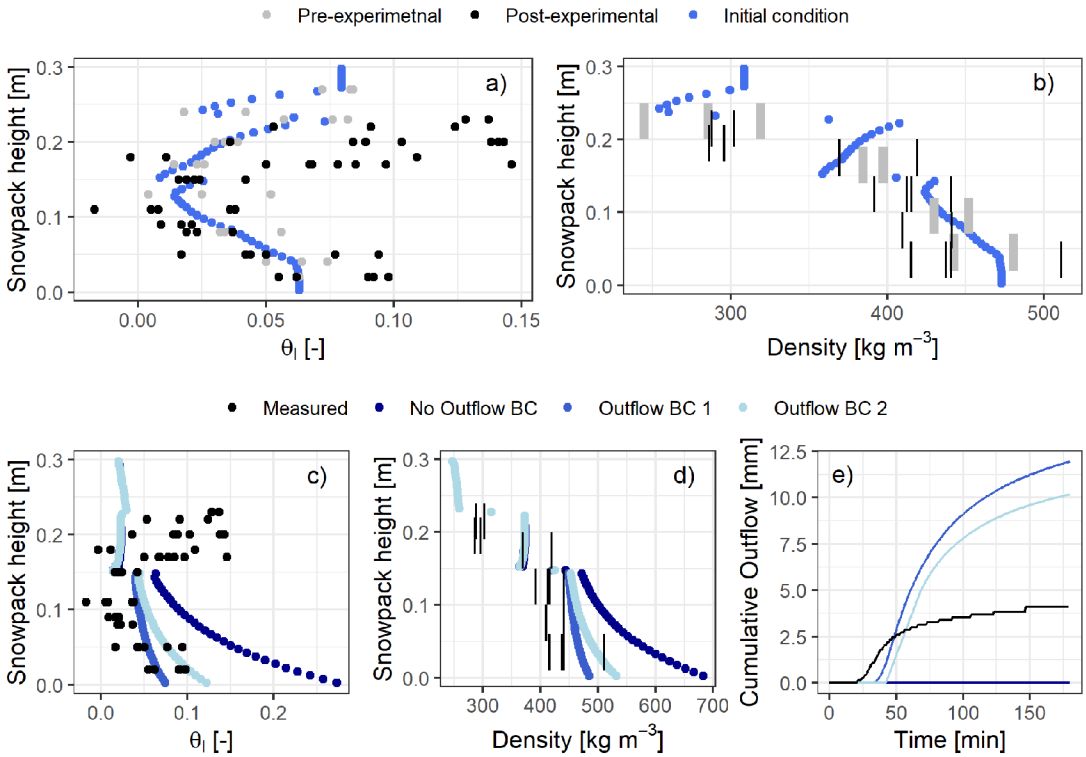

Figure 6.12: Measured pre-experimental and post-experimental of a: liquid water content and b: snow density (liquid + dry snow) with a: initial liquid water content and b: initial snow density used for simulations; Post-experimental measured and simulated (180 minutes after initial sprinkling) for c: liquid water content and d: snow density (liquid + dry snow); e: Cumulative outflow over time of the rain-on-snow experiment on the 16th of March 2019 in Kubová Huť (Ski school site)

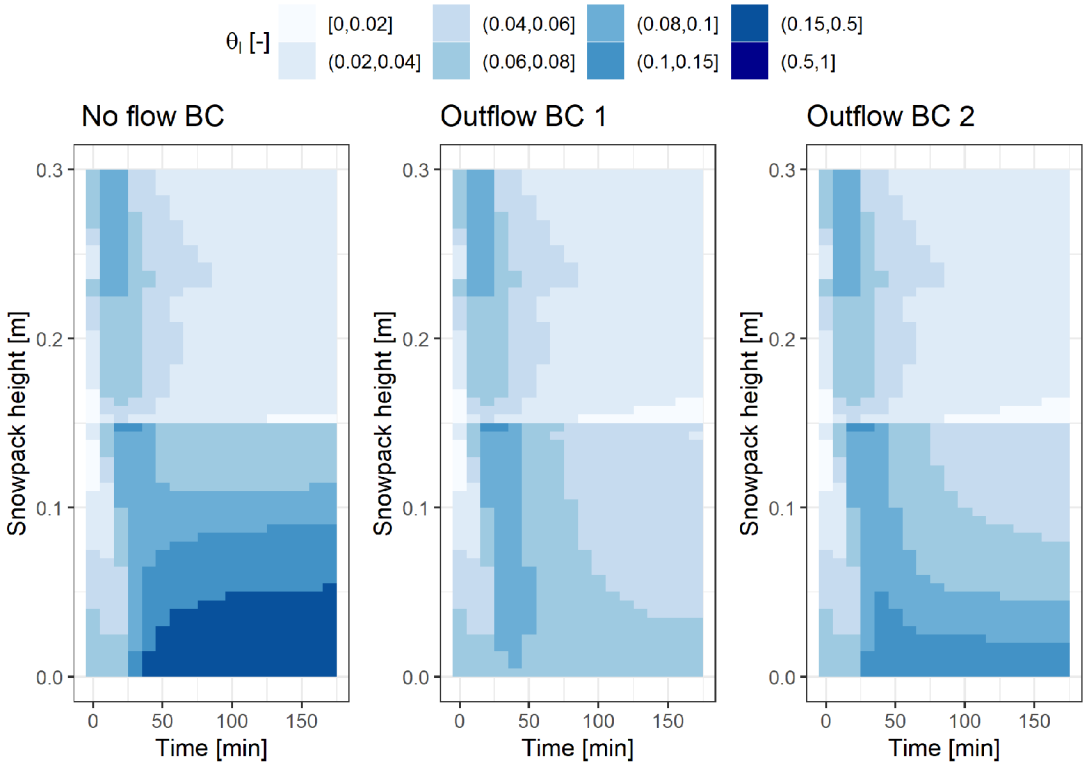

Figure 6.13: Simulated liquid water content, ice content and temperature over height in 10 minute stripes for the rLTE and ICENE models of the rain-on-snow experiment conducted on the 16th of March 2019 in Kubová Huť (Ski school site).

6.4.7 Discussion

Two rain-on-snow experiments conducted in January and March 2019 at different sites in Kubová Huť were simulated with one-dimensional coupled heat and water flow model setups. The results indicate that the model based on the Clausius-Clapeyron equation may not be suitable to model water and heat flow in snow as initial conditions and instantaneous melting at 0 °C do not reflect the physics in snow well. The model assumes that the porous medium is completely liquid at 0 °C, which is the temperature at the bottom of the snow between the snow-soil interface. This model therefore fails to reproduce the dual existence of liquid water and snow at 0 °C. The ICENE model was adapted to estimate melting and freezing on a heat-based approach, and was therefore not the non-equilibrium companion to the rLTE model. The heat-based approach allows that liquid water and ice can co-exist at 0 °C.

The lateral barriers produced in the first ROS experiment did not seem to be explained by capillary barriers, at least the retention and hydraulic conductivity values derived based on density and grain diameter measurements did not result in functions that would have allowed the reproduction of capillary barriers. This is why the author would like to bring forward the idea that the progression of liquid water from the top may change the snow grain structure in a way to induce lateral instead of vertical flow, where a parameterization of anisotropy could be dependent on some melt rate. Closer inspection of the flow patterns even indicates that some lateral barriers exist between every single snow material boundary, which should be explored further. Calonne et al. (2012) explored anisotropy in the permeability of snow and found that especially depth hoar can exhibit anistropic behavior. For the second rain-on-snow experiment, dry snow density values were unknown and had to be derived based on wet snow density measurements and Denoth meter emissivity readings. This introduced uncertainties, which made it difficult to reproduce hydraulic parameters. Whereas no outflow was observed in the first experiment, some outflow was observed in the second experiment, which could not be recreated. This may also be due to the complex flow behavior, i.e. preferential flow. Although the second snowpack was less heterogeneous, its layering could only be partially predicted based on the snowpit observations of the pre-experimental profile. This might indicate that even small differences in observed snow properties can cause lateral flow barriers, which cannot be explained with effective mean grain diameter and density. Measurements of liquid water content are only point-based and we show how the blue fraction of dark blue corresponds to liquid water content. It may be promising to create a database of dyed snow with measurements of liquid water content to be used for further image processing to obtain estimates of liquid water distribution from photographs.

Parameterizations of flow parameters are usually defined by snow structure variables such as grain

size and density. Additional snow microstructural variables such as bond size, dendricity and sphericity determine the grain type (Lehning et al. 2002). These variables are even more difficult to objectively determine in the field, but are important for the evolution of the snow pack and may be necessary to determine more accurate parameterizations in the future.

Although examples of diffusive flow were reproduced in some ROS experiments, water in the experiments presented here moved preferentially, which should be included in the modeling. Some researchers attribute preferential flow paths to heterogeneities in the snowpack properties (Marsh and Woo 1985b). Different approaches to simulate preferential flow currently exist using the Richards equation. The first is to assume two different flow domains, which can also be used in one-dimensional models, and second to define heterogeneous material properties. However, preferential flow may also be induced due to heterogeneity in the boundary conditions, i.e. heterogeneity of rain, which for snow remains unexplored. Examples of the first include Wever et al. (2016) and Würzer et al. (2017) who divided the flow process in snow into two domains: a matrix and a preferential domain. They applied a so-called dual-domain approach developed to represent preferential flow in soils as in Germann (1990) and Gerke and Genuchten (1993). This approach was scrutinized by Leroux and Pomeroy (2017) as it is not physical for snow. In soil, a dual domain system is often present due to root canals, earth worm channels and fractures, which are absent in snow. Snow has not been described as a porous medium with a dual system containing both macropores or fractures and matrix domains. However, snow can exhibit complex ice layers and channels. The dual domain approach may be useful to recreate preferential flow behavior, but it is doubtful whether it has predictive qualities as it lacks physical meaning in its present stage. Hirashima et al. (2014) and Leroux and Pomeroy (2017) developed multi-dimensional transport models for snowpack in order to reproduce preferential flow and visualize preferential flow paths in infiltration experiments. The liquid water fluxes were calculated with mixed-form formulation where water between voxels for wet snow would move according to the Darcy-Buckingham law, and for dry snow according to a different artificial gradient, which was dependent on the grain size. Here, preferential flow only occurred when an adapted flux formulation was used in combination with heterogeneity. To create heterogeneity, the density and grain size were randomly varied in each voxel, which were then used as input parameters for cryo transfer functions. Consequently, Hirashima et al. (2014) found that that the preferential flow path was negatively correlated to grain size, and positively correlated to water supply rate. Moreover, grain size and grain density both affect the size of preferential flow paths and the arrival time of the liquid water at the base. A similar modelling approach was recently put forward by Kmec et al. (2021) to create fingering flow using

a two-dimensional semi-continuous model, where the Darcy-Buckingham law is also adapted. Kmec et al. (2021) show that preferential flow paths highly depend on the initial saturation. This is also observed in snow, where the tendency to form preferential flow is greater in dry cold snowpacks. In contrast to these simulations, Katsushima et al. (2013) conducted experiments on preferential flow in snow and concluded that fingering flow occurs in initially homogeneous snow. This was also supported by experimental findings by Avanzi et al. (2017) using CT scans, who show that wet snow metamorphism can be very localized and heterogeneous and thereby change the porous medium. So far, however, these effects can only be recreated with an initially heterogeneous varying distribution of hydraulic properties with some sort of adaptation of the Darcy-Buckingham law, where water could only move down or sideways, but not diagonally. Some empirical equations for wet snow metamorphism exist that allow the simulation of an increase in grain size with moisture and temperature. For homogeneous snow to become heterogeneous, a stochastic process could be introduced for snow metamorphism based on these equations that would then create spatial variability.

6.5 Conclusion

In this chapter, two models for freezing and thawing of soils were adapted for snow. These models were tested on synthetic infiltration examples and two rain-on-snow experiments that were conducted in 2019. For the synthetic infiltration, only the ICENE model with a high non-equilibrium time constant resulted in similar distributions to the original proposed by Illangasekare et al. (1990) and reproduced by Daanen and Nieber (2009). Their models neglected heat convection, but both considered instantaneous freezing. It was shown that neglecting heat convection can mask the non-equilibrium of the ice-phase. The first model adapted for snow is the regularized model based on the Clausius-Clapeyron equation and assumes instantaneous freezing. One major assumption that had to be made was a saturated water content of 1, as a total hydraulic head is derived that accounts for both the ice and liquid water content. The model assumes that the porous medium is completely liquid at 0 °C, which is the temperature at the bottom of snow between the snow-soil interface. This model therefore fails to reproduce the dual existence of liquid water and snow at 0 °C. The ICENE model was adapted to estimate melting and freezing on a heat-based approach, and was therefore not the non-equilibrium companion to the rLTE model. The heat-based approach allows that liquid water and ice can co-exist at 0 °C. This model is reliant on adequate time steps, which means that the time constant should not be smaller than the time step.

Hydraulic and thermal properties were calculated based on effective mean grain size and dry snow

density. We show that despite detailed knowledge of these two parameters, they are not sufficient to reproduce the heterogeneity and were not sufficient to reproduce lateral barriers at material boundaries. A limitation of this study was the use of a one-dimensional model setup. The one-dimensional model assumes that the vertical gradient outweighs horizontal gradients. Both experiments showed that this may not be applicable. For a two-dimensional model, the development of parameterization for anisotropy may be vital.

There is experimental evidence that capillary barriers are important in snow (Katsushima et al. 2013), but the prevalence of preferential flow makes it questionable whether capillary forces and hydraulic functions based on these forces provide a promising way forward.

Chapter 7

Conclusion

7.1 Summary of thesis

In this thesis several coupled water and heat flow models for freezing soil and snow were developed and implemented into DRUtES, and are now available for everyone to use and modify. A novel parameterization for non-equilibrium freezing was developed for freezing soil, which can be used to simulate freezing and thawing. To allow liquid water and snow to exist at 0 °C, a heat based non-equilibrium model was developed and implemented. Several rain-on-snow experiments were conducted and processed to be used for model testing. Further tools were developed in cooperation with several master students to analyze these experiments. These include an R package for image processing of flow paths, as well as methodologies for grain size analysis. The results of this thesis showed that the application of regularization of the discontinuous term successfully stabilizes the computation and can remove oscillations in freezing and thawing soil. As the degree of regularization is problem dependent, a simple method to determine optimal regularization parameters was presented. Simulations of volumetric water content and temperature profiles of previously published soil freezing experiments are represented well. This approach can be added to other codebases and the method therefore allows for broad applicability. For the non-equilibrium ice-phase model, the change in the ice content was solved in a separate equation and then linked back as a non-linear zero-order term. The zero-order term contains a non-equilibrium time constant and we found these time constants can vary dramatically. With freezing soil experiments, it was shown that higher equilibrium constants can successfully decrease overestimation reported, but also inhibits the propagation of the freezing front into freezing soils. Non-equilibrium ice-phase models therefore seem promising, but the parameterization may need to be adjusted to depend on the speed of temperature change.

For snow, hydraulic and thermal properties are difficult to measure. Some simple cryo-transfer functions based on snow's density and mean snow grain diameter exist. Snow exhibits very steep retention properties. With retention properties based on the snow grain and snow density, the moisture distribution and outflow are difficult to recreate. In this thesis, we confirm that snow often results in complicated flow patterns, showing fingering flow and horizontal flow structures. Some of the horizontal flow structures seemed like capillary barriers, which were impossible to predict based on data from pre-experimental snow pit measurements. Specifically, no remarkably strong difference in grain size and dry snow density were observed, which are the important input values to state-of-the-art cryo-transfer functions for hydraulic properties. It may be that additional mechanisms have to be taken into account to understand how lateral flow patterns are created. One aspect may be to look at anisotropy of permeability of snow. Further, we confirm that the heterogeneity in flow patterns makes it difficult to take representative point measurements of moisture and temperature that can be used for comparison. We also show that image processing could help to obtain a general overview of flow paths after the experiment and may be used to obtain a fast automated overview of preferential flow paths and lateral flow structures as well as regions indicating moisture.

7.2 Fulfillment of targets

In this thesis numerical models of water and heat flow for freezing soil with two different assumptions were derived and implemented into DRUtES and subsequently adapted to simulate water and heat flow in snow. This thesis showed successful applicability of regularization in managing oscillations on a coupled water and heat flow model in freezing soil. A novel parameterization for non-equilibrium freezing was developed for freezing soil, which can be used to simulate freezing and thawing. This thesis presented the limited applicability of instantaneous freezing derived with the Clausius-Clapeyron equation in modeling coupled water and heat flow in snow. We presented a non-equilibrium freezing formulation which allows the existence of liquid water and ice to be present at 0 °C.

7.3 Further extensibility and recommendations

7.3.1 Numerical Modeling

For one-dimensional coupled problems, LU decomposition is implemented for sparse matrices. Since the distance between diagonal and non-diagonal bands is always equal to the block sub-matrix dimension,

non-efficient overfilling of the sparse matrix can be prevented with a reordering mechanism. In our implementation we use the Cuthill-McKee algorithm (Cuthill and McKee 1969) with details in Saad (2003). The Cuthill-McKee algorithm is designed for symmetric-positive-definite matrices. However, due to non-symmetric coupling terms and the convection term in the heat flow equation, the matrix is non-symmetric. With this approach, a strong regularity of the reordered matrix and an optimal pivot selection (see Cheney and Kincaid (2008)) is not guaranteed, nor is assigning non-zero to diagonal elements, which could lead to a solver failure (division by zero). The reordering has not yet been implemented for the ICENE model. Here, the ice term should be decoupled, which would allow the use of the reordering mechanism on the water and heat flow blocks. Further extensibility of the models include the ability to efficiently compute two-dimensional problems. Due to the modular setup of DRUtES, the model itself is implemented, but still requires an efficient and robust solver. However, the matrix structure poses some challenges due to lack of diagonal dominance and high eigen-values leading to high condition numbers. The default algorithm for non-symmetric matrices is a conjugate gradient for normal equations, and development of pre-conditioners is vital.

7.3.2 Hysteresis, lateral and preferential flow in snow

Snow is a non-conservative medium and hysteresis would be an ambitious extension to include. Two types of hysteresis could be considered. First, a porous medium is not only defined by one, but two retention and conductivity curves, which are different for wetting and drying. Scaling functions exists, such as Kool and Parker (1987), however, no experimental data exists and this form of hysteresis has only been used in (Leroux and Pomeroy 2017). More snow specific is snow metamorphism, which is the change of grain structure due to temperature or moisture. Examples include a formulation by Brown et al. (2001), where the grain growth is updated based on temperature and sphericity under dry conditions and Brun (1989), who developed an equation for grain growth for wet snow metamorphism. The updated grain diameter and density can then be used to update retention parameters, saturated conductivity and thermal conductivity. Further, it was hypothesized that the anisotropy may be an important factor to create lateral flow in snow. However, currently no parameterization exists to formulate anisotropy, although findings by Calonne et al. (2012) would support this. Several studies have shown that heterogeneity itself is not sufficient to reproduce preferential flow, but that the flux formulation is also important. Moreover, experimental evidence exists that show that initially homogeneous snow can produce heterogeneous properties due to snow metamorphism which aid preferential flow paths. A probabilistic approach to snow metamorphism

may be key to allow homogeneous snow to become heterogeneous.

Local thermal non-equilibrium

Most coupled water and heat flow models are based on the assumption of local thermal equilibrium (LTE) between the phases. However, local thermal non-equilibrium (LTNE) is the known intrinsic state for the infiltration of liquid water infiltrating into a frozen porous medium. In such non-equilibrium conditions, the standard approach of LTE models may no longer be valid because the infiltrating water can have a different temperature than the solid matrix. To address this, one could use separate heat equations with separate phase temperatures for each phase, which can exchange heat between each other. Separating the phase temperatures would also permit the assumption that the temperature dependence of the hydraulic parameters for the liquid water movement would be limited to the liquid water phase temperature. Being able to assign separate phase boundary conditions could provide a more thermodynamic consistent formulation and thus the LTNE approach could help to model infiltration into frozen soil or snow more physically. Heinze and Blöcher (2019) derived an LTNE model for unfrozen unsaturated soil, which was recently extended to freezing soil in Heinze (2021). However, Heinze (2021) did not include aspects commonly considered such as the temperature dependence of the redistribution of water. The freezing rate is also instantaneous, but based on available heat and not based on the Clausius-Clapeyron equation, which means that liquid water cannot exist at sub-zero temperatures and would completely freeze.

7.3.3 Experiments and processing of experimental data

After the first round of experiments in 2019, considerable effort went into designing an improved setup with more photographic equipment. Unfortunately, due to lack of snow in the beginning of 2020, followed by Covid-related restrictions, no further experiments were conducted in 2020. The improvements included the purchase of an infrared camera to obtain estimates of specific surface area, which can be used to obtain profile wide estimates of grain size. As part of a master thesis by Dytrt (2020), a new frame design to take profile pictures was proposed and constructed. Additionally, crystal cards used to determine snow type and grain size were redesigned to improve grain size estimates based on image processing. Processing these photos to obtain effective mean grain size is not simple, and further research on suitable automated algorithms is needed. Bello (2019) started processing photographs of previous snow profiles after dye tracer experiments, which laid the foundation to improve the image processing to automate identification of flow structures and would allow to better visualize the variability of lateral and preferential flow paths

caused by rain-on-snow events.

Appendix A

Data and Code

The models were implemented into the open-source codebase DRUtES. The code is freely available and accessible on github `https://github.com/michalkuraz/drutes-dev`, with more information on system requirements on `www.drutes.org`.

For freezing soil, data used for model validation was obtained by digitizing experiments in Jame (1977), Jame and Norum (1980) and Hansson et al. (2004).

The R package "Bluesnow" is available on: `https://github.com/Jorub/bluesnow`.

Appendix B

Appendix to Chapter 4

Fitting Soil hydraulic and Thermal Properties for the Jame Experiments

For the Jame experiments, both the retention curve and thermal conductivity were fitted to existing data. The retention curve in Fig. B.1 a was estimated from the soil freezing curve data $\theta(T)$ in Jame and Norum (1980). For the conversion, we assumed that the soil was saturated ($h_w = 0$) and $T_f = 273.15$ K. Following Eq. (4.2), we can calculate h_l [m]:

$$h_l = \frac{Lf}{g} \ln \frac{T}{T_f}. \tag{B.1}$$

We used an extended version of the Campbell (1985) parameterisation to model thermal conductivity. We used the unfrozen thermal conductivity measurements in Jame and Norum (1980) to fit the model of Campbell (1985) (Fig B.1 b).

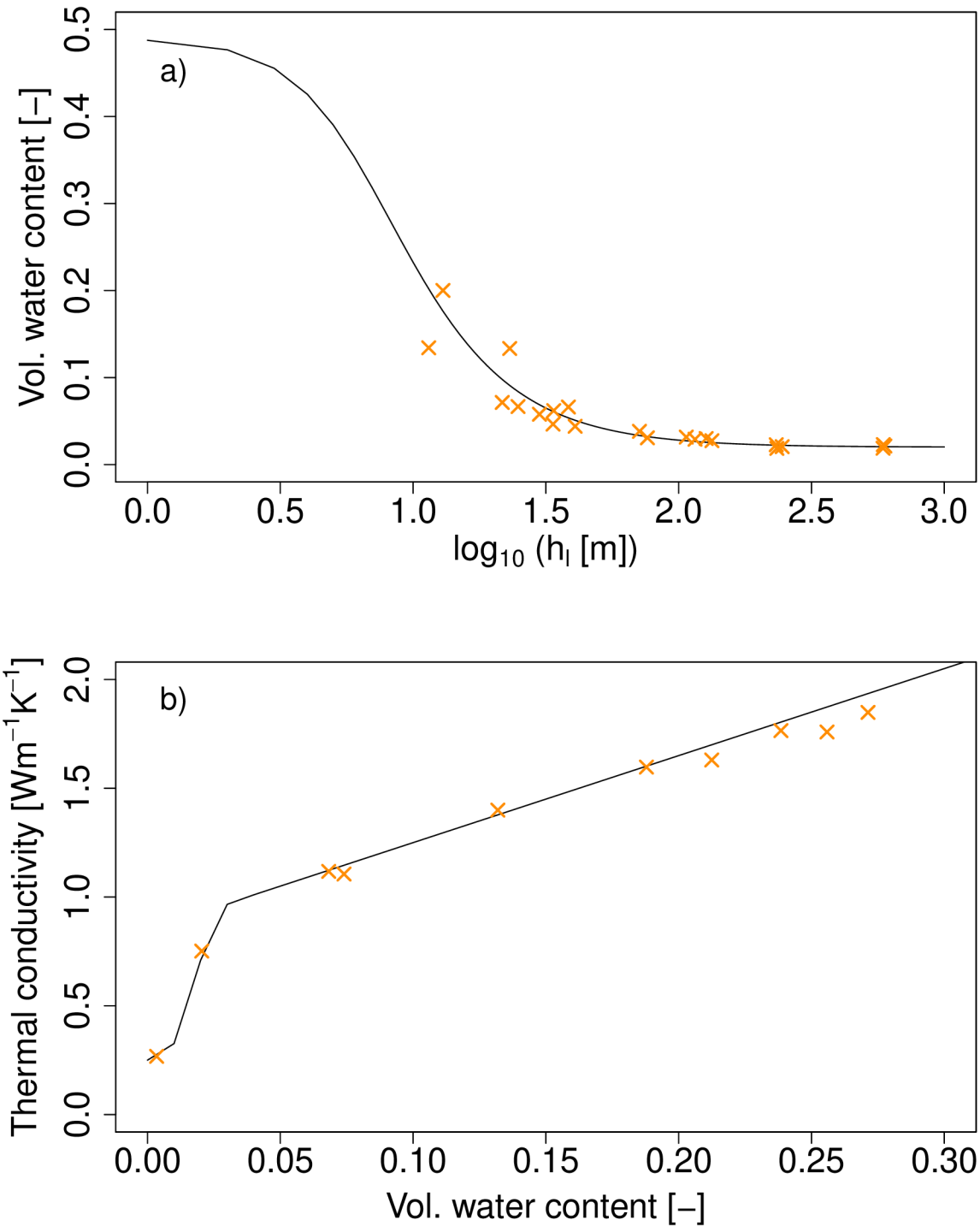

Figure B.1: Models of a) retention curve, b) thermal conductivity (unfrozen), where the black line represent the fit used in the simulations and the orange x represent measured or derived data.

Implementation of the model into DRUtES

DRUtES contains a PDE-pointer system that allows for the implementation of coupled models.

Table B.1: Implementation of the coupled model with freezing according to the DRUtES implementation structure

pde	process	water	heat
	solution	H_w	T
water	capacity	$C(h_w) + (\frac{\rho_i}{\rho_l} - 1)(C(h_w) - C(h_l))$	$(-(\frac{\rho_i}{\rho_l} - 1)C(h_l)\frac{\mathrm{d}h_l}{\mathrm{d}T}$
water	diffusion	K_{lh}	$K_{lh}\frac{\mathrm{d}h_l}{\mathrm{d}T} + K_{lT}$
heat	capacity	$T(C_l C(h_l) + C_i(C(h_w) - C(h_l)) - C_a C(h_w))$ $- (C(h_w) - C(h_l))\, L f \rho_i$	$C_p + T(C_l - C_i)C(h_l)\frac{\mathrm{d}h_l}{\mathrm{d}T} + C(h_l)\frac{\mathrm{d}h_l}{\mathrm{d}T} L f \rho_i$
heat	diffusion	$C_l T K_{lh}$	$\lambda + C_l T(K_{lh}\frac{\mathrm{d}h_l}{\mathrm{d}T} + K_{lT})$
heat	advection	$C_l \vec{q_l}$	

Integrating the Liquid Pressure Head

In order to obtain h_l after the regularization of $\frac{\mathrm{d}h_l}{\mathrm{d}T}$, we need to perform numerical integration on $\frac{\mathrm{d}h_l}{\mathrm{d}T}$ when $\mathrm{T} < \mathrm{T}f$:

$$h_l = h_w + \int_{T_f}^{T} \bar{\Phi}r(T)\frac{\mathrm{d}h_l}{\mathrm{d}T}\mathrm{d}T \tag{B.2}$$

We calculate temperatures bounds $T_{\bar{\Phi}r} = \{T_f, ..., T\}$ depending on the regularization with narrower intervals for steeper curves up to $\bar{\Phi}r(T) = 1$ for the numerical integration. We use three-point Gaussian quadrature to numerically integrate across these bounds. If $T \leq T_r$, the following would be calculated:

$$h_l = h_w + \frac{Lf}{g}\ln\frac{T}{T_r} + \sum_{i=1}^{n}\int_{T_{\bar{\Phi}r}(i)}^{T_{\bar{\Phi}r}(i+1)} \bar{\Phi}r(T)\frac{\mathrm{d}h_l}{\mathrm{d}T}\mathrm{d}T, \tag{B.3}$$

where $T\bar{\Phi}r = \{T_f, ..., T_r\}$ and T_r is the temperature at $\bar{\Phi}r(T) = 1$. If $\bar{\Phi}r(T) < 1$, the model calculates h_l from $T\bar{\Phi}r = \{T_f, ..., T\}$ as follows:

$$h_l = h_w + \sum_{i=1}^{n}\int_{T_{\bar{\Phi}r}(i)}^{T_{\bar{\Phi}r}(i+1)} \bar{\Phi}r(T)\frac{\mathrm{d}h_l}{\mathrm{d}T}\mathrm{d}T. \tag{B.4}$$

Discrete Representation of the Coupled Model

The resulting governing equations (4.33) were implemented into our in-house project DRUtES (Kuraz et al. 2020), where the spatial derivatives are approximated by the continuous linear Galerkin finite element method and the temporal derivatives are approximated by the implicit Rothe method. DRUtES has been successfully applied to a range of real world and theoretical cases combining the Richards equation and the advection-dispersion-reaction equation (Kuraz et al. 2013b; Kuraz et al. 2013a; Kuraz et al. 2015). The weak formulation for a similar coupled problem implemented in DRUtES (particularly dual permeability regime for Richards equation and advection-dispersion-reaction equation) is given in Kuraz et al. (2013b). More simple explanations for the standard Richards equation are given in Kuraz et al. (2013a). The non-linear operator has been treated by a fixed point (Picard) iteration scheme. We use an adaptive time step scheme, where the time step is controlled by the convergence rate of the Picard iteration.

Following the methodology given in Kuraz et al. (2013b), for each time and iteration level the resulting governing equations (4.33) are discretely represented by a sparse matrix $\mathbf{A}$, vector $\vec{x}$ and b-side vector $\vec{b}$.

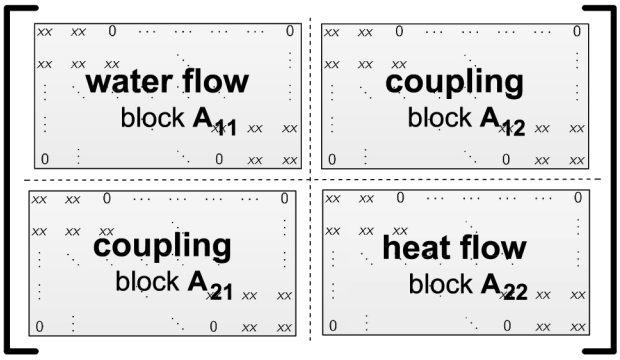

Figure B.2: Scheme of discrete matrix representation of (4.33).

For each iteration level, we solve a system, which can be block-wise represented as

$$\begin{pmatrix} \mathbf{A}_{11} & \mathbf{A}_{12} \\ \mathbf{A}21 & \mathbf{A}_{22} \end{pmatrix} \begin{pmatrix} \vec{x}H_w \\ \vec{x}T \end{pmatrix} = \begin{pmatrix} \vec{b}H_w \\ \vec{b}T \end{pmatrix}, \tag{B.5}$$

where block $\mathbf{A}_{11}$ represents operations with the unknown Hw in the water flow equation (Richards equation), coupling block $\mathbf{A}_{12}$ represents operations with the unknown T in the water flow equation, coupling block $\mathbf{A}_{21}$ represents operations with the unknown Hw in heat flow equation, block $\mathbf{A}_{22}$ represents operations with the unknown T in heat flow equation, sub-vectors $\vec{x}H_w$ and $\vec{x}T$ are approximation coefficients for unknown Hw and T, sub-vector $\vec{b}Hw$ and sub-vector $\vec{b}T$ are the b-side vectors for unknown Hw and T, see figure B.2. For one-dimensional problems the discrete represention of (4.33) is a 2×2 block matrix, where each block is a 3-diagonal matrix.

Solving the discrete system

A popular strategy to solve the coupled system (B.5) is to decouple it into water flow and heat flow blocks and employ an iterative scheme, such as the block-Jacobi method, to solve the entire coupled system (B.5) iteratively. In this approach, one diagonal block (flow equation) is solved after the other and inner iterations are performed. This technique e.g. Jacobi/Gauss-Seidel, is only highly efficient if the diagonal blocks **A**11 and **A**22 are dominant (Saad 2003; Golub and Loan 1996; Varga 2000). Under freezing, the coupling blocks **A**12 and **A**21 involve non-zero capacity terms (i.e. time step divisions) and the diagonals of the coupling blocks reach values of similar magnitude as the diagonals of the main blocks. Reducing the time step cannot improve the diagonal dominance of the main blocks. Therefore, application of block

Jacobi/Gauss-Seidel iterative schemes under freezing may result in convergence failures. In contrast, for the dual permeability model (Gerke and Genuchten 1993), where the coupling blocks are constructed out of first order transfer terms, reducing the time step can improve diagonal dominance of the main blocks, and so the application of block-wise iterations techniques can be efficient. And so we propose to solve the entire system (B.5) at once (without employing any inner iteration scheme), which requires slightly more sophisticated approaches regarding computer memory and numerical linear algebraic techniques.

For one-dimensional problems, we apply direct LU decomposition implemented for sparse matrices. Since the distance between diagonal and non-diagonal bands is always equal to the block sub-matrix dimension, we can prevent non-efficient overfilling of our sparse matrix with a reordering mechanism. In our implementation we use the Cuthill-McKee algorithm (Cuthill and McKee 1969), for a detailed description of the algorithm, we refer to Saad (2003). The Cuthill-McKee algorithm is designed for symmetric-positive-definite matrices. However, due to non-symmetric coupling terms and the convection term in the heat flow equation, the matrix and is non-symmetric. With this approach, a strong regularity of the reordered matrix is not guaranteed. It means that we cannot guarantee an optimal pivot selection (see Cheney and Kincaid (2008)), or assigning non-zero to diagonal elements, which could lead to a solver failure (division by zero). For details about the strong regularity we refer to Fiedler (2013). Note, we haven't experienced any solver failures during any of our simulations. A check of the diagonal values could help detect solver failures, and one could switch to an iterative solver such as conjugate gradient for normal equation or GMRES.

Freezing and thawing problems can have high condition numbers, which can strongly effect the convergence of iterative solvers, which are required for 2D and 3D problems. Developing pre-conditoners that lower the condition number are vital. A similar study as to that of Gohardoust et al. (2021), who compared the efficiency of a range of pre-conditioners and iterative solvers for water and solute transport may be helpful in finding the most efficient setup for freezing and thawing problems in porous media.

Appendix C

Appendix to Chapter 5

C.1 Implementation of the model

Table C.1: Implementation of the non-equilibrium ice phase model

pde	process	water	heat	ice
	solution	H_l	T	θ_i
water	capacity	$C(h_l)$	-	-
water	diffusion	K_{lh}	K_{lT}	-
water	0 order reaction	$-\frac{\rho_i}{\rho_l} v_f$	-	-
heat	capacity	$T(C_l - C_a)C(h_l)$	C_p	
heat	diffusion	$C_l T K_{lh}$	$\lambda + C_l T K_{lT}$	.
heat	advection	$C_l \vec{q_l}$	-	.
heat	0 order reaction	$(L_f \rho_i) v_f$	-	-
heat	1st order reaction	$-(C_i - C_a) v_f$	-	-
ice	capacity	-	-	1
ice	0 order reaction	-	-	v_f

C.2 Model comparison

Model verification of the ICENE model without freezing is depicted in Fig. C.1 and with freezing in Fig. C.2. rLTE freezes faster, but in this example ICENE "catches-up". We see the delay of freezing with β_f = 2000 s in comparison to β_f = 1000 s.

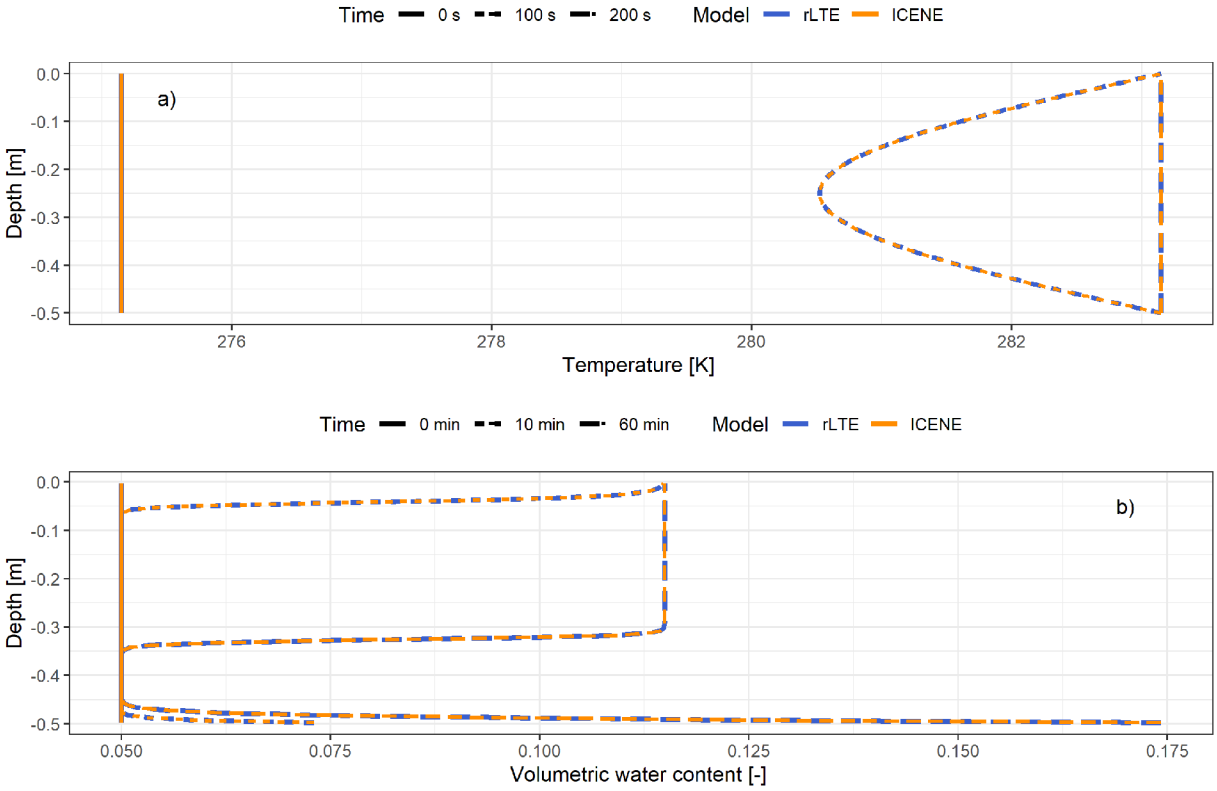

Figure C.1: Model comparison of rLTe and ICENE model without freezing. a: Temperature experiment where the profile warms up until a steady-state temperature profile is reached b: Infiltration of water into soil.

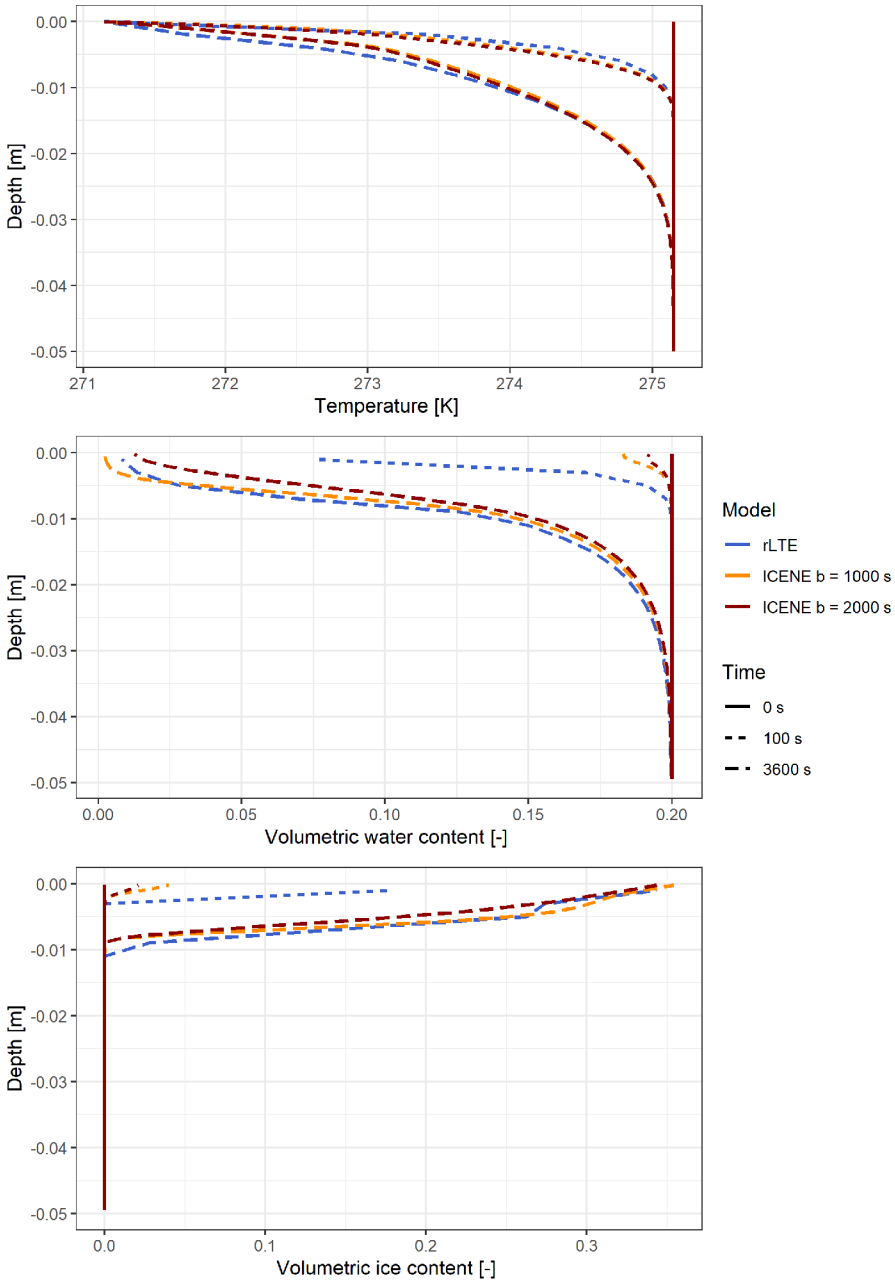

Figure C.2: Simulated temperature, volumetric water content and volumetric ice content with rLTe (blue) and ICENE model with two equilibrium constants (β_f = 1000 s in orange and β_f = 2000 s in dark red) modeling freezing

Appendix D

Appendix to Chapter 6

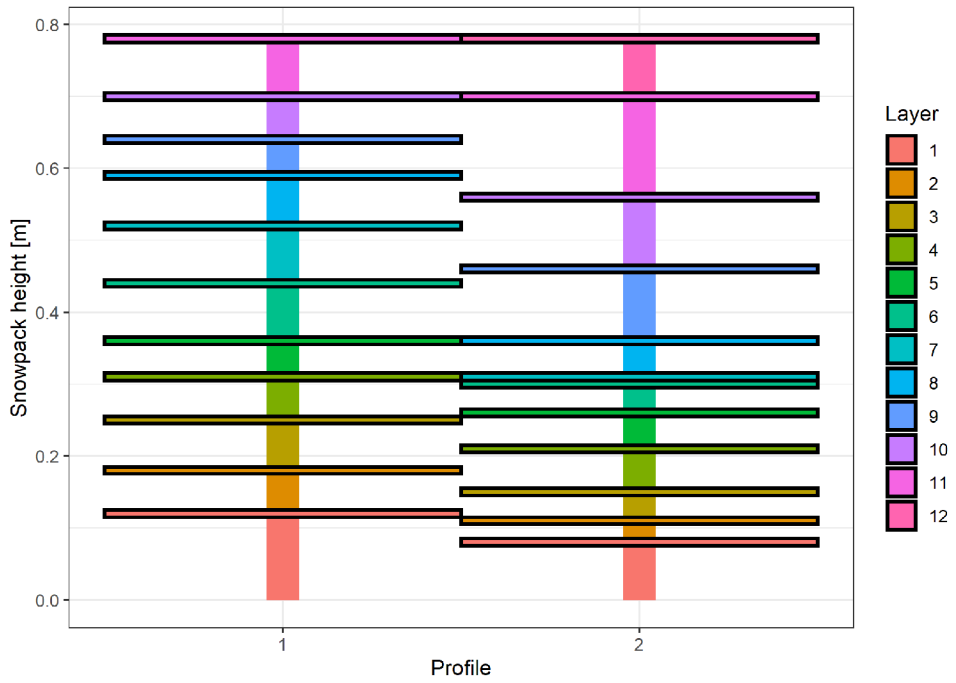

Figure D.1: Identified layers based on snow structure, hardness and changes in density for Kubova Hut.

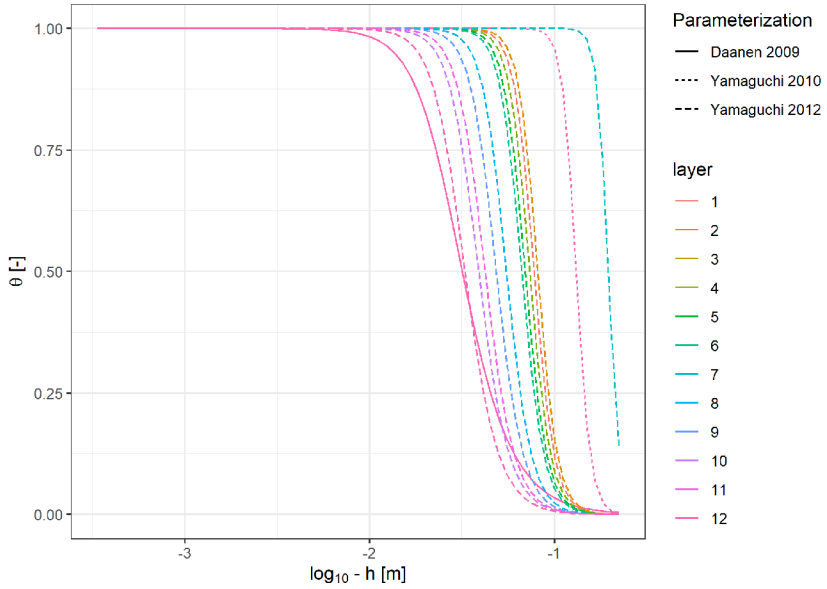

Figure D.2: Effect of different cryo-transfer functions on the retention curve for the experiment conducted in January 2019 in Kubova Hut for the second pre-experimental profile with Daanen and Nieber (2009), Yamaguchi et al. (2010) and Yamaguchi et al. (2012).

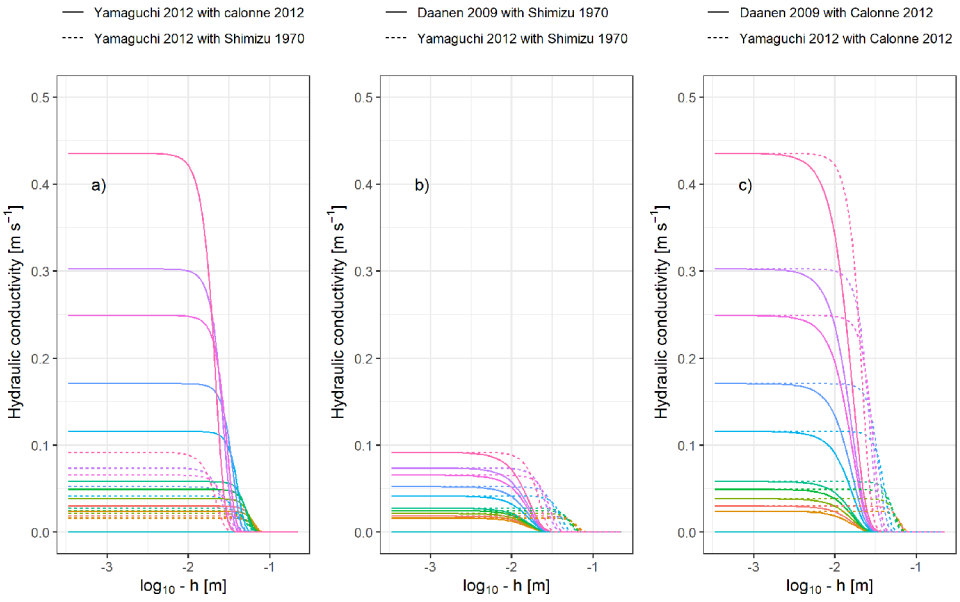

Figure D.3: Effect of different cryo-transfer functions on the unsaturated hydraulic conductivity curve for the experiment conducted in January 2019 in Kubova Hut for the second pre-experimental profile. a) Comparison of saturated conductivity parameterized with Shimizu (1970) and Calonne et al. (2012). b) Comparison of parameterization of α and n with Daanen and Nieber (2009) and Yamaguchi et al. (2012) in combination with saturated conductivity of b) Shimizu (1970) and c) Calonne et al. (2012).

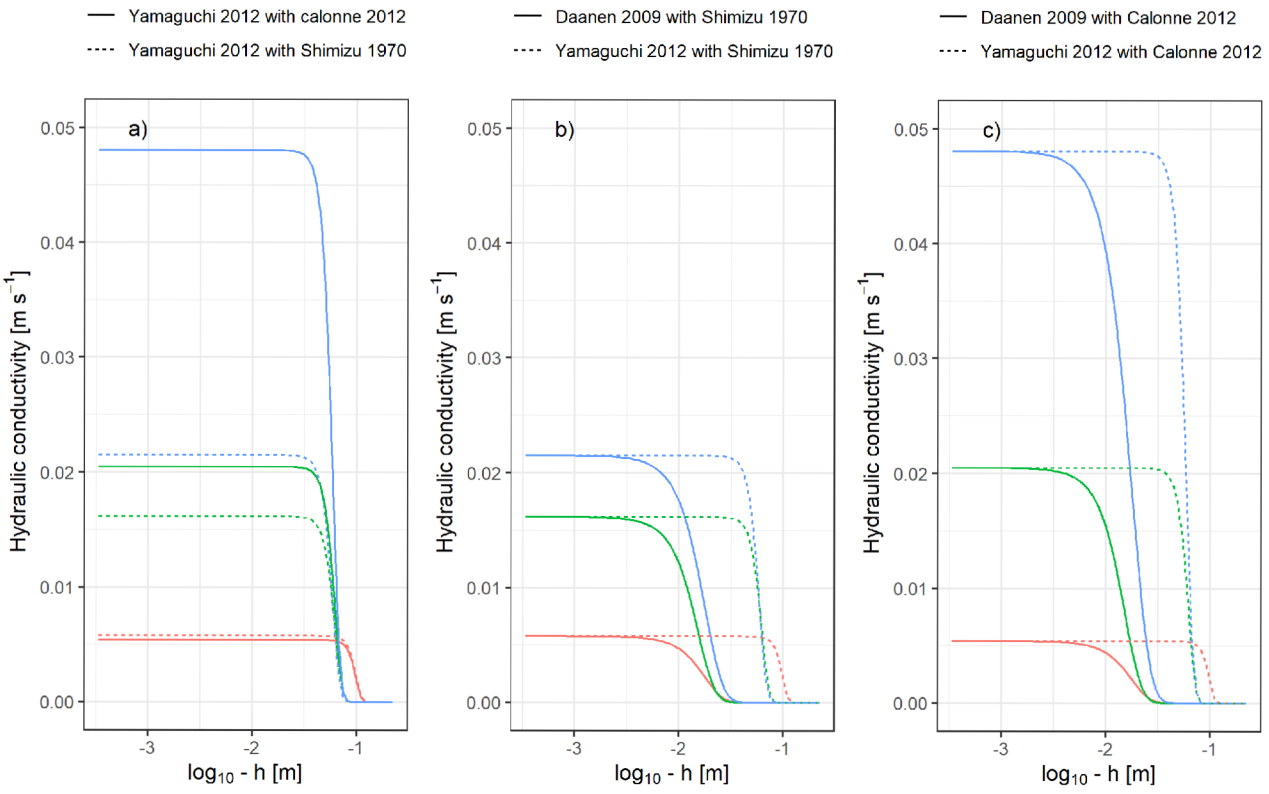

Figure D.4: Effect of different cryo-transfer functions on the unsaturated hydraulic conductivity curve for the experiment conducted in March 2019 in Kubova Hut for the second pre-experimental profile. a) Comparison of saturated conductivity parameterized with Shimizu (1970) and Calonne et al. (2012). b) Comparison of parameterization of α and n with Daanen and Nieber (2009) and Yamaguchi et al. (2012) in combination with saturated conductivity of b) Shimizu (1970) and c) Calonne et al. (2012).

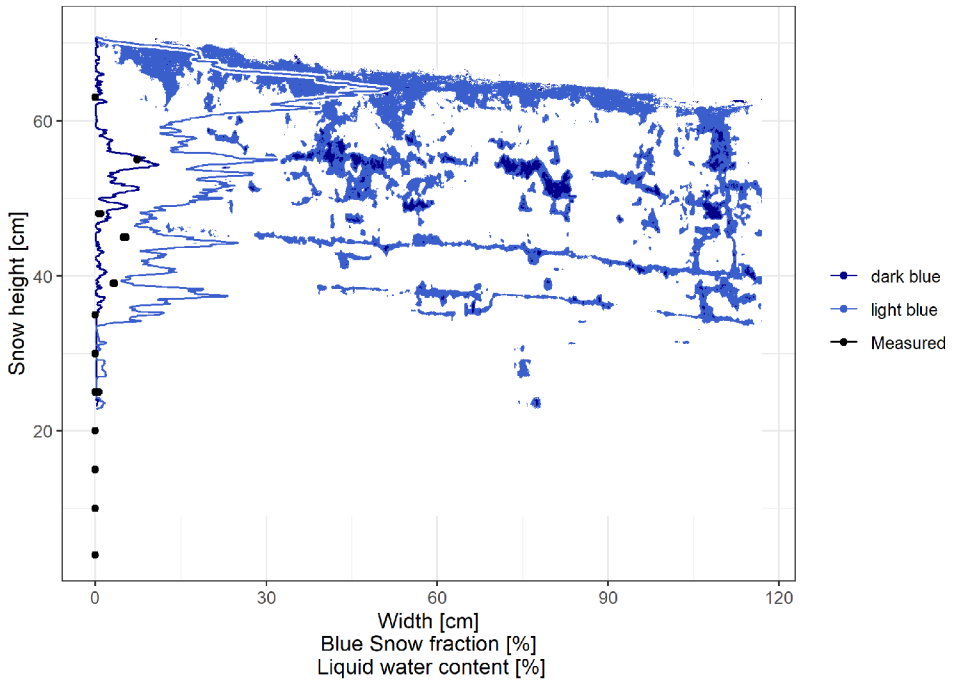

Figure D.5: Dark and light blue dye highlighted in the profile and summarized in the vertical blue snow fraction [%] and measured liquid water content for the rain-on-snow experiment conducted in January in Kubova Hut.

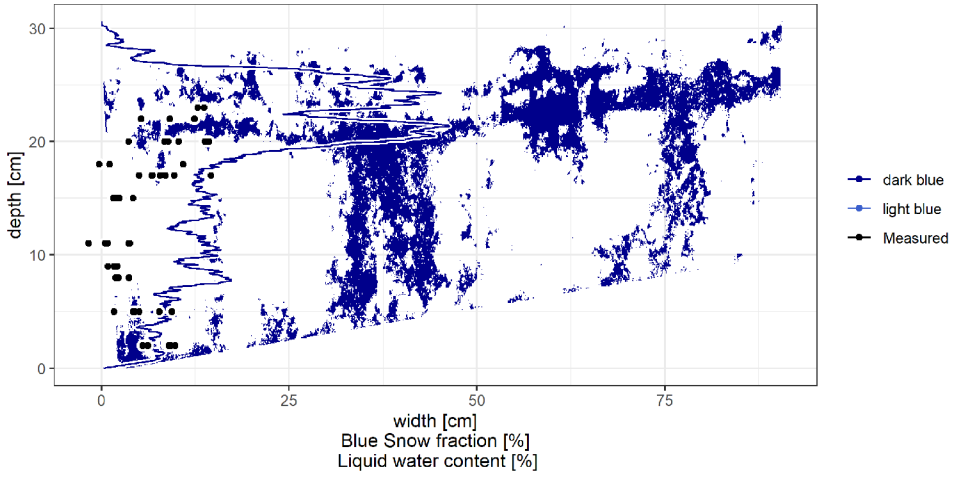

Figure D.6: Dark and light blue dye highlighted in the profile and summarized in the vertical blue snow fraction [%] and measured liquid water content conducted in March in Kubova Hut.

Bibliography

Amiri, Erfan A., James R. Craig, and Barret L. Kurylyk (2018). "A theoretical extension of the soil freezing curve paradigm". In: *Advances in Water Resources* 111, pp. 319–328. ISSN: 0309-1708. DOI: 10.1016/j.advwatres.2017.11.021.

Arzanfudi, Mehdi Musivand and Rafid Al-Khoury (Sept. 2018). "Freezing-thawing of porous media: An extended finite element approach for soil freezing and thawing". In: *Advances in Water Resources* 119, pp. 210–226. ISSN: 0309-1708. DOI: 10.1016/j.advwatres.2018.07.013.

Avanzi, Francesco, Giacomo Petrucci, Margret Matzl, Martin Schneebeli, and Carlo De Michele (2017). "Early formation of preferential flow in a homogeneous snowpack observed by micro-CT". In: *Water Resources Research* 53.5, pp. 3713–3729. ISSN: 0043-1397. DOI: 10.1002/2016WR019502.

Bartelt, Perry and Michael Lehning (Nov. 2002). "A physical SNOWPACK model for the Swiss avalanche warning: Part I: numerical model". In: *Cold Regions Science and Technology* 35.3, pp. 123–145. ISSN: 0165-232X. DOI: 10.1016/S0165-232X(02)00074-5.

Bello, Ibrahim (2019). "Image processing of flow characteristics of rain-on-snow experiments". MA thesis. Prague: Czech University of Life Sciences.

Blöschl, Günter et al. (2019). "Twenty-three unsolved problems in hydrology (UPH) – a community perspective". In: *Hydrological Sciences Journal* 64.10, pp. 1141–1158. DOI: 10.1080/02626667.2019.1620507.

Brown, R. L, P. K Satyawali, Michael Lehning, and Perry Bartelt (Dec. 2001). "Modeling the changes in microstructure of snow during metamorphism". In: *Cold Regions Science and Technology*. ISSW 2000:International Snow Science Workshop 33.2, pp. 91–101. ISSN: 0165-232X. DOI: 10.1016/S0165-232X(01)00032-5.

Brun, E. (1989). "Investigation on Wet-Snow Metamorphism in Respect of Liquid-Water Content". In: *Annals of Glaciology* 13, 22–26. DOI: 10.3189/S0260305500007576.

Burt, TP and PJ Williams (1976). "Hydraulic conductivty in frozen soils". In: *Earth Surface Processes and Landforms* 1.4, pp. 349–360. ISSN: 0197-9337. DOI: 10.1002/esp.3290010404.

Calonne, N., F. Flin, S. Morin, B. Lesaffre, S. Rolland du Roscoat, and C. Geindreau (2011). "Numerical and experimental investigations of the effective thermal conductivity of snow". In: *Geophysical Research Letters* 38.23. ISSN: 1944-8007. DOI: 10.1029/2011GL049234.

Calonne, N., C. Geindreau, F. Flin, S. Morin, B. Lesaffre, S. Rolland du Roscoat, and P. Charrier (2012). "3-D image-based numerical computations of snow permeability: links to specific surface area, density, and microstructural anisotropy". In: *The Cryosphere* 6.5, pp. 939–951. ISSN: 1994-0424. DOI: 10.5194/tc-6-939-2012.

Campbell, G. S. (Nov. 1985). *Soil Physics with BASIC: Transport Models for Soil-Plant Systems*. en. Google-Books-ID: VvTNYMUQuLEC. Elsevier. ISBN: 978-0-08-086982-7.

Cheney, Elliott Ward and David Ronald Kincaid (2008). *Numerical Mathematics and Computing*. 6th ed. Brooks/Cole. ISBN: 978-0-495-38472-4.

Colbeck, S C (1974). "The capillary effects on water percolation in homogeneous snow". In: *Journal Of Glaciology* 67, pp. 143–151.

Colbeck, S. C. (Jan. 1978). "The Physical Aspects of Water Flow Through Snow". In: *Advances in Hydroscience* 11, pp. 165–206.

Colbeck, S C and G Davidson (1973). "Water percolation through homogeneous snow". In: *The Role of Snow and Ice in Hydrology, (Proc.Banff Symp., 1972), Unesco-WMO-IAHS.* Vol. 107. IAHS Publ. 107, pp. 242–257.

Colbeck, Samuel C (1971). *One-dimensional water flow through snow.* Tech. rep. Honover, New Hampshire: CRREL, pp. 1–16.

Conway, H. and C. F. Raymond (1993). "Snow stability during rain". In: *Journal of Glaciology* 39.133, pp. 635–642. ISSN: 0022-1430, 1727-5652. DOI: 10.3189/S0022143000016531.

Cuthill, Elizabeth H. and James McKee (1969). "Reducing the Bandwidth of Sparse Symmetric Matrices". In: *Proceedings of the 1969 24th National Conference.* ACM '69. New York, NY, USA: Association for Computing Machinery, pp. 157–172. ISBN: 978-1-4503-7493-4. DOI: 10.1145/800195.805928.

Daanen, Ronald P. and John L. Nieber (June 2009). "Model for Coupled Liquid Water Flow and Heat Transport with Phase Change in a Snowpack". In: *Journal of Cold Regions Engineering* 23.2, pp. 43–68. DOI: 10.1061/(ASCE)0887-381X(2009)23:2(43).

Dall'Amico, M., S. Endrizzi, S. Gruber, and R. Rigon (2011). "A robust and energy-conserving model of freezing variably-saturated soil". In: *The Cryosphere* 5.2, pp. 469–484. ISSN: 1994-0416. DOI: https://doi.org/10.5194/tc-5-469-2011.

D'Amboise, C. J. L., K. Müller, L. Oxarango, S. Morin, and T. V. Schuler (Sept. 2017). "Implementation of a physically based water percolation routine in the Crocus/SURFEX (V7.3) snowpack model". In: *Geosci. Model Dev.* 10.9, pp. 3547–3566. ISSN: 1991-9603. DOI: 10.5194/gmd-10-3547-2017.

Diamantopoulos, Efstathios and Wolfgang Durner (Aug. 2012). "Dynamic Nonequilibrium of Water Flow in Porous Media: A Review". In: *Vadose Zone Journal* 11.3. ISSN: 1539-1663. DOI: 10.2136/vzj2011.0197.

Dytrt, Krystof (2020). "Experimental methods for investigating rainwater behaviour in the snowpack". MA thesis. Prague: Czech University of Life Sciences.

Essery, Richard, Samuel Morin, Yves Lejeune, and Cécile B Ménard (2013). "A comparison of 1701 snow models using observations from an alpine site". In: *Advances in Water Resources.* Snow–Atmosphere Interactions and Hydrological Consequences 55, pp. 131–148. ISSN: 0309-1708. DOI: 10.1016/j.advwatres.2012.07.013.

Fiedler, Miroslav (2013). *Special Matrices and Their Applications in Numerical Mathematics: Second Edition.* Dover Books on Mathematics. Dover Publications. ISBN: 978-0-486-78348-2.

Fierz, Charles, Armstrong R.L, Durand Y, Etchevers P, Ethan Greene, D Mcclung, K Nishimura, Pramod Satyawali, and Sergey Sokratov (2009). *The international classification for seasonal snow on the ground (UNESCO, IHP (International Hydrological Programme)–VII, Technical Documents in Hydrology, No 83; IACS (International Association of Cryospheric Sciences) contribution No 1).*

Frampton, Andrew, Scott L. Painter, and Georgia Destouni (2013). "Permafrost degradation and subsurface-flow changes caused by surface warming trends". In: *Hydrogeology Journal* 21.1, pp. 271–280. ISSN: 1435-0157. DOI: 10.1007/s10040-012-0938-z.

Genuchten, M.Th. van (1980). "Closed-form equation for predicting the hydraulic conductivity of unsaturated soils". In: *Soil Science Society of America Journal* 44.5, pp. 892–898. DOI: 10.2136/sssaj1980.03615995004400050002x.

Gerke, H. H. and M. T. van Genuchten (1993). "A dual-porosity model for simulating the preferential movement of water and solutes in structured porous media". In: *Water Resources Research* 29.2, pp. 305–319.

Germann, Peter F. (Dec. 1990). "Preferential Flow and the Generation of Runoff: 1. Boundary Layer Flow Theory". In: *Water Resources Research* 26.12, pp. 3055–3063. ISSN: 1944-7973. DOI: 10.1029/WR026i012p03055.

Godsey, S. E., J. W. Kirchner, and C. L. Tague (2014). "Effects of changes in winter snowpacks on summer low flows: case studies in the Sierra Nevada, California, USA". In: *Hydrological Processes* 28.19, pp. 5048–5064. ISSN: 1099-1085. DOI: 10.1002/hyp.9943.

Gohardoust, Mohammad R., Jirka Šimůnek, Horst Hardelauf, and Markus Tuller (May 2021). "Adaptation and validation of the ParSWMS numerical code for simulation of water flow and solute transport in soilless greenhouse substrates". en. In: *Journal of Hydrology* 596, p. 126053. ISSN: 0022-1694. DOI: 10.1016/j.jhydrol.2021.126053.

Golub, Gene H. and Charles F. van Loan (1996). *Matrix Computations*. The Johns Hopkins University Press.

Grenier, Christophe, Hauke Anbergen, Victor Bense, Quentin Chanzy, Ethan Coon, Nathaniel Collier, François Costard, Michel Ferry, Andrew Frampton, Jennifer Frederick, Julio Gonçalvès, Johann Holmén, Anne Jost, Samuel Kokh, Barret Kurylyk, Jeffrey McKenzie, John Molson, Emmanuel Mouche, Laurent Orgogozo, Romain Pannetier, Agnès Rivière, Nicolas Roux, Wolfram Rühaak, Johanna Scheidegger, Jan-Olof Selroos, René Therrien, Patrik Vidstrand, and Clifford Voss (2018). "Groundwater flow and heat transport for systems undergoing freeze-thaw: Intercomparison of numerical simulators for 2D test cases". In: *Advances in Water Resources* 114, pp. 196–218. ISSN: 0309-1708. DOI: 10.1016/j.advwatres.2018.02.001.

Hansson, Klas, Jirka Šimůnek, Masaru Mizoguchi, Lars-Christer Lundin, and Martinus Th van Genuchten (May 2004). "Water Flow and Heat Transport in Frozen Soil Numerical Solution and Freeze–Thaw Applications". In: *Vadose Zone Journal* 3.2, pp. 693–704. ISSN: 1539-1663. DOI: 10.2113/3.2.693.

Harlan, R. L. (1973). "Analysis of coupled heat-fluid transport in partially frozen soil". en. In: *Water Resources Research* 9.5, pp. 1314–1323. ISSN: 1944-7973. DOI: 10.1029/WR009i005p01314.

Heilig, A., C. Mitterer, L. Schmid, N. Wever, J. Schweizer, H.-P. Marshall, and O. Eisen (2015). "Seasonal and diurnal cycles of liquid water in snow—Measurements and modeling". en. In: *Journal of Geophysical Research: Earth Surface* 120.10, pp. 2139–2154. ISSN: 2169-9011. DOI: 10.1002/2015JF003593.

Heinze, T. (2021). "A Multi-Phase Heat Transfer Model for Water Infiltration Into Frozen Soil". en. In: *Water Resources Research* 57.10, e2021WR030067. ISSN: 1944-7973. DOI: 10.1029/2021WR030067.

Heinze, Thomas and Johanna R Blöcher (2019). "A model of local thermal non-equilibrium during infiltration". In: *Advances in Water Resources* 132. Publisher: Elsevier, p. 103394.

Hirashima, Hiroyuki, Satoru Yamaguchi, and Takafumi Katsushima (2014). "A multi-dimensional water transport model to reproduce preferential flow in the snowpack". In: *Cold Regions Science and Technology* 108, pp. 80–90. ISSN: 0165-232X. DOI: 10.1016/j.coldregions.2014.09.004.

Hirashima, Hiroyuki, Satoru Yamaguchi, Atsushi Sato, and Michael Lehning (2010). "Numerical modeling of liquid water movement through layered snow based on new measurements of the water retention curve". In: *Cold Regions Science and Technology*. International Snow Science Workshop 2009 Davos 64.2, pp. 94–103. ISSN: 0165-232X. DOI: 10.1016/j.coldregions.2010.09.003.

Iden, Sascha C., Johanna R. Blöcher, Efstathios Diamantopoulos, and Wolfgang Durner (2021). "Capillary, Film, and Vapor Flow in Transient Bare Soil Evaporation (1): Identifiability Analysis of Hydraulic Conductivity in the Medium to Dry Moisture Range". In: *Water Resources Research* 57.5. ISSN: 1944-7973. DOI: 10.1029/2020WR028513.

Iden, Sascha C, Johanna R. Blöcher, Efstathios Diamantopoulos, Andre Peters, and Wolfgang Durner (2019). "Numerical test of the laboratory evaporation method using coupled water, vapor and heat flow modelling". In: *Journal of Hydrology* 570. Publisher: Elsevier, pp. 574–583.

Illangasekare, Tissa H., Rodney J. Walter, Mark F. Meier, and W. Tad Pfeffer (1990). "Modeling of meltwater infiltration in subfreezing snow". In: *Water Resources Research* 26.5, pp. 1001–1012. ISSN: 0043-1397. DOI: 10.1029/WR026i005p01001.

Jame, Yih-Wu (1977). "Heat and mass transfer in freezing unsaturated soil". en. PhD thesis. University of Saskatchewan.

Jame, Yih-Wu and Donald I. Norum (1980). "Heat and mass transfer in a freezing unsaturated porous medium". In: *Water Resources Research* 16.4, pp. 811–819. ISSN: 1944-7973. DOI: 10.1029/WR016i004p00811.

Juras, R, J Pavlasek, P Ded, V Tomasek, and P Maca (2013). "A portable simulator for investigating rain-on-snow events". In: *Zeitschrift Fur Geomorphologie* 57, pp. 73–89. ISSN: 0372-8854. DOI: 10.1127/0372-8854/2012/S-00088.

Juras, R., S. Würzer, J. Pavlásek, T. Vitvar, and T. Jonas (Sept. 2017). "Rainwater propagation through snowpack during rain-on-snow sprinkling experiments under different snow conditions". In: *Hydrol. Earth Syst. Sci.* 21.9, pp. 4973–4987. ISSN: 1607-7938. DOI: 10.5194/hess-21-4973-2017.

Juras, Roman, Johanna R Blöcher, Michal Jenicek, Ondrej Hotovy, and Yannis Markonis (2021). "What affects the hydrological response of rain-on-snow events in low-altitude mountain ranges in Central Europe?" In: *Journal of Hydrology*. Publisher: Elsevier, p. 127002. DOI: https://doi.org/10.1016/j.jhydrol.2021.127002.

Juras, Roman, Jirka Pavlasek, Tomas Vitvar, Martin Sanda, Jirka Holub, Jakub Jankovec, and Miloslav Linda (2016). "Isotopic tracing of the outflow during artificial rain-on-snow event". In: *Journal of Hydrology* 541, pp. 1145–1154. ISSN: 0022-1694. DOI: 10.1016/j.jhydrol.2016.08.018.

Karra, S., S. L. Painter, and P. C. Lichtner (2014). "Three-phase numerical model for subsurface hydrology in permafrost-affected regions (PFLOTRAN-ICE v1.0)". English. In: *The Cryosphere* 8.5. Publisher: Copernicus GmbH, pp. 1935–1950. ISSN: 1994-0416. DOI: https://doi.org/10.5194/tc-8-1935-2014.

Katsushima, Takafumi, Satoru Yamaguchi, Toshiro Kumakura, and Atsushi Sato (Jan. 2013). "Experimental analysis of preferential flow in dry snowpack". In: *Cold Regions Science and Technology* 85, pp. 206–216. ISSN: 0165-232X. DOI: 10.1016/j.coldregions.2012.09.012.

Kelleners, T. J. (2013). "Coupled Water Flow and Heat Transport in Seasonally Frozen Soils with Snow Accumulation". en. In: *Vadose Zone Journal* 12.4. ISSN: 1539-1663. DOI: 10.2136/vzj2012.0162.

Kelleners, Thijs J., Jeremy Koonce, Rose Shillito, Jelle Dijkema, Markus Berli, Michael H. Young, John M. Frank, and W. J. Massman (2016). "Numerical Modeling of Coupled Water Flow and Heat Transport in Soil and Snow". In: *Soil Science Society of America Journal* 80.2, pp. 247–263. ISSN: 0361-5995. DOI: 10.2136/sssaj2015.07.0279.

Kmec, Jakub, Tomáš Fürst, Rostislav Vodák, and Miloslav Šír (Feb. 2021). "A two dimensional semi-continuum model to explain wetting front instability in porous media". In: *Scientific Reports* 11.1, p. 3223. ISSN: 2045-2322. DOI: 10.1038/s41598-021-82317-x.

Knowles, Noah, Michael D. Dettinger, and Daniel R. Cayan (2006). "Trends in Snowfall versus Rainfall in the Western United States". In: *Journal of Climate* 19.18, pp. 4545–4559. ISSN: 0894-8755. DOI: 10.1175/JCLI3850.1.

Kool, J. B. and J. C. Parker (1987). "Development and evaluation of closed-form expressions for hysteretic soil hydraulic properties". In: *Water Resources Research* 23.1, pp. 105–114. ISSN: 1944-7973. DOI: 10.1029/WR023i001p00105.

Koopmans, RW and RD Miller (1966). "Soil Freezing and soil water characteristic curves". In: *SOIL SCIENCE SOCIETY OF AMERICA PROCEEDINGS* 30.6, pp. 680–&. DOI: 10.2136/sssaj1966.03615995003000060011x.

Kuraz, Michal, Petr Mayer, and Johanna Ruth Blöcher (2020). *DRUtES – an opensource library for solving coupled nonlinear convection-diffusion-reaction equations*. URL: http://www.drutes.org.

Kuraz, Michal, Petr Mayer, Vojtech Havlicek, and Pavel Pech (2013a). "Domain decomposition adaptivity for the Richards equation model". en. In: *Computing* 95.1, pp. 501–519. ISSN: 0010-485X, 1436-5057. DOI: 10.1007/s00607-012-0279-8.

Kuraz, Michal, Petr Mayer, Vojtěch Havlíček, Pavel Pech, and Jirka Pavlásek (2013b). "Dual permeability variably saturated flow and contaminant transport modeling of a nuclear waste repository with capillary barrier protection". In: *Applied Mathematics and Computation* 219.13, pp. 7127 –7138. ISSN: 0096-3003. DOI: https://doi.org/10.1016/j.amc.2011.08.109.

Kuraz, Michal, Petr Mayer, and Pavel Pech (2015). "Solving the nonlinear and nonstationary Richards equation with two-level adaptive domain decomposition (dd-adaptivity)". In: *Applied Mathematics and Computation* 267, pp. 207 –222. ISSN: 0096-3003. DOI: https://doi.org/10.1016/j.amc.2015.03.130.

Kurylyk, Barret L. and Kunio Watanabe (2013). "The mathematical representation of freezing and thawing processes in variably-saturated, non-deformable soils". In: *Advances in Water Resources* 60, pp. 160–177. ISSN: 0309-1708. DOI: 10.1016/j.advwatres.2013.07.016.

Lamontagne-Hallé, Pierrick, Jeffrey M. McKenzie, Barret L. Kurylyk, John Molson, and Laura N. Lyon (2020). "Guidelines for cold-regions groundwater numerical modeling". In: *WIREs Water*, e1467. ISSN: 2049-1948. DOI: 10.1002/wat2.1467.

Lehning, Michael, Perry Bartelt, Bob Brown, Charles Fierz, and Pramod Satyawali (Nov. 2002). "A physical SNOWPACK model for the Swiss avalanche warning: Part II. Snow microstructure". In: *Cold Regions Science and Technology* 35.3, pp. 147–167. ISSN: 0165-232X. DOI: 10.1016/S0165-232X(02)00073-3. URL: http://www.sciencedirect.com/science/article/pii/S0165232X02000733.

Leroux, Nicolas R. and John W. Pomeroy (2017). "Modelling capillary hysteresis effects on preferential flow through melting and cold layered snowpacks". In: *Advances in Water Resources* 107, pp. 250–264. ISSN: 0309-1708. DOI: 10.1016/j.advwatres.2017.06.024.

Liu, Zhen, Ye Sun, and Xiong Bill Yu (2012). "Theoretical basis for modeling porous geomaterials under frost actions: A review". In: *Soil Science Society of America Journal* 76, pp. 313–330.

Lundin, Lars-Christer (1990). "Hydraulic properties in an operational model of frozen soil". In: *Journal of Hydrology* 118.1, pp. 289–310. ISSN: 0022-1694. DOI: 10.1016/0022-1694(90)90264-X.

Markonis, Y., S. M. Papalexiou, M. Martinkova, and M. Hanel (2019). "Assessment of Water Cycle Intensification Over Land using a Multisource Global Gridded Precipitation DataSet". In: *Journal of Geophysical Research: Atmospheres* 124.21, pp. 11175–11187. ISSN: 2169-8996. DOI: 10.1029/2019JD030855. (Visited on 01/27/2022).

Marsh, Philip and Ming-Ko Woo (1985a). "Meltwater Movement in Natural Heterogeneous Snow Covers". In: *Water Resources Research* 21.11, pp. 1710–1716. ISSN: 1944-7973. DOI: 10.1029/WR021i011p01710.

— (1985b). "Meltwater Movement in Natural Heterogeneous Snow Covers". In: *Water Resources Research* 21.11, pp. 1710–1716. ISSN: 1944-7973. DOI: 10.1029/WR021i011p01710.

McCauley, CA, DM White, MR Lilly, and DM Nyman (Apr. 2002). "A comparison of hydraulic conductivities, permeabilities and infiltration rates in frozen and unfrozen soils". In: *COLD REGIONS SCIENCE AND TECHNOLOGY* 34.2, pp. 117–125. ISSN: 0165-232X. DOI: 10.1016/S0165-232X(01)00064-7.

Mizoguchi, M. (1990). "Water, heat and salt transport in freezing soil. sensible and latent heat flow in a partially frozen unsaturated soil." Japanese. PhD thesis. University of Tokyo.

Mualem, Y. (1976). "A catalogue of the hydraulic properties of unsaturated soils". In: *A Catalogue of the Hydraulic Properties of Unsaturated Soils*.

Muskett, Reginald R. (Nov. 2012). "Remote Sensing, Model-Derived and Ground Measurements of Snow Water Equivalent and Snow Density in Alaska". In: *International Journal of Geosciences* 3.5, pp. 1127–1136. DOI: 10.4236/ijg.2012.35114.

Niu, Guo-Yue and Zong-Liang Yang (2006). "Effects of Frozen Soil on Snowmelt Runoff and Soil Water Storage at a Continental Scale". In: *Journal of Hydrometeorology* 7.5, pp. 937–952. ISSN: 1525-755X. DOI: 10.1175/JHM538.1.

Painter, S. L., J. D. Moulton, and C. J. Wilson (2013). "Modeling challenges for predicting hydrologic response to degrading permafrost". In: *Hydrogeology Journal* 21.1, pp. 221–224. ISSN: 1435-0157. DOI: 10.1007/s10040-012-0917-4.

Painter, Scott L. (2011). "Three-phase numerical model of water migration in partially frozen geological media: model formulation, validation, and applications". In: *Computational Geosciences* 15.1, pp. 69–85. ISSN: 1573-1499. DOI: 10.1007/s10596-010-9197-z.

Painter, Scott L., Ethan T. Coon, Adam L. Atchley, Markus Berndt, Rao Garimella, J. David Moulton, Daniil Svyatskiy, and Cathy J. Wilson (2016). "Integrated surface/subsurface permafrost thermal hydrology: Model formulation and proof-of-concept simulations". In: *Water Resources Research* 52.8, pp. 6062–6077. ISSN: 1944-7973. DOI: https://doi.org/10.1002/2015WR018427.

Peng, Zhenyang, Fuqiang Tian, Jingwei Wu, Jiesheng Huang, Hongchang Hu, and Christophe J. G. Darnault (2016). "A numerical model for water and heat transport in freezing soils with nonequilibrium ice-water interfaces". In: *Water Resources Research* 52.9, pp. 7366–7381. ISSN: 1944-7973. DOI: 10.1002/2016WR019116.

Pradhanang, Soni M., Allan Frei, Mark Zion, Elliot M. Schneiderman, Tammo S. Steenhuis, and Donald Pierson (2013). "Rain-on-snow runoff events in New York". In: *Hydrological Processes* 27.21, pp. 3035–3049. ISSN: 1099-1085. DOI: 10.1002/hyp.9864.

R Core Team (2021). *R: A Language and Environment for Statistical Computing*. R Foundation for Statistical Computing. Vienna, Austria. URL: https://www.R-project.org/.

Ross, P. J. and K. R. J. Smettem (2000). "A Simple Treatment of Physical Nonequilibrium Water Flow in Soils". In: *Soil Science Society of America Journal* 64.6, pp. 1926–1930. ISSN: 1435-0661. DOI: 10.2136/sssaj2000.6461926x.

Rössler, O., P. Froidevaux, U. Börst, R. Rickli, O. Martius, and R. Weingartner (2014). "Retrospective analysis of a nonforecasted rain-on-snow flood in the Alps-A matter of model limitations or unpredictable nature?" In: *Hydrology and Earth System Sciences* 18.6, pp. 2265–2285. ISSN: 16077938. DOI: 10.5194/hess-18-2265-2014.

Saad, Yousef (2003). *Iterative Methods for Sparse Linear Systems*. 2nd. USA: Society for Industrial and Applied Mathematics. ISBN: 0-89871-534-2.

Saito, Hirotaka, Jiri Šimůnek, and Binayak P. Mohanty (May 2006). "Numerical Analysis of Coupled Water, Vapor, and Heat Transport in the Vadose Zone". en. In: *Vadose Zone Journal* 5.2, pp. 784–800. ISSN: 1539-1663. DOI: 10.2136/vzj2006.0007.

Schneider, Caroline A., Wayne S. Rasband, and Kevin W. Eliceiri (2012). "NIH Image to ImageJ: 25 years of image analysis". In: *Nature Methods* 9.7, pp. 671–675. ISSN: 1548-7105. DOI: 10.1038/nmeth.2089.

Shimizu, Hiromu (1970). "Air Permeability of Deposited Snow". In: *Contributions from the Institute of Low Temperature Science* A22, pp. 1–32. ISSN: 0073-2931.

Spaans, Egbert J. A. and John M. Baker (1996). "The Soil Freezing Characteristic: Its Measurement and Similarity to the Soil Moisture Characteristic". In: *Soil Science Society of America Journal* 60.1, pp. 13–19. ISSN: 1435-0661. DOI: 10.2136/sssaj1996.03615995006000010005x.

Sturm, Matthew, Michael A. Goldstein, and Charles Parr (2017). "Water and life from snow: A trillion dollar science question". In: *Water Resources Research* 53.5, pp. 3534–3544. ISSN: 0043-1397. DOI: 10.1002/2017WR020840.

Tadono, T., H. Ishida, F. Oda, S. Naito, K. Minakawa, and H. Iwamoto (2014). "Precise Global DEM Generation by ALOS PRISM". In: *ISPRS Annals of the Photogrammetry, Remote Sensing and Spa-*

tial Information Sciences. Vol. II-4. ISSN: 2194-9042. Copernicus GmbH, pp. 71–76. DOI: 10.5194/isprsannals-II-4-71-2014.

Tan, Xianjun, Weizhong Chen, Hongming Tian, and Junjie Cao (2011). "Water flow and heat transport including ice/water phase change in porous media: Numerical simulation and application". In: *Cold Regions Science and Technology* 68, pp. 74–84. ISSN: 0165-232X. DOI: 10.1016/j.coldregions.2011.04.004.

Van Genuchten, M.T., J. Simunek, FJ Leij, and SR Yates (1991). *The RETC Code for Quantifying the Hydraulic Functions of Unsaturated Soils*. Riverside, California.

Varga, Richard S. (2000). *Matrix Iterative Analysis*. Springer-Verlag Berlin Heidelberg.

Voytkovskiy, KF and VN Golubev (1973). "Mechanical properties of ice as a function of the conditions of its formation". In: *2nd International Conference on Permafrost. Proceedings, National Academy of Sciences, Washington DC*.

Watanabe, Kunio and Markus Flury (2008). "Capillary bundle model of hydraulic conductivity for frozen soil". In: *Water Resources Research* 44.12, W12402. ISSN: 1944-7973. DOI: 10.1029/2008WR007012.

Watanabe, Kunio and Tomomi Wake (2009). "Measurement of unfrozen water content and relative permittivity of frozen unsaturated soil using NMR and TDR". In: *Cold Regions Science and Technology* 59.1, pp. 34–41. ISSN: 0165-232X. DOI: 10.1016/j.coldregions.2009.05.011.

Wever, N., C. Fierz, C. Mitterer, H. Hirashima, and M. Lehning (2014). "Solving Richards Equation for snow improves snowpack meltwater runoff estimations in detailed multi-layer snowpack model". In: *The Cryosphere* 8.1, pp. 257–274. ISSN: 1994-0424. DOI: 10.5194/tc-8-257-2014.

Wever, N., S. Würzer, C. Fierz, and M. Lehning (2016). "Simulating ice layer formation under the presence of preferential flow in layered snowpacks". In: *The Cryosphere* 10.6, pp. 2731–2744. ISSN: 1994-0424. DOI: 10.5194/tc-10-2731-2016.

Würzer, S., N. Wever, R. Juras, M. Lehning, and T. Jonas (Mar. 2017). "Modelling liquid water transport in snow under rain-on-snow conditions – considering preferential flow". In: *Hydrol. Earth Syst. Sci.* 21.3, pp. 1741–1756. ISSN: 1607-7938. DOI: 10.5194/hess-21-1741-2017.

Yamaguchi, Satoru, Takafumi Katsushima, Atsushi Sato, and Toshiro Kumakura (2010). "Water retention curve of snow with different grain sizes". In: *Cold Regions Science and Technology*. International {Snow} {Science} {Workshop} 2009 {Davos} 64.2, pp. 87–93. ISSN: 0165-232X. DOI: 10.1016/j.coldregions.2010.05.008.

Yamaguchi, Satoru, Kunio Watanabe, Takafumi Katsushima, Atsushi Sato, and Toshiro Kumakura (2012). "Dependence of the water retention curve of snow on snow characteristics". In: *Annals of Glaciology* 53.61, pp. 6–12. ISSN: 0260-3055, 1727-5644. DOI: 10.3189/2012AoG61A001.

Zhang, Yinsuo, Sean K. Carey, and William L. Quinton (2008). "Evaluation of the algorithms and parameterizations for ground thawing and freezing simulation in permafrost regions". In: *Journal of Geophysical Research: Atmospheres* 113.D17. DOI: https://doi.org/10.1029/2007JD009343.

Zhao, Litong and D. M. Gray (1999). "Estimating snowmelt infiltration into frozen soils". In: *Hydrological Processes* 13.12-13, pp. 1827–1842. ISSN: 1099-1085. DOI: 10.1002/(SICI)1099-1085(199909)13:12/13<1827::AID-HYP896>3.0.CO;2-D.

Čejková, Veronika (2019). "Analysis of rainwater flow in snowpack". MA thesis. Czech University of Life Sciences.